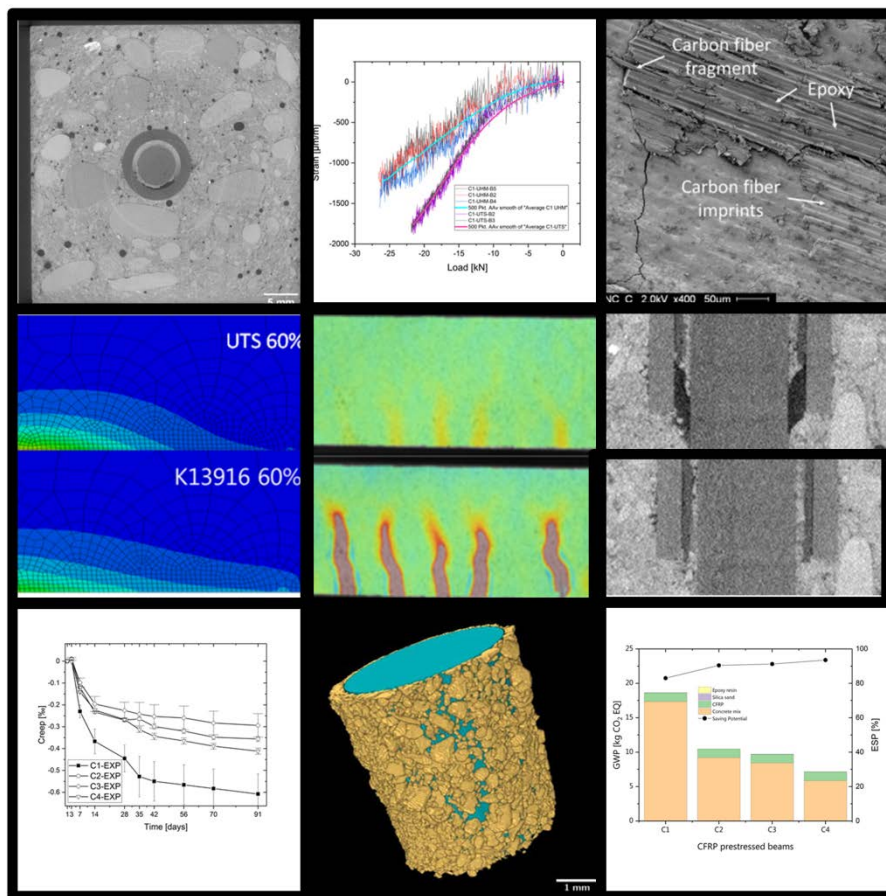


Development of novel low-clinker high-performance concrete elements prestressed with high modulus carbon fibre reinforced polymers

DISS. ETH NO. – 25890



Tobias Dominik Lämmlein

March 2019

Empa – Mechanical Systems Engineering Laboratory

ETH Zurich – Institute for Building Materials (IfB)

DISS. ETH NO. – 25890

**Development of novel low-clinker high-performance
concrete elements prestressed with high modulus
carbon fibre reinforced polymers**

A thesis submitted to attain the degree of
DOCTOR OF SCIENCES of ETH ZURICH
(Dr. sc. ETH Zurich)

presented by
TOBIAS DOMINIK LÄMMLEIN

MSc ETH ME, ETH Zurich

born on 20.09.1985
citizen of Germany

accepted on the recommendation of

Prof. Dr. Pietro Lura
Dr. Giovanni P. Terrasi
Prof. Dr. Janet M. Lees
Prof. Dr. Guillaume Habert

2019



Eidgenössische Technische Hochschule Zürich
Swiss Federal Institute of Technology Zurich



Departement Bau, Umwelt und Geomatik
Department of Civil, Environmental and Geomatic Engineering

Your Doctoral Thesis: Declaration of Your Personal Contribution

Name: Lämmlein

First Name: Tobias Dominik

Title of Thesis: Development of novel low-clinker high-performance concrete elements prestressed with high modulus carbon fibre reinforced polymers

Thesis Supervisor: Prof. Dr. Pietro Lura

Study Programme (CE, EE, G&P, REIS): -

I, Tobias Dominik Lämmlein, declare that this thesis is my own work and has not been submitted in any form for another degree or diploma at any university or other institute. Information derived from the published and unpublished work of others has been acknowledged in the text and a list of references is given in the bibliography.

Declaration of Your Personal Contribution

Briefly describe your contribution as well as that of your co-authors, if any, by chapter/paper. Where published or submitted papers form the basis of a chapter/chapters in your thesis, provide the full reference of each and clearly specify the corresponding chapter(s) in your thesis.

My contribution to the Thesis entitled "Development of novel low-clinker high-performance concrete elements prestressed with high modulus carbon fibre reinforced polymers" was organisation, conducting, presenting, planning, writing, performing experiments and simulations as well as their doing their analysis. The Chapters 2-4 are based on papers written based on results gained during this thesis. In these Chapters I was assisted by my co-authors. In particular, by M. Griffa for the X-ray tomography (Ch2), F. Messina and M. Wyrzykowski for the concrete recipe development (Ch2-Ch3), J. Justs for the beam manufacturing (Ch4) and overall by G.P. Terrasi and P. Lura who always critically reviewed my work (Ch0-Ch7). In addition Chapter 5 is in part based on Zingg et al. (2016) and I was assisted bei F.Pittau during the final LCA. All references are clearly marked in the Thesis and given at the respective places in the Chapters.

I confirm that the individual contributions are correctly declared.

Place, Date: Zürich, den 10.02.2019

Signature Doctoral Student: _____

Acknowledgements

Firstly, I'd like to thank both of my excellent supervisors Prof. Dr. P. Lura and Dr. G. P. Terrasi for their great guidance, their continuous support and their never-ending inspiration during many talks and steps of this Thesis.

Further, I would like to express my gratitude to Prof. Dr. J. M. Lees and Prof. Dr. G. Habert for serving in my PhD committee and their support during the final stage of this Thesis.

A special thanks goes to Dr. Michele Griffa, Lee Völker, Vanessa Rohr, Iurii Burda, Francesco Messina and Dr. Mateusz Wyrzykowski for their direct support of this Thesis and their fruitful discussions and inputs.

Moreover, I would like to thank the whole work group in the joint Concrete Solution project. Especially, I would like to address my gratitude to Sharon Zingg and Francesco Pittau for managing the project and their support while performing the LCA analysis.

I would like to acknowledge Empa for the financial support and the Swiss National Science Foundation (SNSF) for funding the joint project "Concrete Solutions" within the framework of the NRP70 "Energy Turnaround".

A big thanks goes to the staff of both research laboratories I've been working in at Empa. In particular I would like to thank Daniel Völki for his patience during my extensive mechanical testing program, Janis Justs for keeping his composure when I managed to stop the 250 l concrete mixer and Daniel Käppeli, Marcel Käppeli, Walter Bollier, Nikolajs Toropovs, Sebastiano Valvo and Angelo Scioscia for their help to solve this fiasco but also for their great support all over this project, without these guys my project would not have been possible. In addition, I would like to thank Dr. M. Barbezat for giving me access to his composite group laboratory whenever I needed, Peter Ebschner for the best lunchtime I could imagine, Gabor Kovacs for taking me to the best possible work trips, Walter Trindler for organizing the best late night lab activities, Lukas Düring for some great days of skiing and Roland Koller for keeping an eye on my physical exercise outside of work and teaching me the basics of tennis.

Moreover, I would like to thank my family, for their continuous support and help during my studies, for motivating me and for always being around when needed.

Finally, and most importantly I would like to thank my girlfriend Caroline who managed to survive the last 8 years with me on her side and in particular for showing a remarkable stress load capacity during the final path of this thesis.

Abstract

In this thesis, new ideas for reducing the environmental impact and, at the same time, increasing the mechanical performance of carbon fibre reinforced polymer (CFRP) prestressed high performance concrete (HPC) elements were studied. This involved in particular, the initial characterization of sand coated ultra-high-modulus (UHM)-CFRP tendons and the assessment about their suitability for prestressing applications, the development of novel low clinker high performance concretes (LCHPCs) and the final proof of concept on structural level with the development of a 2nd generation of UHM-CFRP LCHPC beam elements.

At first, the sand coated UHM-CFRP prestressing tendons were investigated on their bond to concrete. With the aid of a combined experimental and numerical approach, employing X-ray CT, scanning electron microscopy (SEM) and the finite element software Abaqus 6.14, a numerical model could be formulated to describe the tendon pull-out behaviour up to failure. The tendon draw-in behaviour was significantly affected by the longitudinal stiffness of the CFRP tendon. In contrast, the experimentally tested ultimate bond strength between sand-coated tendon and concrete was only dependent on the chosen sand-coating and found independent from the tendon's stiffness.

Secondly, starting from an industry reference HPC, novel LCHPCs were developed by substituting significant amounts of cement with limestone filler, metakaolin and silica fume. Three LCHPC recipes were developed with clinker replacement levels of 54, 58 and 70 %. All three recipes reached a compressive strength between 77 MPa and 88 MPa. Due to their low cement content, they showed less shrinkage and creep in comparison to a reference HPC. Based on these results a finite element model was developed in Abaqus 6.14, considering concrete shrinkage and creep, to estimate the performance of the novel LCHPCs and the UHM-CFRP prestressing tendons in a fictitious prestressing application. This model showed that high longitudinal stiffness of the UHM-CFRP tendons will lead to increased prestress losses. Low shrinkage and creep of LCHPCs, in contrast, were predicted to contribute to a high remaining prestress level the fictitious prestressed elements.

Thirdly, the gained knowledge on LCHPCs and UHM-CFRP prestressing tendons was combined and three meter long UHM-CFRP prestressed LCHPC beam elements were designed. In these elements, the prestress loss over time was experimentally studied by the aid of fibre optic sensors placed inside the CFRP-prestressing tendons. Further, the beams were tested in 4-point bending and their structural behaviour was analysed by a digital image correlation system (DIC). The experimental results confirmed the previously developed numerical model. UHM-CFRP tendons showed much higher prestress loss over time. In the four point bending tests, UHM-CFRP tendons contributed to a significantly reduced beam deflection in particular when the beam was loaded in the cracked state. The LCHPCs showed no significant effect during the 4-point bending tests performed 28 days after casting. This confirmed the expectations and showed that these recipes are ready for application in CFRP-prestressed concrete elements.

This work was concluded by performing a life cycle assessment (LCA) on the new beam elements using the measures of global warming potential (GWP), cumulative energy demand (CED) and ecological scarcity method (UBP). In comparison to a reinforced concrete structure

savings of 80% for the CED measure and even up to 90% for the GWP and UBP measure could be reached by using CFRP-prestressed LCHPC beam elements. A direct application of LCHPCs as replacement for HPC would lead to savings between 25% and 50% for recipes containing metakaolin and up to 55-70% for a recipe which used only limestone and silica fume as cement replacement.

The results of this research could be transferred without large adaptations into praxis and would significantly help to reduce the CO₂ footprint of future infrastructure. In addition, this thesis sets the basis for the use of UHM-CFRP prestressing tendons in prestressed concrete and developed the first LCHPC recipes for applications in CFRP prestressed structural concrete elements.

Zusammenfassung

Diese Arbeit behandelt neue Ansätze zur Verbesserung der strukturellen Tragfähigkeit von Kohlenstofffaser vorgespannten Spannbetonelementen. Darüber hinaus hat diese Arbeit das Ziel die Umweltbelastung dieser Elemente in Form von CO₂ Emissionen zu senken und somit einen Beitrag für eine nachhaltige Schweiz zu leisten. Um dies zu erreichen wurden hochsteife sandbeschichtete Vorspanndrähte aus Kohlenstofffaser verstärkten Kunststoffen (UHM-CFK) ausgewählt und neue Hochleistungsbetone mit einem geringen Anteil an Zementklinker entwickelt. Die Eigenschaften der neuen Materialien wurden anschliessend verknüpft, vorgespannte Tragbalken der neusten Generation entwickelt und deren Leistungsfähigkeit nachgewiesen.

Begonnen wurde diese Arbeit damit die sandbeschichteten UHM-CFK Spanndrähte zu charakterisieren um anschliessend ihre Verbundeigenschaften zu hochfestem Betonen zu bestimmen. Hierzu wurden numerischen Methoden (Finite Elemente Methode) mit experimentellen Auszugsversuchen kombiniert. Unter der Zuhilfenahme von Röntgen Computertomographie und Rasterelektronenmikroskopie wurde das Drahtauszugsverhalten bis zum Verbundversagen analysiert und beschrieben. Es zeigte sich, dass das Drahtauszugsverhalten signifikant von der Längssteifigkeit des UHM-CFK Spanndrahtes abhängt. Im Gegensatz dazu war die maximale Verbundfestigkeit zwischen dem sandbeschichteten Spanndraht und dem Beton nur von der gewählten Sandbeschichtung abhängig, nicht aber von der Spanndrahtsteifigkeit.

Parallel dazu wurden, ausgehend von einem industriellen Referenzbeton, neue Hochleistungsbetone entwickelt in denen grosse Teile des Zements durch Kalkstein, Metakaolin und Silikastaub ersetzt wurden. Hierbei konnten drei neue Rezepturen entwickelt werden die eine Zementreduktion von 54, 58 und 70% aufweisen. Die gemessene Druckfestigkeit der drei Mischungen lag zwischen 77 und 88 MPa was sie als „hochfest“ klassifiziert. Auf Grund des stark reduzierten Zementanteils zeigten sich diese Mischungen zudem ein deutlich verbessertes Schwind- und Kriechverhalten. Basierend auf diesen Erkenntnissen wurde ein Finite-Elemente-Modell entwickelt, welches die mechanischen Eigenschaften der neuen Spanndrähte, aber auch der Betone sowie zusätzlich deren Schwind und Kriecheigenschaften berücksichtigt. Mit diesem Modell war es möglich abzuschätzen welche Auswirkungen die Verwendung der beiden neuen Materialien in einem fiktiven vorgespannten Element haben würde. Das Model zeigte das durch die hohe Längssteifigkeit der UHM-CFK Spanndrähte grosse Vorspannungsverluste zu erwarten sind. Durch die neuen Betonmischungen konnten diese Vorspannungsverluste jedoch teilweise wieder kompensiert werden. Das macht die neuen Betone insbesondere für Anwendungen in vorgespannten Elementen interessant.

Um die Leistungsfähigkeit der beiden neuen Materialien auch auf struktureller Ebene beurteilen zu können wurden die gewonnenen Resultate genutzt und UHM-CFK vorgespannte Biegebalken mit drei Meter Länge entworfen. Die CFK Spanndrähte in diesen Elementen waren mit faseroptischen Sensoren ausgerüstet um damit die auftretenden Vorspannungsverluste experimentell zu bestimmen. Die Balken wurden 28 Tage nach ihrer Herstellung, in 4-Punkt Biegeversuchen, belastet und ihre Tragfähigkeit ermittelt. Das strukturelle Verhalten der Balken

wurde während den Versuchen mit einem digitalen Bildkorrelationssystem (DIC) aufgezeichnet und analysiert. Die Ergebnisse der experimentellen Untersuchung bestätigten die Erwartungen des numerischen Modelles. Wie schon das Modell, zeigten die Experimente einen erhöhten Vorspannungsverlust bei der Verwendung von UHM-CFK Spanndrähten. In den 4-Punkt Biegeversuchen konnten die UHM-CFK Spanndrähte jedoch ihre Stärken ausspielen und verminderten die Durchbiegung des Balkens im gerissenen Zustand immens. Die neuen Betone zeigten sich während den 4-Punkt-Biegeversuche unauffällig was sehr positiv zu bewerten ist. Dies bestätigte die Erwartungen und zeigt, dass diese Rezepte für ihre Verwendung in CFK-Spannbetonelementen einsatzbereit sind.

Abschliessend wurden die neuen Balkenelemente mittels einer Ökobilanz auf ihre Umweltauswirkungen und ihre CO₂ Einsparpotentiale untersucht. Dabei wurden verschiedene Bewertungskennziffern eingesetzt; ein Mass für den Beitrag zur Erderwärmung (GWP), ein Ökofaktor auf Basis der Methode der ökologischen Knappheit (UBP) und ein Mass für die enthaltene Menge an Grauenergie (CED).

Im Vergleich zu einer Stahlbetonkonstruktion konnten mit den neuen Materialien Einsparungen von 80% nach CED und sogar bis zu 90% nach GWP und UBP erzielt werden. Eine direkte Anwendung der neuen Betone im Austausch für einen herkömmlichen Hochleistungsbeton alleine würde bereits zu Einsparungen zwischen 25% und 50% für Betonmischungen mit Metakaolin führen, und sogar Einsparungen von 55-70% bei einem Rezept, bei dem nur Kalkstein und Silikastaub als Zementersatz verwendet wurden.

Die Ergebnisse dieser Forschung können ohne große Anpassungen in die Praxis übertragen werden und würden erheblich dazu beitragen, die CO₂ Bilanz zukünftiger Bauten zu reduzieren. Darüber hinaus bildet diese Arbeit die Grundlage für den Einsatz von UHM-CFK-Spanndrähten in Spannbetonanwendungen. Ebenso entwickelte diese Arbeit die ersten Hochleistungsbetone mit einem stark reduzierten Zementanteil für die Anwendung in CFK vorgespannten Betonelementen.

Table of Contents

Acknowledgements	I
Abstract	II
Zusammenfassung	IV
Table of Contents	VI
List of Tables	VIII
List of Figures	IX
Nomenclature	XIV
CHAPTER 1 Introduction.....	1
1.1 Background and Motivation.....	1
1.2 Objective and Scope.....	11
1.3 Content and Structure of this Thesis.....	12
CHAPTER 2 Bond performance of sand coated UHM CFRP tendons in high performance concrete	15
2.1 Introduction	16
2.2 Materials and Methods.....	17
2.3 Experimental Results and Discussion.....	22
2.4 Summary and Discussion.....	32
2.5 Conclusions	33
CHAPTER 3 Low clinker high performance concretes and their potential in CFRP-prestressed structural elements	35
3.1 Introduction	36
3.2 Materials and Methods.....	38
3.3 Results	42
3.4 Discussion	44
3.5 Conclusions	50
CHAPTER 4 Prestressing low clinker structural concrete elements by ultra-high modulus carbon fibre reinforced polymer tendons	52
4.1 Introduction	53
4.2 Materials and Methods.....	55
4.3 Results	60

4.4	Discussion	63
4.5	Conclusions	68
CHAPTER 5 Life Cycle Analysis of CFRP prestressed LCHPC		69
5.1	Introduction	70
5.2	Material and Methods.....	70
5.3	Results and Discussion.....	73
5.4	Conclusions	78
5.5	Outlook	78
CHAPTER 6 Summary and Conclusion.....		80
CHAPTER 7 Outlook		84
Bibliography		86
Curriculum Vitae		96

List of Tables

Table 1: Properties of Concretes	18
Table 2: Properties of CFRP Tendons	18
Table 3: Sand coating characteristics and their application in this work	19
Table 4: Oxide composition for cement, fly-ash, metakaolin and silica fume	40
Table 5: Concrete composition and fresh concrete properties	40
Table 6: Compressive strength and E-modulus of the LCHPCs and their reference HPC	42
Table 7: Development of compressive strength and elastic modulus in compression over time in respect to their 28d properties (100%)	45
Table 8: Properties of Concretes	56
Table 9: Specified FBG sensing point position along the concrete beam	58
Table 10: Moments of inertia of cracked and un-cracked beams and the modular ratio between CFRP and concrete	64
Table 11: Longitudinal properties of CFRP tendons	65
Table 12: Overview of the functional units I-III as they were used in the LCA. In particular the relevant data of the functional unit I was taken from [124]. The data for functional units II and III were calculated based on the model developed in [124].	72

List of Figures

Figure 1: Microstructure of hardened cement paste with w/c ratio of 0.3 after 28 days, taken from [14].	2
Figure 2: Backscattered electron image of the interfacial transition zone (ITZ) in concrete. The white lines are drawn at approximately 20 and 50 μm apart from the aggregate which is visible on the left. The most significant changes in the ITZ can be found within the first 15-20 μm . Content adapted after and figure taken from [17].	3
Figure 3: Schematic of tensile and compressive load behaviour of concrete. The pre-stress moves the initial situation of zero stress and zero strain in a structural concrete element at point I into the compressive prestressed condition of point P. The prestress “activates” an additional load-bearing capacity which is visualized with the bracket in the graphic.	4
Figure 4: Schematic of prestress transfer and possible prestress losses according to [26].	4
Figure 5: Schematic cutout of a UD-FRP including related stresses in longitudinal, transverse and shear directions, taken from [34].	5
Figure 6: Mid-span deflection of three pole specimens loaded in 4-point bending over time. Graph taken from [41].	6
Figure 7: Mid-span deflection of two simply-supported slab specimens loaded in self-weight loading conditions over time. The geometry of the test setup was chosen so that the concrete reached the point of decompression in the middle of its span on the tensile side of the slab. Graph taken from [41].	7
Figure 8: Building façade elements produced with CFRP prestressed HPC; Location: Zürich, Switzerland.	7
Figure 9: Centrifugally-cast, CFRP-prestressed HPC lamp pole; Location: Zurich, Switzerland.	8
Figure 10: Slender, CFRP-prestressed HPC pole setup as a design element in a housing complex; Location: Uster, Switzerland.	8
Figure 11: Global warming expressed as temperature anomaly from the year 1880 until today. Data taken from and redrawn after [50].	9
Figure 12: Three strategies for improving a concrete structure`s sustainability, slide by P. Lura	9
Figure 13: Schematic visualization of the three main objectives in this thesis.	11
Figure 14: Schematic of testing/modelling interaction for this project.	12
Figure 15: Specimen details: (A) CFRP-tendon and bond-breaker arrangement before casting; and (B) demoulded samples before testing.	20
Figure 16: Pull-Out test configuration: Overview of mounted sample in experimental set-up.	20
Figure 17: Influence of different sand-epoxy coating options on bond: (A) absolute bond strength comparison for different sand coating options; and (B) tendon draw-in behaviour. The	

sudden drop in load after failure is cut-off from the graphs to allow a better visualization up until failure. This graph has to be studied from right to left along its x-axis and shows the means and the standard deviation for all tested configurations.....23

Figure 18: Results of visual analysis of the failure surface outside the concrete prism for no-coating, fine-coating, old-coarse-coating and new coating.....23

Figure 19: Influence of tendon stiffness on bond (UTS5631 136 GPa, K63A12 463 GPa, K13916 509 GPa). (A) Absolute bond strength comparison. All samples are coated with the new coarse coating and tested in C1 and Cind, respectively. (B) Tendon draw-in behaviour. The sudden drop in load after failure is cut-off from the graphs to allow a better visualization up until failure.24

Figure 20: Analysis of failure area for different tendon materials. Upper row: Visual results indicate the sand-epoxy layer shear off outside the concrete prism; and Lower row: SEM images show pull-out failure surface of different CFRP tendons. This supports the hypothesis that the weak interface lies in between tendon and epoxy-sand coating, independent of the different CFRP materials used.....25

Figure 21: Bond performance of UHM-CFRP in C1 (A) maximum bond strength after seven days (7 d) and 28 days (28 d); and (B) tendon draw-in and -out. These graphs show the average including the standard deviation up to failure. The darker colour indicates the mixture tested after 28 d and the lighter colour the same mixture tested after 7 d. The sudden drop in load after failure is cut-off from the graphs to allow a better visualization up until failure. Starting from the point of zero draw-in-out, negative values indicate the tendon draw-in at the unloaded side and positive values the draw-out at the loaded side of the tendon.....26

Figure 22: 2D vertical, digital vertical cross-sections from the X-ray tomograms acquired after loading the sample up to 50.5%, 70.5%, Reference 100% and 100% failure, from left to right, respectively.27

Figure 23: Overview of all components in the FEA.....28

Figure 24: Validation of FE model. The calculated stresses inside the concrete as well as the CFRP tendon are compared. The blue graph indicates the concrete and the black graph represents the values of the CFRP tendon.....29

Figure 25: Tendon draw FEM compared to related Sensor measurements. (A) Draw in for FEM UTS and FEM UHMK13916. Results show the same trend as experiments in terms of the higher tendon draw in for the UHM tendon. Sensor data is shown as reference. (B) Draw-in and -out modelled using Cind, UTS and UHMK13916. Sensor 28d of UHMK13916 properties are shown as a reference.30

Figure 26: Influences on tendon draw-in and -out behaviour: (A) relative displacement between concrete and CFRP at the beginning (draw-out) and the end (draw-in) of the bond length; and (B) shear stress in the middle of the sand-epoxy segment, $t = 44 \mu\text{m}$, along the bond length for two CFRP materials at 10% load.....30

Figure 27: Shear stress distribution in longitudinal direction of the prism up to 22.39 MPa (100%) bond stress: (A) modelled using Cind and a UTS tendon in pull-out; and (B) modelled using Cind and UHMK13916 tendon in pull-out.....31

Figure 28: Sensitivity of FE model. (A) Thickness of the adhesive layer. In this visual, the adhesive thickness in μm is indicated by the number behind the label, e.g., Bond-Stress-25 represents an adhesive layer thickness of 25 μm ; (B) Variation of cohesive stiffness and their influence on the tendon draw-in behaviour.....	33
Figure 29: Scheme of the loading procedure – the stress applied on the samples at different ages is shown. The stress corresponded to 20% of the compressive strength (see Table 6) at the time of changing the load.....	41
Figure 30: Shrinkage (left) and creep (right). In creep measurements, the load was increased to correspond to 20% of compressive strength at 3, 7 and 28d. C1 represents an industrial self-compacting HPC as it is currently used in the Swiss precast industry. C2-C4 correspond to the newly-developed LCHPCs.....	43
Figure 31: Bond performance of UHM-CFRP to LCHPC (C2-C4) and the reference concrete C1; data of C1 taken from [127].....	44
Figure 32: Overview of the Abaqus FEA-model. The concrete prism is visualized in blue, the four prestressing tendons in red colour.....	47
Figure 33: Validation of the FEA creep and shrinkage material models. The left graph (A) shows the results of the shrinkage modelling as colored lines in comparison to the experimental shrinkage data. The experimental shrinkage data is shown as symbols including their standard deviations. The right graph (B) shows the results including creep and shrinkage.....	48
Figure 34: FEA results of the prestress transfer behaviour. The left graph (A) shows the longitudinal stress distribution inside the concrete prism for specified time points. After the prestress release, this visualization shows the redistribution of the stresses inside the concrete prism due to concrete creep. As expected, the stresses in the higher loaded areas of the concrete prism were reduced. The right graph (B) shows the tendon stress along the specimen's longitudinal axis evaluated at critical time points during the FEA analysis, with and without creep and shrinkage. Here, the results are exemplarily shown for C1 and a UHM-K13916 prestressing tendon. The general behaviour of the LCHPCs prestressed with UHM-K13916 CFRP prestressing tendons was comparable. However, differences were present due to the different levels of prestress transfer, concrete creep and concrete shrinkage.....	49
Figure 35: Calculated prestress inside the CFRP tendon from the time point of prestress release until 91 days after casting. In the FEA, the prestress was released 3 days after casting; the value of 100% prestress corresponds to the prestress inside the CFRP tendon right before the prestress release. Due to shrinkage, this value was already slightly lower than the initial 800 MPa. The presented curves include all modelled sources of prestress losses; shrinkage, creep and elastic shortening. The labeling of the lines expresses the chosen concrete in first position, then the CFRP material and the CFRP prestress level, in MPa, in third position.....	50
Figure 36: Prestress losses related to shrinkage, creep and elastic shortening after 91 d based on FEA analysis. The labelling of the columns expresses the chosen concrete in first position, then the CFRP material and the CFRP prestress level, in MPa, in third position.....	50
Figure 37: Cross section of CFRP prestressed concrete beam.....	57

Figure 38: Four point bending test configuration: Overview of mounted sample in experimental set-up.....	59
Figure 39: Prestress transfer length development over time. The bars show the averaged value of the beams investigated including their standard deviations. The drop in prestress transfer length for the C4-UHM-CFRP beams after 28 days is caused by the loss of one sensing tendon after the 21 day measurement.....	60
Figure 40: Prestress level development over time. The bars show the averaged value of the beams investigated including their standard deviations.....	61
Figure 41: Results of 4p-bending tests performed, 28 days after casting, on CFRP prestressed beam specimens. Orange indicates the new C4-UHM-CFRP beam type, dark grey the C1-UHM-CFRP beams and light grey the current industry standard C1-UTS-CFRP type. All beams were initially prestressed to the same level of 800 MPa. The averaged bi-linear load deflection behaviour for the different beams is shown in (A), including their standard deviations. The corresponding maximum load bearing capacity is visualized in (B), also including their respective standard deviations.	62
Figure 42: Visualization of the surface strain pattern along the horizontal direction of the beam's vertical face at selected load levels. Level A corresponds to a load of 5 kN, level B to the cracking load and level C to 20kN. The left column represents a beam of type C1-UHM-CFRP, the middle column an industry standard type C1-UTS-CFRP and the right column the new C4-UHM-CFRP beam type. The distance between the cracks in the pattern of the different beam types was similar; all showed about 6 cracks in the same field of view. The crack width was visually larger for beams prestressed with C1-UTS CFRP tendons. A precise crack width analysis was not performed.	62
Figure 43: Influences on a prestressed beam's deflection behavior: A: Analytical deflection modelling, based on the approach of Rezazadeh et al. [58], in comparison to the experimental results. B: Development of the concrete's top fibre strain for C1-UHM-CFRP beams and C1-UTS-CFRP-beams during loading.....	65
Figure 44: FEA results showing the vertical stress component (S_{22}) in the CFRP tendons at ultimate load condition. A: For a C1-UHM-CFRP beam. B: For a C1-UTS-CFRP prestressed beam.	66
Figure 45: Prestress loss assessment. A: Comparison of experimental results with FEA predictions. B: Breakdown of prestress losses into the three main contributions of shrinkage, creep and elastic shortening based on the FEA.....	67
Figure 46: Environmental saving potential for different prestressed concrete elements in comparison to a conventional reinforced concrete structure. This comparison is based on one linear meter of the functional unit I, see Table 12. For steel-prestressed and CFRP-prestressed HPC elements, the recipe of C1, see Chapter 3, was considered; for the estimation of CFRP prestressed HPC-optima a concrete with a fictitious 40% clinker content was used. The data was taken from and the graph redrawn after [124].	74

Figure 47: Assessment of the LCA measures, UBP, CED and GWP for the developed LCHPCs C2-C4 and their reference mixture C1. The environmental saving potential (ESP) was calculated for the LCHPC recipes in comparison to C1. All results presented above are based on one cubic meter of concrete, which corresponds to the functional unit II, see Table 12.....76

Figure 48: Assessment of the LCA measures, UBP, CED and GWP for the developed CFRP prestressed LCHPC beam specimens, see Chapter 4. This assessment was based on one linear meter of the CFRP-prestressed beam elements, which corresponds to the functional unit III given in Table 12. The environmental saving potential (ESP) was calculated in comparison to a conventional reinforced concrete structure. This calculation was simplified by assuming the ESP of the CFRP-prestressed HPC, see Figure 46 to be equal to the ESP of the CFRP prestressed C1 beam element. The ESP calculation of the CFRP prestressed LCHPC beams was finally based thereon.77

Nomenclature

°	Degree
°C	Degree Celsius
μA	Microampere
μm	Micrometer
cm ² /g	Specific surface or Blaine fineness
d	Days
d ₅₀	Median particle diameter
GPa	Gigapascal
kg	Kilogramme
kg/m ³	Density
kgCO ₂ EQ	Kilogramme CO ₂ equivalent
kN	Kilo newton
kNm	Kilo newton meter
kV	Kilovolt
min	Minute
MJ	Mega Joule
mm	Millimeter
mm ³	Cubic millimeter
MPa	Megapascal
N/m ³	Cohesive stiffness
s	Seconds
t	Tonne
€	Euro
ACI	American Concrete Institute
AFm	Aluminate ferrite monosulfate
ANOVA	Analysis of Variance
BBC	British Broadcasting Corporation
BOS	Burnt Oil Shale

CED	Cumulative Energy Demand
CFRP	Carbon fibre reinforced polymers
CHF	Swiss franc
C_{ind}	Industry reference HPC
CO ₂	Carbon dioxide
C-S-H	Calcium Silica Hydrates
CT	Computed tomography
DIC	Digital Image Correlation
E	Young's modulus
E_{11}	Longitudinal Young's modulus in FRPs
E_{22}	Transverse Young's modulus in FRPs
$E_{c_{xxd}}$	Compressive elastic Young's modulus after xx days
ESP	Environmental savings potential
FBG	Fibre Bragg grating
$f_{c_{max}}$	Ultimate compressive strength
FCMK	Flash-calcined metakaolin
$f_{c_{xxd}}$	Compressive strength after xx days
F_e	Effective prestressing force
FE	Finite element
FEA	Finite element analysis
FEM	Finite element method
F_i	Prestressing force after transfer
F_j	Jacking force
FOV	Field of view
FRP	Fiber-reinforced polymers
$f_{t_{max}}$	Ultimate tensile strength
f_{vc} , FVC	Fiber volume content
GFRP	Glass fibre reinforced polymer
$g_R(t)$	Shear relaxation modulus
GWP	Global Warming Potential
HPC	High performance concrete

HPSCC	High performance self-compacting concrete
HRWRA	high range water reducing admixtures
I_{cr}	Cracked moment of inertia
I_g	Gross moment of inertia
$Impact_{ref}$	Environmental impact (GWP, CED or UBP) of the reference technology
$Impact_x$	Environmental impact of the improved technology
ITZ	Interfacial transition zone
$k_R(t)$	Bulk relaxation modulus
LCA	Life cycle assessment
LCC	Low-clinker concretes
LCHPCs	Low-clinker high-performance concretes
LVDT	Linear variable differential transformer
M	Bending moment
MCC	Minimum cement content
M_{cr}	Cracking moment
n	# of specimens
$n = E_{cfRP} / E_c$	Modular ratio between CFRP tendon and concrete
NRP	National Research Project
NRP70	National Research Project 70 "Energy Turnaround"
\emptyset	Diameter
p	Pixel
\tilde{p}	Effective voxel size of the tomogram
PAN	Polyacrylonitrile
PP	Polypropylene
PVC	Polyvinyl chloride
RH	Relative humidity
S_{11_u}	Tensile strength
$S_{11_{u,beams}}$	Ultimate tendon stress in beams
$S_{11_{uD}}$	Design tensile strength
S22	Vertical stress component
SBE	Sustainable Built Environment

SCM	Supplementary cementitious materials
SEM	Scanning electron microscopy
SNSF	Swiss National Science Foundation
SP	Superplasticizer
Stdv	Standard deviation
$\theta_k, \Delta\theta$	Radiograph orientation over 360°
UBP	Ecological scarcity method
UD	Unidirectional
UD-FRP	Unidirectional fiber-reinforced polymers
UHM	Ultra-high modulus
UHPC	Ultra-high performance concrete
UTS	Ultra-high tenacity strength
w/b	Water-to-binder-ratio
w/c	Water to cement ratio
WMO	World Meteorological Organization
XA3	Exposure class according to EN 206-1
XS3	Exposure class according to EN 206-1
ϵ_{tmax}	Ultimate tensile strain CFRP
ν	Poisson ratio
σ_{tmax}	Ultimate tensile strength of CFRP
σ_U	Ultimate bond strength
τ - δ curve	Tendon draw-in curve

CHAPTER 1

Introduction

1.1 Background and Motivation

In modern infrastructure the use of concrete is pervasive and can be found in manifold shapes and applications. In fact, there is a very high chance that the reader of these lines may find some concrete within a few meters of his or her position. The success of concrete was and is based on its wide and easy availability but also on its price, strength and durability. In a recent BBC news online publication [1], Lucy Rodgers described the vast use of concrete as follows:

“Concrete is the most widely used man-made material in existence. It is second only to water as the most-consumed resource on the planet.”, Lucy Rodgers, BBC News 2018 [1].

Translated into numbers, this means that each year about 10 km³ of concrete are produced [2]. As a comparison, this enormous volume corresponds to about 16 times the volume of the upper 1000 vertical meters of the Matterhorn summit [3, 4] and about to one fifth of the total volume of the Swiss glaciers in 2018 [5, 6]. Tragically, the current production of concrete, due to its contribution to CO₂ emissions and global warming, is leading to further melting of the glaciers and hence this relation will change towards one fourth or even one third in the future as the glaciers melt away.

1.1.1 From ancient times to CFRP prestressed structural elements

Somewhat surprising from a first perspective, however, is the fact that concrete generally is not a modern invention. For thousands of years, concrete-like materials have been used in construction. Some of the first evidences of manmade concrete were found in floorings of crude shelters on the banks of the river Danube, about 5600 BC [7]. Also the Egyptians developed a cement-like binder material based on lime and gypsum. Greek and then Roman engineers significantly improved lime-based cements by adding volcanic ash (pozzolan) [7]. The higher strength and hardness of this hydraulic cement enabled the production of stronger concrete and hence the construction of monumental buildings such as the Pantheon in Rome, some of which are still in excellent condition today [8]. As the roman concrete and binder knowledge was lost in the meantime, the 1824 patent by Joseph Aspdin and the work of his son William started the development that led to Portland cement [9] and to modern concrete technology [10].

Concrete (general)

Concrete has three basic components; cement aggregates and water. The cement consists mainly of anhydrous calcium silicates (principally, tricalcium silicate), which start hydrating when

they get in contact with water. Calcium silicate hydrate (C-S-H), the largest reaction product by volume, is mainly responsible for the development of the mechanical properties in the cement paste [11, 12]. It forms bridges between the original cement particles to a strong matrix which surrounds and binds the inert aggregates. With time, the hydration of the cement progresses, the porosity of the matrix decreases and the strength of concrete develops. An example for the microstructure of a hardened cement paste can be found in Figure 1. The typical strength of concrete is measured 28 days after casting on cube or cylinder specimens [12] following standards, e.g. EN12390 [13].

Depending on the chosen concrete recipe and hence the relative portions of the main components, the final properties of concrete can be very different. A high water to cement ratio (w/c) results in more workable and fluid fresh concrete but may cause aggregate segregation. Due to the additional water, these concretes typically show higher porosity when hardened and hence low strength. In contrast, using a low w/c , results in reduced concrete porosity and consequently, increased strength and modulus [12]. However, the reduction in w/c comes at the cost of workability. To produce concretes with high strength at a low w/c , superplasticizers are commonly employed [12]. Aggregates of different size, modulus and amount are used to increase the stiffness, the strength and restrain shrinkage and creep accordingly. Different types of concrete are designed according to their intended application, which may require special strength, durability, density, stiffness, workability or other properties. The compressive strength values range from about 20-40 MPa for normal strength concretes up to 80-100 MPa for HPC and more than 120-150 MPa for UHPC.

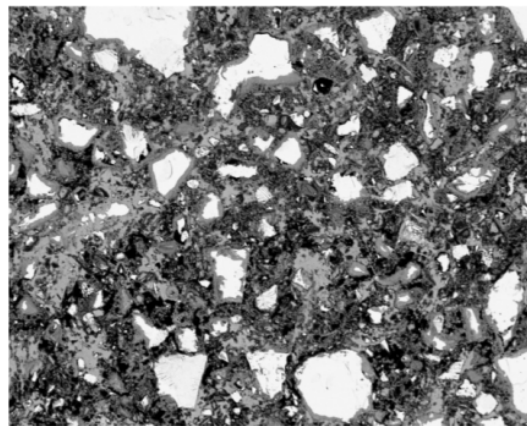


Figure 1: Microstructure of hardened cement paste with w/c ratio of 0.3 after 28 days, taken from [14].

The structural use of unreinforced concrete is however limited by its low tensile strength. The hydrated cement paste contains voids, micro cracks and pores [12]. The low tensile strength can be explained by stress concentrations around these discontinuities following the principles of Griffith [15]. The tensile failure is often initiated by a thin and weak area between the coarse aggregates and the hydrated cement paste, usually referred to as interfacial transition zone. This zone has a higher porosity in comparison to the hydrated cement paste and may contain micro cracks due to restrained deformations (especially hygral shrinkage) even before the concrete has been subjected to mechanical loads, see Figure 2. Under tension, these micro cracks are pulled apart and grow quickly until tensile failure. Loaded in compression, the structure is able to withstand much higher loads until the extension of the crack network yields to compression

failure [12]. The tensile strength of a HPC can be assumed to be about 7-8% of its compressive strength [16].

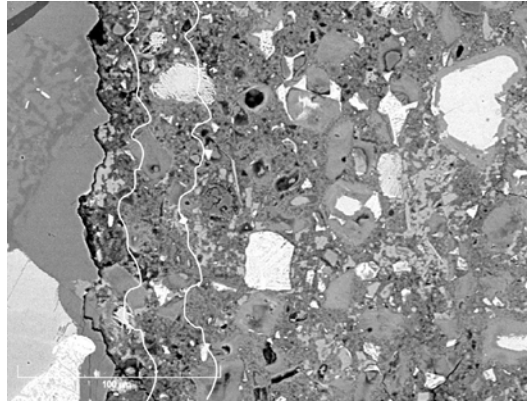


Figure 2: Backscattered electron image of the interfacial transition zone (ITZ) in concrete. The white lines are drawn at approximately 20 and 50 μm apart from the aggregate which is visible on the left. The most significant changes in the ITZ can be found within the first 15-20 μm . Content adapted after and figure taken from [17].

Strengthening for structural applications (general)

To overcome concrete's low tensile strength, structural concrete is generally passively reinforced with steel bars. When reinforced concrete members are subjected to bending moments, they will crack and the tensile load will be transferred to the steel bars [18]. The failure of the concrete member in bending is generally a ductile failure due to yielding of the steel. However, for specific structural applications, especially for high loads and long spans, passive reinforcement may result in uneconomically large structural members and would also need large amounts of steel bars.

A more efficient way of strengthening structural concrete is prestressing, which can be realized either by pre-tensioning or post-tensioning the reinforcement. The difference between both techniques is the time when the tendons are stressed and the way the stress is transferred to the concrete. In post-tensioned concrete, the tendons are anchored at the ends of the concrete structure to the concrete and the stress is applied after casting of the prestressed concrete element [19]. In the case of pre-tensioning, high strength steel tendons are prestressed in tension prior to the casting of the related structural element. After concrete hardening, this prestress is released and transfers, due to the bond between the tendons and the concrete, to the concrete and puts the concrete under compression.

Pre-compression of the concrete allows the loading of structures until a certain level without inducing tension into the concrete. This delays load-related cracking to higher loads and, at the same time, results in less deflection due to the intact cross section of the structure [20], see Figure 3. Prestressing of structural concrete elements is most efficient when tendons with high-strength are used in combination with high performance concretes.

The idea of prestressing dates back to the year 1888, when P. H. Jackson formulated the idea of prestressing in a patent about the „Construction of artificial-stone or concrete pavements“ [21, 22]. However, it took until the 1920`ies when high strength steels became available and this technique could be applied in praxis [23]. Ever since, prestressing of concrete is applied for structural components and buildings when needed.

With time, the prestress in a structural member does not remain constant. First prestress losses occur immediately after the stress release due to elastic shortening of the concrete element. In the long term, concrete shrinkage (time-dependent, negative strain caused by moisture loss) and creep (time-dependent strain caused by external loads) further reduce the remaining prestress and hence the load-bearing capacity in a structural member [24, 25], see Figure 4. For design engineers, precise knowledge about the losses and their behaviour over time is needed to guarantee the long term serviceability of prestressed concrete structures.

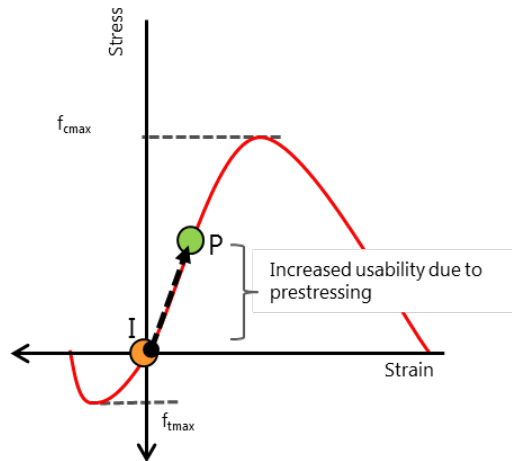


Figure 3: Schematic of tensile and compressive load behaviour of concrete. The pre-stress moves the initial situation of zero stress and zero strain in a structural concrete element at point I into the compressive prestressed condition of point P. The prestress “activates” an additional load-bearing capacity which is visualized with the bracket in the graphic.

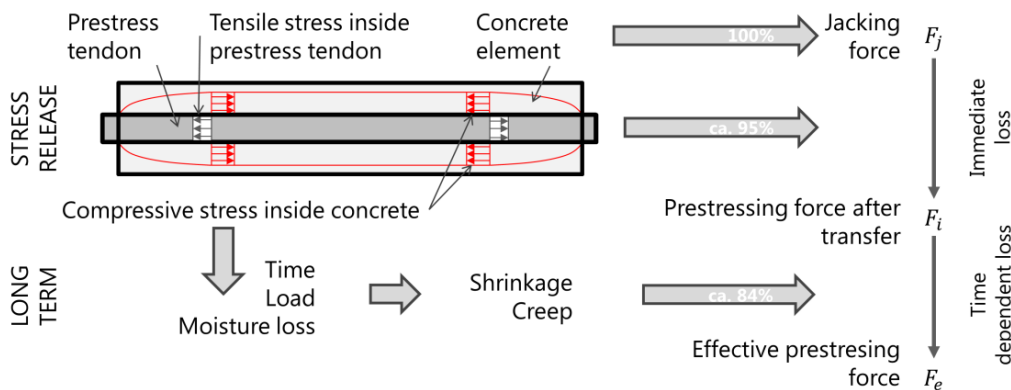


Figure 4: Schematic of prestress transfer and possible prestress losses according to [26].

A main durability issue in steel-prestressed concrete is guaranteeing the passivation of the prestressing steel over the planned service life [27]. In addition, beside other risks of corrosion and due to the high stress inside the prestressing tendons, steel prestressed structures may also be prone to stress-corrosion [28]. In fact, for prestressed concrete exposed to the environment, depending on the exposure class, a concrete cover of 30-65 mm has to be provided to protect the steel reinforcement from corrosion (see SIA 262). The need for passivation forces a limit to the design possibilities in steel prestressed concrete by giving these elements a minimum allowable thickness. The use of HPC in prestressed structures has the advantage of high strength and a lower porosity and permeability (thus better durability) than conventional concrete [29].

This motivated some researchers to reduce the concrete cover to a minimum, while still guaranteeing the corrosion protection of prestressing steel tendons and wires [30]. However, this did not lead to any relevant reduction of the dimension of prestressed HPC elements. Corrosion-resistant materials with high strength were needed as alternatives to the steel prestressing tendons to reduce weight and to increase the slenderness of prestressed concrete structures. Among the possible alternatives, fibre-reinforced polymers (FRP) [31–33] started to be seen as the ideal candidates and were introduced during the 1990ies for prestressing applications prone to corrosion and in need of a low weight.

Fibre reinforced polymers

FRPs are fibre composite materials consisting of strengthening fibres and a surrounding polymer matrix. In this context, typical fibre types are carbon fibres, glass fibres and aramid fibres. From an engineer's perspective, these fibres mainly separate themselves in their mechanical properties such as strength, stiffness, density and fibre diameter. Among the three fibre types mentioned above, the carbon fibre has the highest strength and stiffness, reaching values of up to 800 GPa in elastic modulus and 7000 MPa in strength. In comparison, glass fibres only reach a modulus of 73–87 GPa and a strength of 1800–3900 MPa, aramid fibres a modulus of 70–130 GPa and a strength of 2500–3000 MPa and [34]. In addition, carbon fibres do not creep [35], which is a downside for aramid fibres. Furthermore, carbon fibres are not subjected to stress corrosion, which is a limitation for glass fibres [36]. Consequently, for prestressing applications, needing high strength, high stiffness and good durability, carbon fibres would be best suited.

The simplest form of FRPs is given when all fibres are aligned along one longitudinal direction, usually referred to as unidirectional (UD) FRP, see Figure 5 and [34]. Accordingly, a UD-FRP is anisotropic and the mechanical properties strongly vary between their longitudinal and transverse direction. Beside the chosen fibre type and polymer matrix, UD-FRPs are characterized by the fibre volume content (fvc). Based on this data, the longitudinal strength and stiffness of UD-FRPs can be estimated by using the rule of mixture [34]. The transverse properties of a UD-FRP can be calculated for isotropic fibres (glass), following Puck [37] and for anisotropic fibres (aramid and carbon) after Schneider, Menges and Peulen [34].

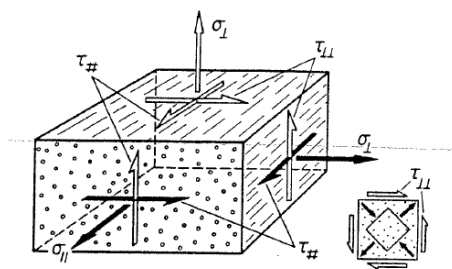


Figure 5: Schematic cutout of a UD-FRP including related stresses in longitudinal, transverse and shear directions, taken from [34].

UD-FRPs with a constant cross section, e.g. like cylindrical prestressing tendons, are produced most efficiently by pultrusion. In this process the dry fibres are first impregnated in an epoxy resin bath, afterwards pulled through a die and heated for fast curing. After curing, the new formed composite is pulled out of the die and cut into length. This process is ideally suited for large scale fibre composite production, allowing a production at reasonable cost, quality and

speed. Typically, composites produced by this method reach a high fibre volume content of around 60 % and hence are efficient in using the fibre properties of high strength and stiffness [34].

Slender, highly-loaded structural elements prestressed with CFRP

In the 1990ies, CFRP was introduced in Switzerland for prestressing applications as a reaction to changes in standards. The adapted standards demanded a much thicker concrete cover over the prestressing steel to prevent corrosion. As a result, the Swiss precast industry was partially in need of alternative solutions and researchers at Empa started investigating the topic of FRP prestressing of concrete [38, 39]. Since steel is absent, pre-tensioned FRP reinforcement allows reducing the thickness of prestressed concrete cross-sections to a minimum. The cover thickness is then only determined by the uptake of static forces and by the thermal compatibility of the FRP reinforcement with the HPC. This launched the research topic of thin, lightweight, pre-fabricated, CFRP-prestressed structural elements [40].

At the start of this research, the durability and creep resistance of such structures was a major concern. Creep test data were already available for UD CFRP pultrusion profiles or epoxy and adhesives, but long-term data for a prestressed pole as a structural element with its new material combination of CFRP and concrete were still missing. Researchers at Empa realized the importance of long term experiments on these novel structures. Therefore, in 1996, they started bending creep tests on three spun-concrete poles [39]. Until today, two of these three poles withstand their loads and show, already since several years, a fairly stable deflection behavior over time, see Figure 6. The highest loaded pole, which showed already a continuous increase in deflection over time, failed in the year 2013 [38]. The permanent load in this pole corresponded to about 72 % of the short term failure load, a level much higher than would be expected in actual structures. The development of CFRP-prestressed elements continued and in 2009 a second long-term study was started at Empa on slender CFRP prestressed slab specimens under self-weight loading conditions. As for the pole specimens, the increase in deflection stabilized in the slabs after about 3 months and showed a promising behaviour with little effects of creep in the long term, see Figure 7 and [41]. Both cases show that CFRP prestressed concrete is durable and the structural elements are reasonably resistant to creep.

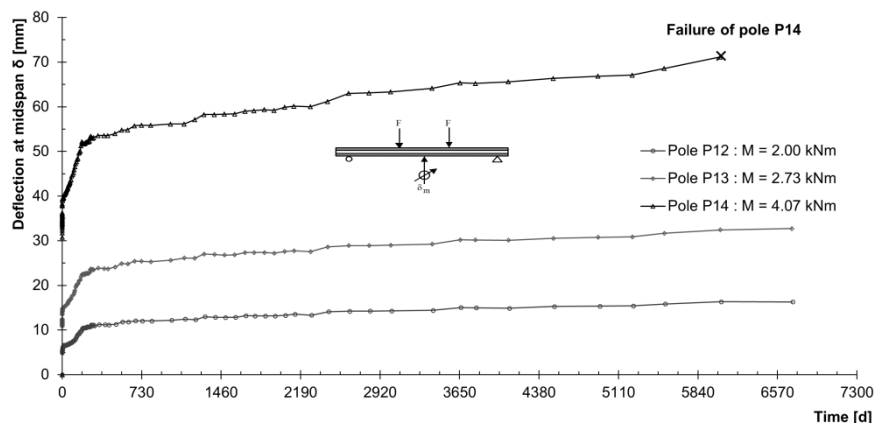


Figure 6: Mid-span deflection of three pole specimens loaded in 4-point bending over time. Graph taken from [41].

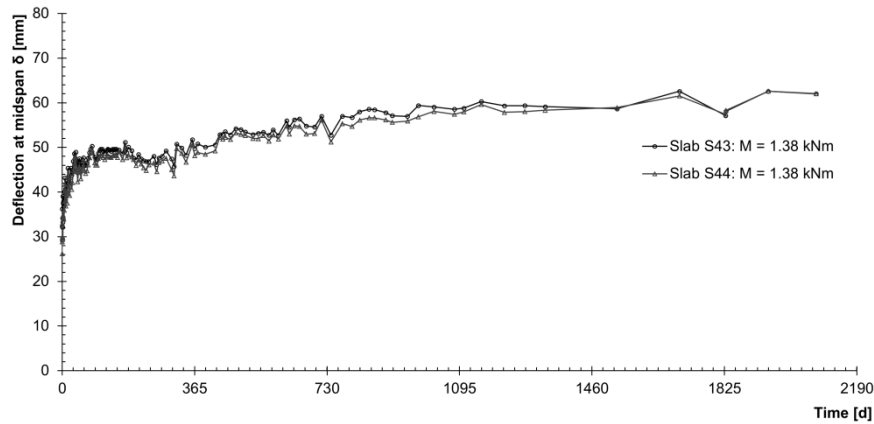


Figure 7: Mid-span deflection of two simply-supported slab specimens loaded in self-weight loading conditions over time. The geometry of the test setup was chosen so that the concrete reached the point of decompression in the middle of its span on the tensile side of the slab. Graph taken from [41].

Current situation

In the Swiss construction market CFRP slender prestressed HPC elements are well established. Thin-walled (30-45 mm) CFRP prestressed HPC lighting poles are produced by the precaster SACAC AG in Lenzburg (Aargau, Switzerland) and sold in Switzerland and on the European market [71]. In addition, filigree concrete shapes are of interest especially on building façades. In recent years this market has developed well in Switzerland and has an estimated volume of CHF 300 million / year [76]. With their outstanding corrosion resistance, low weight, high stiffness and fatigue resistance [42-44], CFRP-prestressed concrete elements are ideally suited for these applications. Examples of this technology can be found at some places in the greater Zurich area, e.g. on the façade of a schoolhouse in Zurich Leimbach, see Figure 8. Further applications are exemplarily shown in Figure 9 and Figure 10.



Figure 8: Building façade elements produced with CFRP prestressed HPC; Location: Zürich, Switzerland.



Figure 9: Centrifugally-cast, CFRP-prestressed HPC lamp pole; Location: Zurich, Switzerland.



Figure 10: Slender, CFRP-prestressed HPC pole setup as a design element in a housing complex; Location: Uster, Switzerland.

1.1.2 Sustainability of concrete and related CO₂ emissions

An aspect long ignored in the construction industry is sustainability. As a fact, global warming is progressing rapidly. Since pre-industrial times, the temperature has already increased on average around 1 °C worldwide [45]. According to current estimates, the temperature increase is seen likely to reach 2°C by 2060 and depending on the chosen emission scenario could reach 3-4°C by 2100 [46], both in comparison to pre industrial times. The steady temperature increase, see Figure 11, causes severe changes for the world's population; e.g. rising sea levels, droughts and extreme weather conditions have already increased and will occur more frequently in the future [47, 48]. The impact of this change on people and environment will be immense and solutions must be found quickly to counter this trend. One approach in this direction is the reduction of CO₂ emissions. According to the recent 2018 WMO Greenhouse Bulletin [49], CO₂, due to the large amounts emitted, is the single most important anthropogenic greenhouse gas, being responsible for 66% of the total radiative forcing and even 82% of the increase of radiative forcing in the last decade.

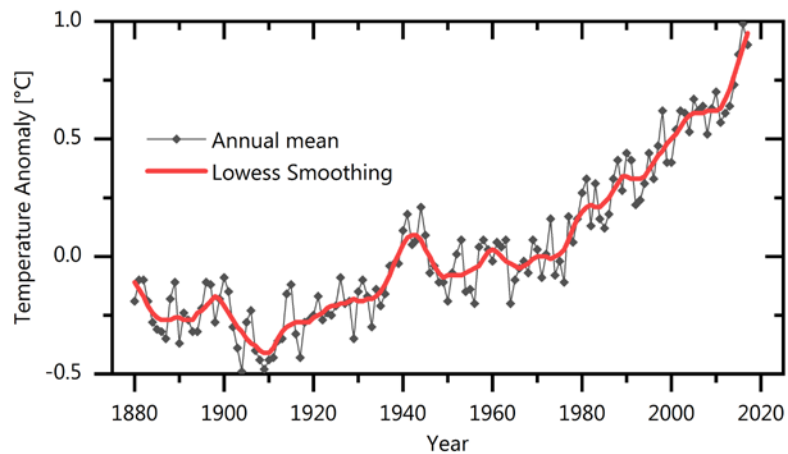


Figure 11: Global warming expressed as temperature anomaly from the year 1880 until today. Data taken from and redrawn after [50].

Concrete structures contain large amounts of cement. The production of cement clinker, however, is accompanied by massive CO₂ emissions. For the production of cement clinker, limestone (calcium carbonate) is decarbonated by the addition of silica and heat (about 1450°C [51]) in a rotating kiln. During this reaction, alite (impure tricalcium silicate, the most reactive phase in the cement clinker) is formed but significant amounts of CO₂ are emitted [52, 53]. Here, decomposition of calcium carbonate is responsible for about 60 % of the total amount of CO₂ emissions during cement production and the supply of energy for about 40% [53, 54]. For the year 1994, the total emission for the production of 1 t of cement was specified by Gartner [52] to be 0.815 t of CO₂. As the CO₂ emissions of the reaction cannot be changed, today's rate can be estimated based on [53, 54] to be around 0.7 t of CO₂ per ton of cement. In 2007, the worldwide annual absolute production of concrete reached about 13 billion tons [55]. As a consequence today's worldwide cement production is responsible for about 5-8% of the anthropogenic CO₂ emissions [54].

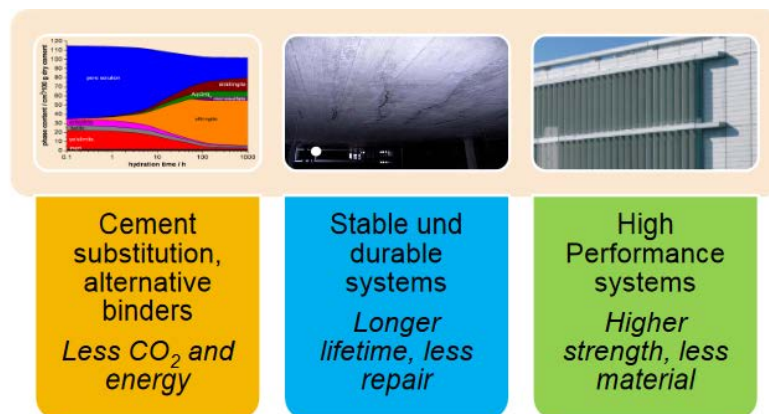


Figure 12: Three strategies for improving a concrete structure's sustainability, slide by P. Lura.

To improve the sustainability of concrete structures, three different strategies are currently being pursued, see Figure 12. First of all, one could replace the currently employed materials with materials that emit less CO₂ during their production [52, 53]. Assuming that these new materials have the same mechanical properties, this would result in a direct saving without the need of

changing current designs. A second approach is to find solutions that extend the lifetime and durability of the structures. This has the effect that the CO₂ emissions that are emitted during the construction are spread over a longer period of time and thus are lower overall than if buildings have to be replaced early. The final approach is to develop high performance systems that have higher strength and also better durability despite the smaller cross-sections. This makes it possible to use less material in structural applications and thus to save CO₂ emissions.

1.1.3 Research needs

The current technology of CFRP-prestressed HPC elements offers excellent structural performance at considerably lower weight than conventional (steel) prestressed concrete elements. However, due to their high clinker content, their grey energy (embedded energy) and CO₂ footprint by volume are remarkably high and these elements are in addition also expensive. Hence, the current use of these elements in industry is still restricted to applications of high architectural standard or concrete poles.

The development of fibre composites progressed rapidly since their first introduction in prestressed concrete pole elements in the 1990ies. Today, CFRP materials with ultra-high modulus (UHM) are commercially available and their stiffness is more than three times higher than traditional CFRP materials with stiffness ~ 150GPa. In the context of prestressed concrete, many studies were published on different aspects influencing the prestress behaviour but only a few consider FRP tendons. None of them investigated the prestressing mechanisms of tendons comparable to the new UHM-CFRP tendons in HPC. In fact, all known studies which investigated CFRP materials in concrete prestressing applications used materials with a longitudinal stiffness of less than 200 GPa [38, 43, 56-59].

Substituting high amounts of cement in concrete (and also in HPC) in practical applications has been limited by standards that dictated a minimum amount of cement for different exposure classes. Hence, progress in developing final recipes with reduced environmental impact was of minor interest. However, this situation is changing and current guidelines in Switzerland (SIA Merkblatt 2049) [60] or standards in Europe (EN-197) [61] allow significant amounts of cement replacement. Researchers showed the possibility of replacing unhydrated cement particles in HPCs with limestone fillers or without significant reduction in the concrete's mechanical performance [62, 63]. Thus, the final development of low-clinker, high-performance concretes (LCHPCs) could be assumed to be reasonable but was not accomplished yet for practical applications. Consequently, no application in prestressed structural concrete elements exists to date.

Both materials trends show a great potential for prestressed structural elements, the LCHPCs may be used for directly reducing the CO₂ footprint and the UHM-CFRP tendons may limit the total deflection, the crack opening behaviour and hence may increase the serviceability of such structures. In addition, the use of corrosion resistant CFRP tendons in LCHPCs would be an ideal choice to avoid difficulties due to a high rate of carbonation in the clinker reduced concrete recipes which would possibly present limitations for classic steel prestressing tendons.

1.2 Objective and Scope

The final goal of this thesis was to develop a 2nd generation of CFRP prestressed structural concrete elements with improved sustainability and an increased mechanical performance. To achieve this goal, the two basic research areas (LCHPC development and bond of UHM-CFRP tendons) were first investigated separately and then finally merged to develop the final UHM-CFRP prestressed concrete elements, see Figure 13.

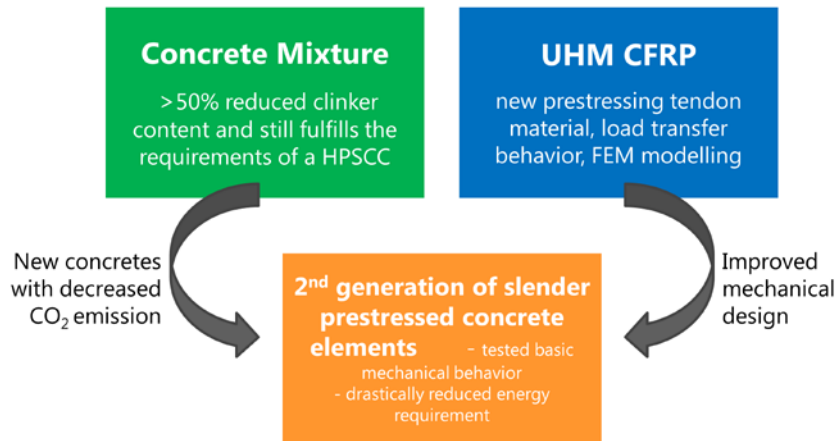


Figure 13: Schematic visualization of the three main objectives in this thesis.

Using this procedure, all three proposed strategies to improve a structure's sustainability, see Figure 12, were applied in one go. The development and application of LCHPCs were directly targeted to reduce the CO₂ emissions of the used concrete material and the application of CFRP tendons enables a durable structure and hence a long service life without issues due to steel corrosion. In addition, the investigation of UHM-CFRP tendons explored the full range of available CFRP materials for prestressing applications and hence allows the design of structures with high strength and less material.

Relevance for science and economy

This thesis provides new insights about the structural behaviour of prestressed HPC, in particular about slender beams prestressed with UHM-CFRP tendons. Special topics in this thesis, that have received little attention so far, are the mechanism of bond and prestress transfer of UHM-CFRP tendons. In addition, by applying and testing LCHPCs, this work opened up a new line of research into these energy- and CO₂-saving materials and explored their mechanical and time-dependent properties (creep, shrinkage).

The final product, lightweight CFRP-prestressed LCHPC elements with reduced clinker amount, do not only have a reduced environmental impact but also have potential to improve the economic feasibility of CFRP-prestressed concrete elements. It could be expected that such elements may expand the volume of the current market to medium and low-cost buildings and hence to extend the use of such elements in Switzerland and abroad.

1.3 Content and Structure of this Thesis

This thesis contains novel research results which were achieved during the development of novel UHM-CFRP prestressed, low-clinker, high performance concrete (LCHPC) elements. This work was conducted within the joint project "Concrete Solutions" in the context of the national research program "Energy Turnaround" (NRP70) of the Swiss National Science Foundation (SNSF) from 2014 until 2019. The overall scope of the joint project was developing solutions for reducing the CO₂ emissions in future infrastructure.

The three main parts of this thesis (chapters 2-4) are presented as scientific papers and ordered in the logical flow followed to reach the goal of developing novel CFRP-prestressed concrete structures. They are either published, submitted or prepared for submission in leading journals. An overview of the interaction between the main chapters of this thesis and the related experimental and modelling sections is given in Figure 14.

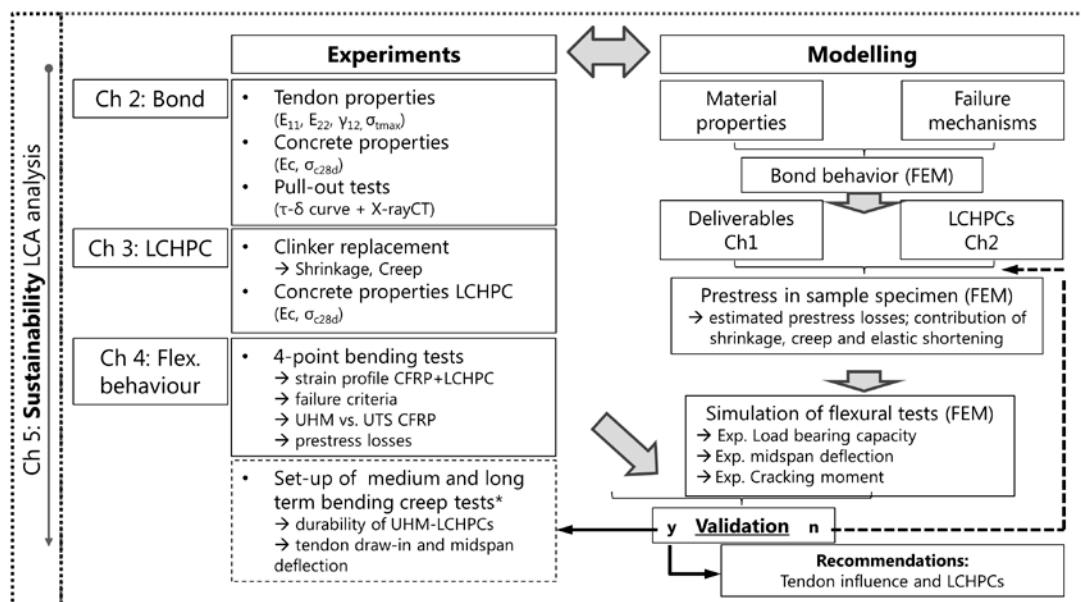


Figure 14: Schematic of testing/modelling interaction for this project.

Chapter 1 Introduction

This chapter introduces the topic of structural applications of CFRP prestressed concrete, recent sustainability needs and their relevance in today's economy in a general manner. Within this context, the aim of this chapter is to define the objective and scope of this thesis. Finally, a brief overview of the conducted work and respective chapters is presented and puts their scientific results in a logical structure to support the goals of this work.

Chapter 2 Bond performance of sand-coated UHM CFRP tendons in high performance concrete

The efficiency and durability of prestressed concrete elements is governed by a good and durable bond between prestressing tendon and concrete. With their very high longitudinal stiffness of up to 509 GPa, the novel UHM CFRP tendons are much stiffer (more than 3 times stiffer) than conventional CFRP tendons (UTS-CFRP). This chapter describes the differences in bond behaviour between UTS-CFRP and UHM-CFRP tendons and sets the basis for the following

chapters. In this process, experimental techniques such as X-ray tomography, pull-out testing and scanning electron microscopy were combined with a FEA in the commercial software Abaqus 6.14.

This chapter was published as an original research paper. The format was adapted to fit the style of this thesis and hence does not necessarily reflect the exact published version. The full bibliography is given here:

*Lämmlein, T.D.; Messina, F.; Griffa, M.; Terrasi, G.P.; Lura, P. Bond Performance of Sand Coated UHM CFRP Tendons in High Performance Concrete. Polymers 2017, 9, 78.
DOI: 10.3390/polym9020078*

Chapter3 Low clinker high performance concretes and their potential in CFRP-prestressed structural elements

Slender CFRP-prestressed structural elements typically use HPC as concrete. These concretes contain large amounts of cement which is linked to large CO₂ emissions due to its energy intensive production. This chapter describes the development of novel LCHPCs in which part of the cement binder were substituted by metakaolin, silica fume and limestone filler. The new LCHPCs recipes were characterized by their strength, stiffness, bond to sand coated CFRP tendons, shrinkage and creep. Finally, this chapter estimates prestress losses in prestressed structural elements, with and without the implementation of LCHPCs and for UTS and UHM-CFRP prestressing tendons. Together with Chapter 2, this chapter forms the basis for the final scientific goal of this thesis, which is the proof of concept at the structural element level.

This chapter was submitted to be considered for publication in the Elsevier Journal "Cement and Concrete Composites" and is currently under review with first revisions submitted. The format was adapted to fit the style of this thesis and hence does not necessarily reflect exactly the submitted version. The current bibliographic information is given here:

*Lämmlein, T.D.; Messina, F.; Wyrzykowski, M.; Terrasi, G.P.; Lura, P. Low clinker high performance concretes and their potential in CFRP prestressed structural elements. Cement and Concrete Composites 100 (2019) 130-138.
DOI: 10.1016/j.cemconcomp.2019.02.014*

Chapter 4 Prestressing low clinker structural concrete elements by ultra-high modulus carbon fibre reinforced polymer tendons

In this chapter, the materials introduced in the previous chapters were combined in a 2nd generation of prestressed structural beam elements. The effects of LCHPCs and UHM-CFRP tendons on prestress losses, prestress transfer and on the load bearing capacity on a full scale prestressed structural element were studied. Experimental techniques such as Digital Image Correlation (DIC), 4 point bending tests and optical fibre strain measurements were combined with analytical and numerical models. Finally, differences in the prestress transfer length, prestress loss and load bearing capacity were quantified and the contribution of the related materials on these properties could be identified.

This chapter is intended to be submitted with small supplements as an original research paper for consideration as publication in the Elsevier Journal "Composites Part B: Engineering". The current bibliographic information is given here:

Lämmlein, T.; Justs J.; Terrasi, G.P.; Lura, P. Prestressing low clinker structural concrete elements by ultra-high modulus carbon fibre reinforced polymer tendons. Intended to be submitted in Composites Part B: Engineering, planned submission Spring 2019.

Chapter 5 Life Cycle Analysis of CFRP prestressed LCHPC

The new generation of LCHPC-CFRP prestressed concrete elements was developed with the aim of reducing future CO₂ emissions. This chapter compares the CO₂ saving potential of the current state-of-the-art technology in CFRP prestressed HPC elements with the accomplished saving in the new UHM-CFRP prestressed LCHPC beams. In this process, three impact assessment methods were employed, namely Global Warming Potential (GWP), Cumulative Energy Demand (CED) and the Ecological Scarcity Method 2013 for calculating the total environmental impact (UBP).

This chapter is in part based on a paper by Zingg et al. presented at the Sustainable Built Environment (SBE) conference in Zurich in 2015. Details about the work extracted and additional work added is given on the front page of Chapter 5. The full bibliography of the work of Zingg et al. is also given here:

S. Zingg, G. Habert, T. Lämmlein, P. Lura, E. Denarié, A. Hajiesmaeili, Environmental assessment of radical innovation in concrete structures, Sustainable Built Environment (SBE) Regional Conference, Zurich, Switzerland, June 15-17, 2016, vdf Hochschulverlag AG, G. Habert, A. Schlueter (Eds.) 2016, p. 687.

Chapter 6 Summary and Conclusions

This chapter briefly summarizes the main results of Chapters 2-5 and puts their outcome into the context of the whole thesis. Furthermore, it shows the links between the different topics investigated and their effects on the final performance of the UHM-CFRP prestressed LCHPC beam elements. Finally, conclusions are drawn considering the novel results gained in this thesis but also in relation to the previous state of the art. Recommendations for future designs of CFRP-prestressed structural elements are also given.

Chapter 7 Outlook

This chapter gives a perspective on possible applications of the knowledge which was developed during this thesis. Furthermore, additional research questions that arose during this thesis, but were not in the direct scope of the thesis, are identified and briefly formulated. This chapter finally concludes on possible scenarios for future developments.

CHAPTER 2

Bond performance of sand coated UHM CFRP tendons in high performance concrete ^a

Abstract

The bond behaviour of novel, sand-coated ultra-high modulus (UHM) carbon fibre reinforced polymers (CFRP) tendons to high performance concrete (HPC) was studied by a combined numerical and experimental approach. A series of pull-out tests revealed that the failure type can vary between sudden and continuous pull-out depending on the chosen sand coating grain size. Measuring the same shear stress vs. tendon draw-in (τ - δ) curves in the same test set-up, for sand coated CFRP tendons with a longitudinal stiffness of 137 and 509 GPa, respectively, indicated that the absolute bond strength in both cases was not influenced by the tendon's stiffness. However, the τ - δ curves significantly differed in terms of the draw-in rate, showing higher draw-in rate for the UHM CFRP tendon. With the aid of X-ray computed tomography (CT), scanning electron microscopy (SEM) and visual analysis methods, the bond failure interface was located between the CFRP tendon and the surrounding sand-epoxy layer. For further investigation, a simplified finite element analysis (FEA) of the tendon pull-out was performed using a cohesive surface interaction model and the software Abaqus 6.14. A parametric study, varying the tendon-related material properties, revealed the tendon's longitudinal stiffness to be the only contributor to the difference in the τ - δ curves found in the experiments, thus to the shear stress transfer behaviour between the CFRP tendon and the concrete. In conclusion, the excellent bond of the sand-coated UHM CFRP tendons to HPC as well as the deeper insight in the bond failure mechanism encourages the application of UHM CFRP tendons for prestressing applications.

Keywords

CFRP; UHM carbon fibre; UTS carbon fibre; prestressing tendon; sand coated; bond; HPC; pull-out test; finite element modelling (FEM); X-ray tomography.

^a This chapter was published as an original research paper. The format was adapted to fit the style of this thesis and hence does not necessarily reflect the exact published version. The full bibliography is given here: Lämmlein, T.D.; Messina, F.; Griffa, M.; Terrasi, G.P.; Lura, P. Bond Performance of Sand Coated UHM CFRP Tendons in High Performance Concrete. *Polymers* 2017, 9, 78. DOI: 10.3390/polym9020078

2.1 Introduction

Slender CFRP prestressed concrete elements have beneficial properties compared to steel prestressed structures. These elements are much lighter, mostly due to the fact that CFRP does not corrode and the concrete cover can be reduced to a minimum dictated only by statics and ease of fabrication [39].

Current applications of slender, CFRP-prestressed elements are mainly used for building façades or as free-standing lighting poles [43]. The concrete used in these elements [39, 43, 64] is usually a high performance concrete (HPC). This choice of material accounts for high loads and facilitates the best possible utilization of the prestressing technique due to its high elastic modulus and low creep coefficient. In addition, the use of HPC also minimizes loss of prestress due to creep, which would lead to considerable loss of prestress in the UHM tendons with time and temperature. In these applications, the elements need to be anchored to a primary structure. The mounting of these elements can only be applied in their regions where the prestress is fully developed. Thus, the prestress transfer length, starting at the end of each element, should be kept as short as possible to reduce the dead weight and the non-usable area of the elements.

In CFRP, a wide choice of carbon fibres can be applied. These fibres vary largely in terms of longitudinal stiffness (230–827 GPa) and tensile strength (1400–7060 MPa) [65]. With a higher stiffness of the tendon, more loads can be transferred at a lower strain. Thus, it is proposed that the transfer length of prestressed elements will also be affected and may be shortened by using stiffer tendons. This would allow a further reduction of material and thus would lead to lighter and more functional designs.

Several studies investigated the stress transfer behaviour between tendons and the surrounding concrete [31, 32, 66–69], which is most important when the dead weight of the elements should be reduced. It was observed that the bond of prestressed tendons is one of the key elements during the design of load introduction and anchorage areas [70].

The bond behaviour of prestressing steel tendons and strands (pretensioning technique) has been studied intensively since the early 1950s (see, e.g., [70–72]). However, there is still little knowledge of the bond behaviour of CFRP tendons in high strength concrete and high performance self-compacting concrete (HPSCC). In contrast to standardized steel reinforcing tendons, the material and surface variants of FRPs are much more manifold and difficult to standardize [73]. Consequently, the possible influences on bond of FRP tendons are various. The effects of the tendon's diameter [74], the bond length [75], the concrete strength [74, 76] and the surface characteristics [77, 78] on the bond are of major importance [79, 80]. Surface features like embedded sand grains were found to be the main contributors to the bond between FRP reinforcements and concrete [81]. The bond of a sand-coated CFRP profile is principally based on adhesion and mechanical interlock between the rough surface of the tendon and its concrete cover. The force transfer of sand-coated FRP bars in concrete [40] showed a development length of only 16 tendon- \emptyset , significantly shorter than steel bars (\sim 80–120 tendon- \emptyset). Thus, a sanded tendon's surface is expected to be a good coating option which should assure a durable prestress as well as a short transfer length [42]. Indeed, sand-coated CFRP tendons proved to be effective to at least 18 years in outdoor four-point bending creep tests

[41]. Another benefit of the sand-coated surface is the application to a clean and intact CFRP tendon surface. In contrast to some alternatives, e.g., machined grooves on the CFRP surface, the tensile strength of the tendon is not lowered by the sand coating. Thus, this technique allows the best possible use of the beneficial CFRP properties.

One study exists dealing with the influence of tendon stiffness on bond between two types of glass fibre reinforced polymer (GFRP) tendons and concrete [82]. However, the GFRP tendons used in that study had longitudinal stiffness values of either 48 or 64 GPa, which is much lower than generally-used CFRP counterparts. The known studies on bond or prestress transfer of CFRP tendons had a longitudinal stiffness in the range of 115–167 GPa [42, 75-78], substantially lower than steel (about 210 GPa).

None of these studies differentiate in detail between the possible influences on the bond between diverse CFRP materials, in terms of their longitudinal tendon stiffness. The UHM-CFRP tendons used in this study reach longitudinal stiffness values of 509 GPa, which is 3–4.5 times stiffer than the mentioned currently-used CFRP tendons and almost 2.5 times stiffer than steel. It is anticipated that this increase in tendon stiffness will heavily influence the stress transfer behaviour between concrete and tendon, thus it needs to be characterized in detail.

The aim of this work is to investigate experimentally the effect of very high tendon stiffness on the bond with a reference HPC. Moreover, the τ - δ -curves as well as the failure surfaces were studied and the information implemented within a FEM model in Abaqus 6.14 (Dassault Systemes Simulia Corp., Providence, RI, USA). This new knowledge about bond will form the basis for the continuation of this research, which focuses on the bending behaviour of UHM-CFRP prestressed structural elements.

2.2 Materials and Methods

This work consists of three experimental and one numerical analysis sections. The used materials, their characterization as well as the applied test procedures are outlined here.

2.2.1 Raw Materials and Composites

An industry based high performance self-compacting concrete (HPSCC) was chosen for the first part of this work to investigate the bond strength of different sand coating options. This concrete mixture ($w/b = 0.37$), which was slightly further developed from [42], mainly consists of ordinary Portland cement CEM I 52.5 R, fly ash, silica fume, sand 0/4, gravel 4/8. PP-fibres, SIKA ViscoCrete20HE superplasticizer (SP) and stabilizer were also used. The basic mechanical properties in compression were tested according to EN12390 [13]. The corresponding tensile properties were measured on specimens slightly adapted and customized in geometry from SIA 2052 [83]. The properties are summarized under the name C_{ind} in Table 1. Furthermore the influence of the longitudinal stiffness of the CFRP tendon on the bond was studied with the same concrete as well as with a slightly adapted mixture. The adapted mixture, named C1 ($w/b = 0.35$), had only minor differences to the previously employed C_{ind} . C1 used as well ordinary Portland cement CEM I 52.5 R and comparable amounts of sand 0/4 and gravel 4/8. In contrast to C_{ind} , C1 did not include any stabilizer and PP-fibres. The basic mechanical properties of C1

were characterized as described above for C_{ind} (see Table 1) and were found to be very close to those of C_{ind} .

Table 1: Properties of Concretes

Concrete	Compressive strength (MPa)	Tensile strength (MPa)	Tensile Young's modulus (GPa)	Density (kg/m ³)
Standard	EN12390-3:2009	SIA 2052 (adapted)	SIA 2052 (adapted)	EN12390-3:2009
#of samples	3 (15 C_{ind})	5	5	3 (15 C_{ind})
C_{ind}	89.18 ± 2.52	6.58 ± 0.40	40.59 ± 2.11	2413 ± 132.18
C1	85.70 ± 1.14	6.59 ± 0.84	42.26 ± 5.48	2299 ± 2.08

In this study, a total of three different CFRP tendons were investigated. The classic production process for unidirectional (UD) CFRP tendons is pultrusion. The carbon fibres are impregnated with epoxy resin and afterwards pulled through a forming and curing die to obtain a circular cross section. An alternative way to produce CFRP tendons is a tape-laying method. To form the circular shape, a thin shrinking foil is wrapped around the laid down and slightly tensioned CFRP prepregs. Curing of this prepreg tendon takes place afterwards by applying heat. The advantage of the latter method is flexibility in terms of batch sizes and changes in materials. The tendons used in this study were produced, as mentioned later, by both of these methods.

The first type is a reference tendon used in industry [43] and was produced by pultrusion. This tendon consists of PAN based carbon fibres from type TENAXTM UTS 5631 (Toho Tenax, Chiyoda, Tokyo, Japan) and a Bakelite Ruetapox VE 4434 (Hexion GmbH, Iserlohn-Letmathe, North Rhine-Westphalia, Germany) epoxy resin. This ultra-high tenacity strength (UTS) CFRP tendon had a diameter of 5.5 mm, a fibre volume content (FVC) of 64.5% and a relatively low longitudinal stiffness of only 137 GPa.

To assess the bond strength between UHM-CFRP tendons and concrete, two further tendon types were selected. Ultra-high modulus (UHM) PITCH based Mitsubishi DIALEDTM carbon fibres (Mitsubishi Rayon Co. Ltd., Chiyoda, Tokyo, Japan), K63A12 and K13916, were chosen as the two different fibre materials for these tendons. Both UHM-fibres were combined with a Huntsman XB3515/AD5021 hot-melt epoxy system to a prepreg. The two tendons were produced in the tape-laying method by Carbolink AG in Fehraltdorf, Switzerland. Both UHM-CFRP tendons had a diameter of 5.3 mm but a slightly different longitudinal stiffness of 464 GPa (K63A12) and 509 GPa (K13916), respectively. A summary of the characterized mechanical properties of all three tendons can be found in Table 2.





Table 2: Properties of CFRP Tendons

CFRP	Shear strength (MPa)	σ_{tmax} (MPa)	E11 (GPa)	ϵ_{tmax} (%)	Poisson ratio	FVC (%)
Standard	DIN 65148	EN 2561	EN 2561	EN 2561	EN 2561	EN 2564
UTS 5631	30.00 ± 0.86	1576.67 ± 111.36	136.84 ± 4.59	1.152 ± 0.043	0.30	60.81
K63A12	28.69 ± 4.47	1029 ± 109.72	463.64 ± 28.16	0.230 ± 0.037	0.26	60.43
K13916	31.83 ± 2.47 ²	1561.98 ± 68.05 ¹	509.12 ± 13.49 ¹	0.307 ± 0.017	0.22	67.08

The CFRP tendons were coated by three different types of quartz sand particles to enhance the bond between the tendons and the concrete. The first two sand types, “fine” and “old-coarse”, were reference coatings used in industry [43] and during earlier work at Empa [41]. In both cases, the sand particles were applied to the tendon’s surface by spray coating in an industrial process directly after pultrusion. The third sand coating, named “new-coarse”, was chosen to further improve the bond strength. This sand coating was applied separately by a sprinkling technique following the tendon production. In this case, a thin layer of Huntsman 5052 epoxy resin was used to glue the sand particles effectively to the tendons surface.

All sand particles were characterized in size and visualized after their application, see Table 3. Furthermore, an overview of the tendon-sand-concrete combinations utilized in the different experimental sections (I–III) of this work can be found in the right part of Table 3. Here, (I) represents the determination of sand coating influence; (II) stands for the CFRP material’s influences on bond; and (III) investigates the bond failure by the aid of X-ray CT and measures the tendon draw-in/-out for UHM-CFRP tendons in a pull-out experiment.

Table 3: Sand coating characteristics and their application in this work.

CFRP material →	Tendon coating		UTS	K63A12	K13916
Sand types ↓	Grain size (mm)	Visual	Pultrusion	Tape laying	
None	-		x		
Fine	0.1–0.2		x		
Old-coarse	0.4–0.68		x	I	
New-coarse	0.063–0.5		x	II	III
				x	x

2.2.2 Test Specimens

All pull-out tests were performed on $40 \times 40 \times 160 \text{ mm}^3$ prisms. This specimen geometry is different from the usual cube type found in the literature [35, 80, 84]. However, in real applications of slender CFRP-prestressed structures, the typical element thickness lies in the range 40–60 mm. Hence, the chosen cross-section in this study should represent a conservative geometry related to the end-goal application.

The bond length was set to be 40 mm and kept equal in all specimens during this study. To enhance the measurement of high bond stresses, as proposed by Losberg [85], the bond length was defined to be in the middle of the longitudinal direction of the specimen. The unbonded area of 60 mm at each side of the bond area was created by the use of PVC-tubes. These PVC-tubes were sealed by a rubber O-ring to prevent direct concrete-to-tendon contact. The placement of the CFRP-tendons inside a steel mould is shown below in Figure 15A. After casting, the specimens were demoulded and stored in 90% RH and 20 °C until testing. An example of the finished pull-out samples can be seen in Figure 15B.

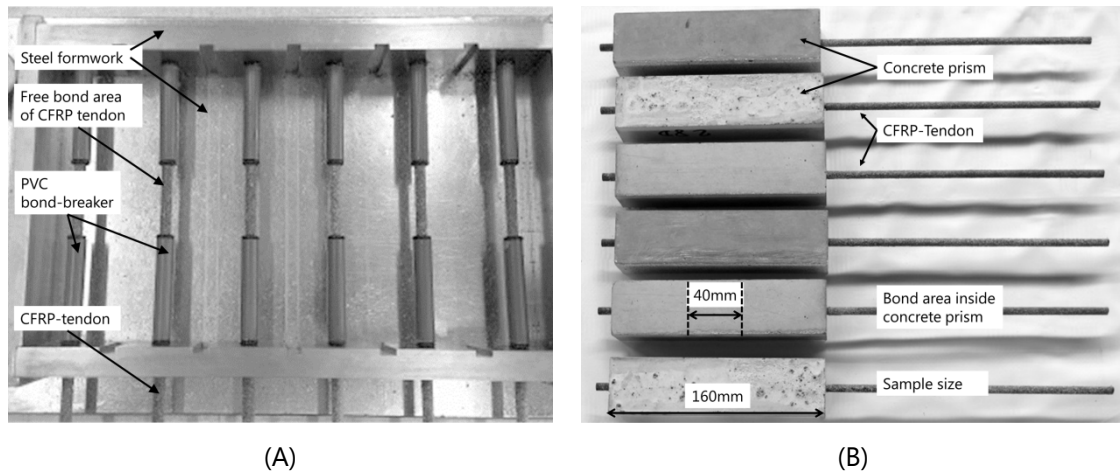


Figure 15: Specimen details: (A) CFRP-tendon and bond-breaker arrangement before casting; and (B) demoulded samples before testing.

2.2.3 Experimental Pull-Out Setup

To compare the influence on the maximum bond strength of different parameters, such as sand-coating and tendon stiffness, the proposed experimental set-up in EN10080 Appendix D was chosen and slightly adapted in geometry after considerations in [73, 85]. Due to the long unbonded distance of 60 mm between the counter holder and the 40 mm long bond area in the middle of the concrete prism, it is anticipated that the influence of concrete confinement due to friction at the counterholder is minimal. This was also checked during pilot testing by applying a 0.5 mm thin rubberlike material (Scotch™ VHB™ 4905, 3M, Mapplewood, MN, USA) between the prism and the counter

holder during pull-out testing. No effect on tendon draw-in and failure type could be detected. An overview of this pull-out set up is shown in Figure 16. The force was applied by a servo hydraulic cylinder and the tendon draw-in at the load free end was measured by a LVDT of type W2ATK HBM (Hottinger Baldwin GmbH (HBM), Darmstadt, Hesse, Germany).

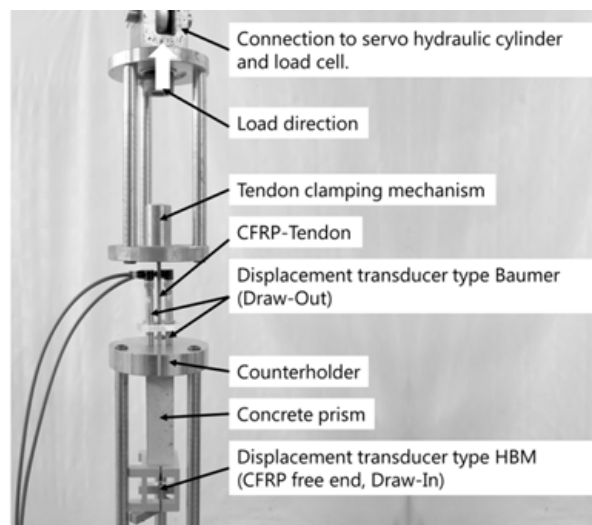


Figure 16: Pull-Out test configuration: Overview of mounted sample in experimental set-up.

To study the bond failure it was of further interest to gain additional knowledge about the tendon draw-out at the loaded side of the tendon. Hence, two additional high-precision analogue sensors of type Baumer IPRM12I9505/S14 were mounted on top of the counter holder to measure the tendon's draw-out. All samples tested were loaded continuously at a constant velocity of 2 mm/min until failure.

2.2.4 SEM, Microscopy and Visual Analysis

For visualization of the details on the bond failure area, electron micrographs were acquired from the surface of the CFRP tendon as well as of the corresponding concrete area failed in pull-out. This was done using a SEM of type FEI ESEM XL30 (Philips, Amsterdam, North Holland, Netherlands) at 2 kV and different magnifications.

In addition, the pull-out samples were split after loading and the failure area at the concrete's side was examined visually. These results were recorded by a Canon PowerShot G10 camera.

The interface thickness between sand coating and CFRP tendon was determined by a Zeiss Axioskop light microscope (Carl Zeiss AG, Jena, Thuringia, Germany). For the microscopic analysis, a cross section of the CFRP tendons was placed in embedment resin, polished and the adhesive thickness was measured afterwards at five points around the tendon's circumference. The measured value of 44 μm (Stdv = $\pm 19 \mu\text{m}$) is used as input parameter in the performed FEA. Due to the large uncertainty of this thickness, the influence of a deviating adhesive thickness on the pull-out behaviour was analysed and the result is shown in Section 2.4 (Figure 28).

2.2.5 X-ray CT

X-ray computed tomography (CT) was performed at Empa's Center for X-ray Analytics with an in-house developed X-ray micro-CT instrument based on a Viscom AG XT9225 TEP[®] X-ray source (Viscom AG, Hanover, Lower Saxony, Germany), with a transmission target consisting of a 9 μm -thick tungsten film, and a Perkin Elmer XRD 1621 CN3 ES[®] X-ray detector (Waltham, MA, USA), consisting of 2048 \times 2048 pixels with physical size $p = 200 \mu\text{m}$. Each pixel consists of CsI(Tl) scintillator layer deposited on top of amorphous silicon. The scintillator layer converts the received X-ray photons into visible light photons, which are then converted into electrical charge by the amorphous silicon material.

The X-ray source was operated at 200 kV accelerating voltage and 45 μA current, for the electron beam irradiating the target, for a total power of 9 W delivered on the target.

One attenuation-contrast X-ray CT measurement consists in acquiring several radiographs of the specimen for different orientations θ_k over 360°, producing a set of projection images. Tomographic reconstruction algorithms are then used to retrieve the object function $\mu(x', y', z')$, representing a 3D image of the interior of the specimen, from the set of linear projections [86].

In our case, we acquired 1441 radiographs over 360° of overall rotation of the specimen with a step of $\Delta\theta = 0.25^\circ$ per successive radiograph. At each orientation angle, each radiograph was actually the result of averaging over 4 of them at the same orientation, in order to increase the radiograph signal-to-noise ratio. The tomographic reconstruction was then performed with an

implementation of the Feldkamp–Davis–Kress cone beam filtered back-projection algorithm [87], a type of tomographic reconstruction algorithm, available in the Octopus Reconstruction[®] software (Ghent, East Flanders, Belgium) suite by Inside Matters (<http://insidematters.eu/>).

The 3D image (also called tomogram) consisted in a stack of 2D digital cross-sections of the volume of $\mu(x', y', z')$, orthogonal to the vertical y -axis and saved as 16 bit unsigned integer TIFF images.

The effective voxel size of the tomogram was $\tilde{p} = 30.53 \mu\text{m}$, corresponding to an effective spatial resolution of the images of about twice \tilde{p} ($61 \mu\text{m}$).

2.2.6 Statistics

To compare the maximum bond strength means, gained during this work for different material combinations (see Table 3), an Analysis of Variance (ANOVA) was conducted. With the Tuckey test, significant differences between specific means were identified. The significance level α was chosen to be 0.05. If the result of Tukey test, a p -value, is smaller than 0.05, the null hypothesis of no significant difference is rejected. The normal distribution of each test series was tested preceding the ANOVA.

2.3 Experimental Results and Discussion

2.3.1 Influence of Sand Coating on Bond Strength (I)

The maximum bond strength obtained with the different sand coatings (Scheme 1) was evaluated by pull out tests. The tendon material (UTS $E_{11} = 136.8 \text{ GPa}$) as well as the concrete mixture C_{ind} was not changed during this test series.

All coating options showed a similar behaviour during the first stage of loading. A continuous increase in bond stress was observed, until the maximum bond strength was reached. The non-coated samples as well as the ones coated with fine-sand softened slightly after reaching their maximum bond strength. Afterwards, they were further pulled out at a bond stress level close to their ultimate bond strength. For all coarse-coated tendons, the recorded load dropped suddenly after reaching its maximum value and stabilized a split second later on a much lower level. However, this level was still as high as (UTS old-coarse, UHM new-coarse) or higher than (UTS new coarse) the level of the UTS fine-sand tendon during further pull out. All tendons failed by slippage and splitting of the concrete [88] prism never occurred.

The results show a clear dependency of the maximum bond strength upon the chosen sand coating. No-coating ($\sigma_u = 1.73 \text{ MPa}$, Stdv = ± 0.12) and fine-sand ($\sigma_u = 4.50 \text{ MPa}$, Stdv = ± 0.75) showed the weakest bond performance. A significant increase was reached by the old-coarse-sand ($\sigma_u = 8.95 \text{ MPa}$, Stdv = ± 1.87) and finally the new-coarse-sand (19.47 MPa , Stdv = ± 3.11). All bond strength means are significantly different despite the two samples no-coating vs. fine-sand and are visualized in Figure 17A.

The particle size (fine or coarse) seems to control the bond failure mechanism (softening vs. sudden failure). If sufficiently coarse sand is applied by the aid of an epoxy resin, the bond

between tendon and sand-coating is found to be fundamental for the overall bond performance. The tendon draw-in vs. bond stress, the so-called τ - δ curve, is shown for all four coating options in Figure 17B. According to these τ - δ curves, the sand coating has also an influence on the draw-in at the unloaded side of the tendon. In this case the mean draw-in at failure is found to be higher for higher maximum mean bond strength. The draw-in for the new-coarse sand reached a value of 0.04 mm while the old-coarse sand had a maximum draw-in of 0.03 mm.

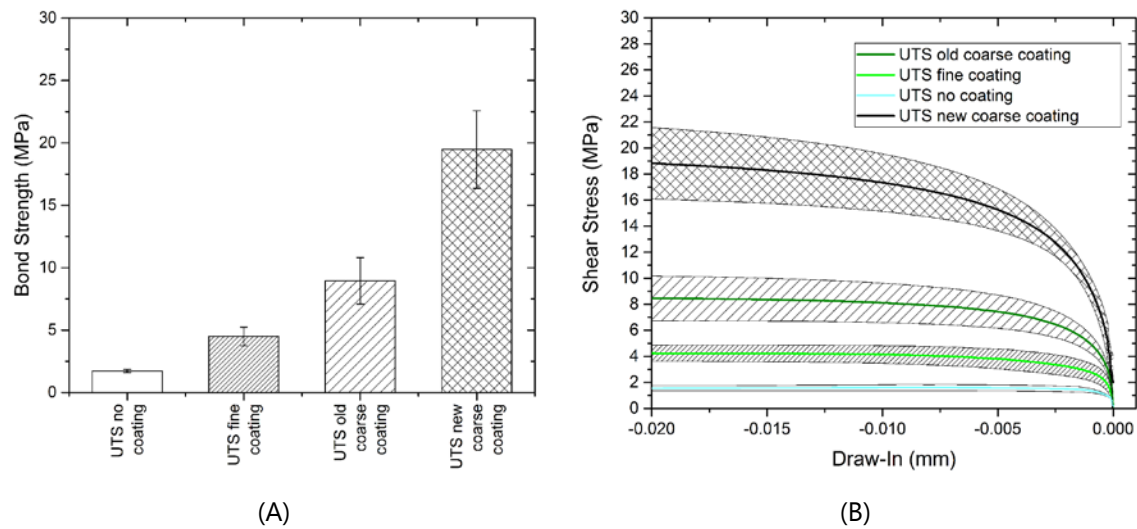


Figure 17: Influence of different sand-epoxy coating options on bond: (A) absolute bond strength comparison for different sand coating options; and (B) tendon draw-in behaviour. The sudden drop in load after failure is cut-off from the graphs to allow a better visualization up until failure. This graph has to be studied from right to left along its x-axis and shows the means and the standard deviation for all tested configurations.

Moreover, the bond area of the four tested surface configurations was investigated visually (see Figure 18). For the two coarse coatings it was found that the sand particles stick together with their corresponding adhesive epoxy resin to the surrounding concrete. This indicates most probably that the overall bond strength is governed by the interface between the sand epoxy adhesive layer and the CFRP tendon's surface. In the case of the fine-sand coating, the grains were also found to be present outside the concrete prism after the pull-out. However, the fine particles were not anymore completely embedded in their adhesive layer. Thus, the bond strength was dependent on the bond between the fine-sand and the coating epoxy. In conclusion, the new-coarse-sand was identified as the best option and was also applied to the specimens studied in the next sections.

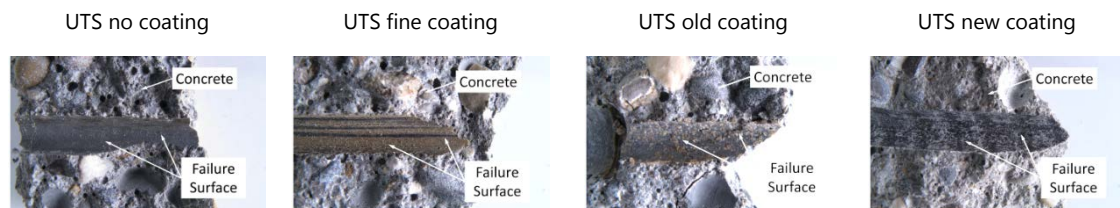


Figure 18: Results of visual analysis of the failure surface outside the concrete prism for no-coating, fine-coating, old-coarse-coating and new coating.

2.3.2 Influence of Tendon Stiffness on Bond (II)

The aim of this program was to compare the maximum bond strength of novel UHM-CFRP sand-coated tendons (K63A12 $E_{11} = 463.6$ GPa, K13916 $E_{11} = 509.1$ GPa) to formerly-used tendons with lower stiffness [43] (UTS $E_{11} = 136.8$ GPa). Both UHM tendons were designed to have approximately the same fibre volume content (62%) as the reference UTS tendon. In addition, all tendons were coated with the same sand-epoxy mixture, which showed the best results in the first section of this work. The pull-out tests were performed in comparable concrete mixtures C_{ind} (UTS), C_{ind} (UHM K63A12) and in C1 (UHM K13916). All samples were loaded continuously at a constant velocity of 2 mm/min until failure.

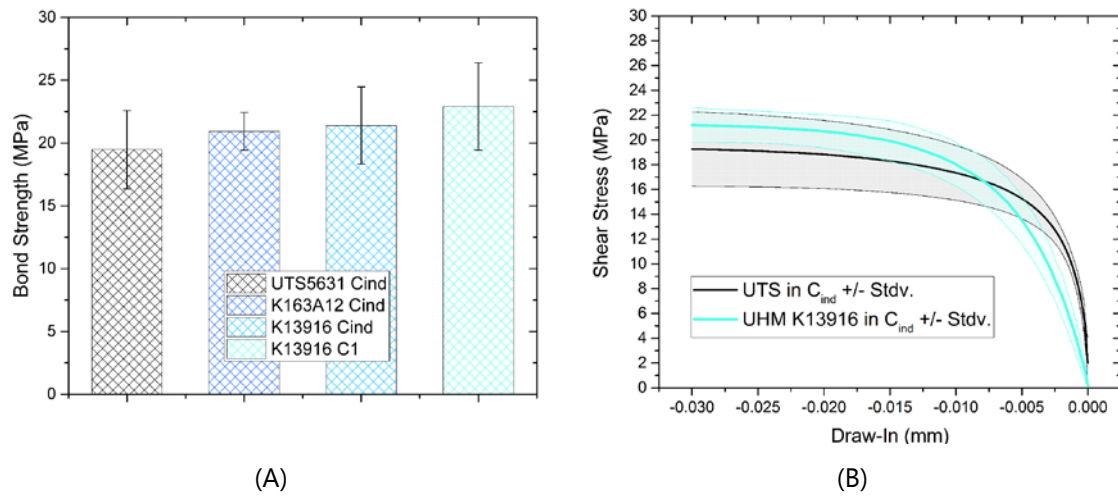


Figure 19: Influence of tendon stiffness on bond (UTS5631 136 GPa, K63A12 463 GPa, K13916 509 GPa). (A) Absolute bond strength comparison. All samples are coated with the new coarse coating and tested in C1 and C_{ind} , respectively. (B) Tendon draw-in behaviour. The sudden drop in load after failure is cut-off from the graphs to allow a better visualization up until failure.

Similar behaviour during loading was observed for all tendons. A continuous load increase until the maximum bond strength was followed by a sudden tendon slip-out failure. The maximum bond strength of all tendons ($\sigma_{u,K63A12} = 21.08$ MPa, $\sigma_{u,K13916} = 22.92$ MPa, $\sigma_{u,UTS} = 19.47$ MPa) was not significantly different (see A). Thus, σ_u seems to be mainly influenced by the adhesion of the sand-coating epoxy to the tendon's surface. However, according to the measured τ - δ curves, the tendon draw-in seems to be influenced by the tendon's stiffness (B). Up to 60% of the maximum bond stress, the averaged tendon draw-in of the means of the two UHM configurations is significantly softer compared to the mean of the UTS samples. To gain more information about this characteristic, the tendon's failure surfaces were investigated with SEM (, lower row). For the UHM CFRP, the SEM analysis showed that the carbon fibres on the failure interface were in good order and epoxy resin was partially spalled away. Thus, the failure of the UHM-tendon occurred at the interface between the carbon fibres and the attached epoxy resin. The UTS-tendon shows a slightly different picture. Here, the fibres are still nicely in touch with the surrounding epoxy resin used as tendon's matrix. This difference between the two tendons can be explained by different fibre surface treatments related to their production process. As before, the failed bond area inside the concrete prism was investigated visually but also by SEM. For all tendons tested, the sand coating remained visually attached as a whole (sand and epoxy resin) to the concrete. SEM reveals epoxy patches but barely any carbon fibres outside the

concrete prism's failure surface. In fact, carbon fibre fragments were found rarely and only very isolated (, upper row). These results indicate a bond failure between sand-epoxy coating and the CFRP tendon. Again, splitting of concrete never occurred in this test series.

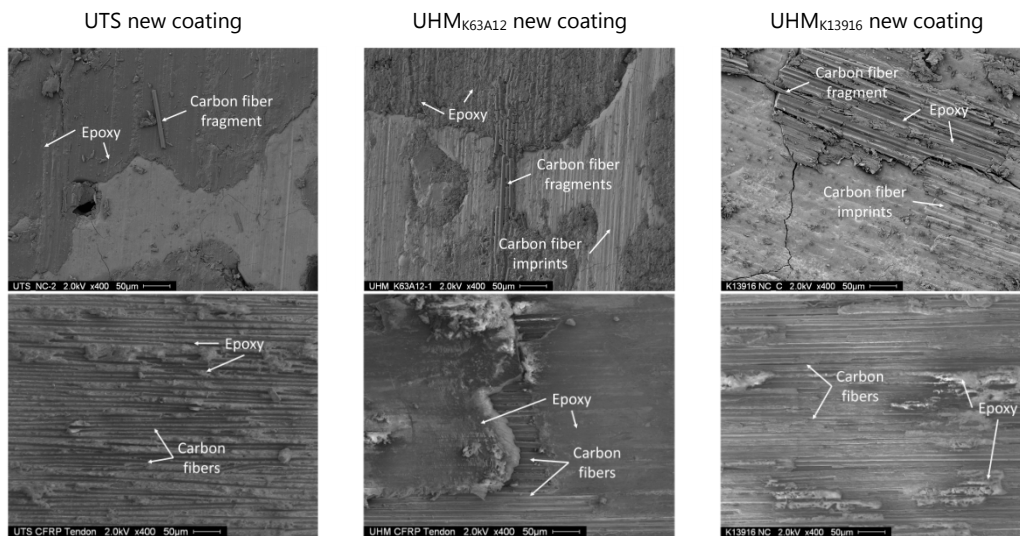


Figure 20: Analysis of failure area for different tendon materials. Upper row: Visual results indicate the sand-epoxy layer shear off outside the concrete prism; and Lower row: SEM images show pull-out failure surface of different CFRP tendons. This supports the hypothesis that the weak interface lies in between tendon and epoxy-sand coating, independent of the different CFRP materials used.

2.3.3 Bond Performance and Bond Failure of Sand Coated UHM CFRP Tendons (III)

The aim of this program was to compare the bond performance as well as the pull-out behaviour of novel UHM-CFRP sand-coated tendons ($E_{11} = 509.1$ GPa) in HPC. All tendons were coated with the same sand-epoxy mixture (Huntsman 5052 and new-coarse-sand), which previously showed the best results in the first section of this work. The pull-out tests were performed in the concrete mixture C1; after seven days (7 d) as well 28 days (28 d) after casting. The samples were loaded continuously at a constant velocity of 2 mm/min until failure.

In addition to the previous pull-out setup, the draw-out at the loaded side of the specimen was recorded by two additional sensors. This additional information should give knowledge about the whole pull-out behaviour of UHM tendons and support the analysis of the failure initiation.

During loading, the monitoring of the tendon draw-in and -out showed a nearly constant increase up to approximately 75% of the final loading. Afterwards, the slip increase accelerated progressively until failure. After that, the tendons were further pulled-out until the remaining pull-out load stabilized at a much lower load level. All 12 samples tested failed by a sudden slip-out after reaching their maximum bond strength. The failure happened in the same manner as all other samples with the same coarse-sand-epoxy coating tested previously. The maximum bond strength means, ranging between 17.33 and 22.92 MPa for 7 and 28 d, respectively, are visualized as a whole in A. Even though the maximum bond strength values look different at first

glance, no significant difference nor a trend could be detected for the different dates of testing by statistics. Thus, the maximum bond-strength averaged over all samples of this test series is 20.13 MPa. The visualization of the corresponding τ - δ curves in B is based on sensor data. Again, in these figures, the mean values of the tested samples and their standard deviation are visualized.

The τ - δ curves suggest that the tendon draw-out rate of samples tested after 7 days is higher compared to the draw-out rate after 28 days. However, based on the shown standard deviations, the effect of specimen age is statistically not significant. Furthermore, the slippage and the tendon draw-in rate at the unloaded side of all samples seems not be influenced by the concrete's age at loading.

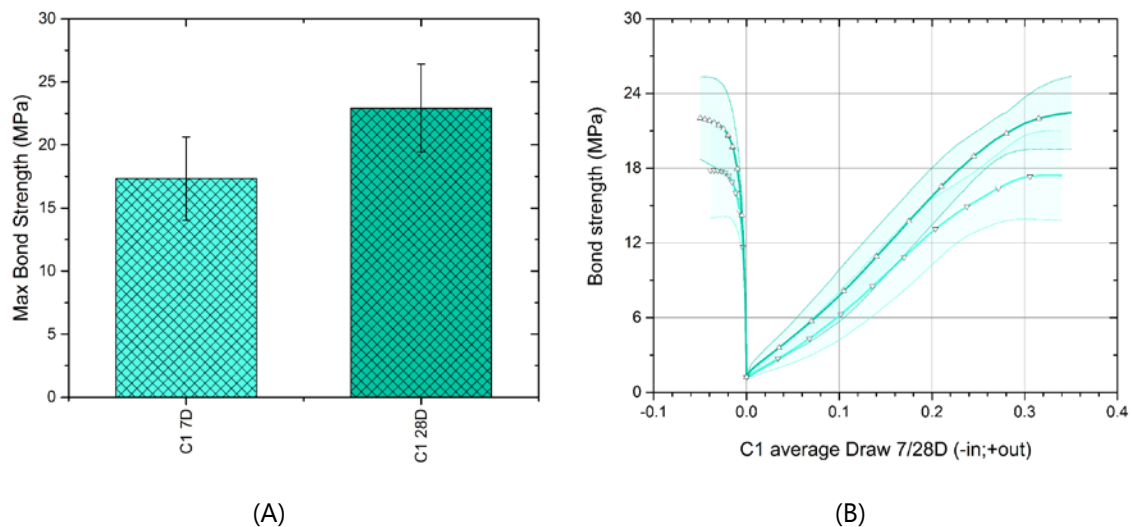


Figure 21: Bond performance of UHM-CFRP in C1 (A) maximum bond strength after seven days (7 d) and 28 days (28 d); and (B) tendon draw-in and -out. These graphs show the average including the standard deviation up to failure. The darker colour indicates the mixture tested after 28 d and the lighter colour the same mixture tested after 7 d. The sudden drop in load after failure is cut-off from the graphs to allow a better visualization up until failure. Starting from the point of zero draw-in-out, negative values indicate the tendon draw-in at the unloaded side and positive values the draw-out at the loaded side of the tendon.

To gain more information of the bond failure initiation and to detect possible internal cracks at low loads, one sample was investigated at different load levels by X-ray CT. This sample was loaded in the same manner as all other tested samples to the following load levels: 50.5%, 70.5%, 100% no failure and 100% including failure. After reaching each level, the load was released instantly and the sample was transferred from the pull-out test setup into the X-ray CT setup. This procedure was repeated after each loading and the generated X-ray scans (Figure 22) were analysed visually. Up to 100% of loading, neither slippage nor cracks could be detected with the given setup configuration. Only after loading the sample until its sudden slip-out failure, the tendon slip could be visualized and was clearly indicated in the interface between the sand-epoxy layer and the CFRP tendon (see right side of Figure 22). The loading until 100% was possible due to online monitoring of the tendon draw-in. As visualized in B, the tendon draw-in rate rapidly increases before failure. At this point, the loading was stopped and immediately released manually. Numerical Modelling

The pull-out behaviour found in the experimental sections of this work is collated and modelled by the Finite Element Method in the commercial software Abaqus 6.14. This model should show the applicability of the idea to reduce the failure behaviour down to the adhesive properties between CFRP tendon and sand-coating epoxy resin. Furthermore, this numerical model allows additional investigations on possible bond-influencing parameters and clarifies the origin of the experimentally-observed softening of the draw-in behaviour of UHM-tendons when compared to the behaviour of UTS tendons.

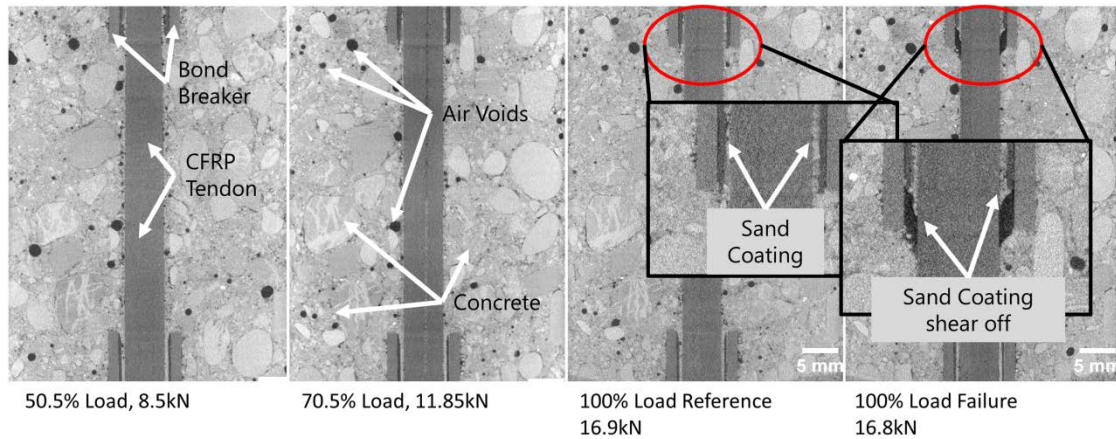


Figure 22: 2D vertical, digital vertical cross-sections from the X-ray tomograms acquired after loading the sample up to 50.5%, 70.5%, Reference 100% and 100% failure, from left to right, respectively.

2.3.4 Finite Element Analysis

The structure of the implemented model is based on the idea of cyclic symmetry. To save computational cost, only a one-degree segment of a cylindrical pull-out prism is modelled. This is a simplification as the original prisms tested have a rectangular cross section. The FEM results show that the shear stress, transmitted from the tendon to the concrete, decreases very fast in radial direction. Hence, the modelled pull-out behaviour is expected to be independent of the actual cross section of the concrete prism. The model consists of three different areas which are related to the main materials and assembled as shown in Figure 23. As found in the experimental work, the sand coating was never ripped out of the concrete prism. Thus, these particles are not modelled in detail and are consequently neglected. However, the bond between the sand coating and the CFRP tendon is modelled by a very thin layer of epoxy resin. The thickness of this layer was chosen according to light microscopy measurements and an explanation of this method can be found in the materials and methods section of this work. In this FEA, only the new coarse coating was considered for the comparison between UTS- and UHM-CFRP.

In this model, the bond between the epoxy layer and the concrete is assumed to be perfect. Between the tendon's surface and the epoxy layer, a surface-to-surface contact interaction of type surface-based cohesive behaviour is embedded. The main parameters controlling this cohesive behaviour are the cohesive stiffness and the damage initiation. Due to the explicitly modelled epoxy layer, which takes the compliance into account, and the infinitely thin interface between tendon and epoxy, the cohesive stiffness should be set to an infinitely high value. In

the presented FEA, the cohesive stiffness was defined to $2 \times 10^6 \text{ N/m}^3$. This value was chosen to achieve a good numerical convergence and to avoid possible issues usually related to high cohesive stiffness values [89]. A sensitivity analysis related to the cohesive stiffness value was performed and can be found in the summary and discussion section. For the damage initiation, the experimentally-found bond strength of 22.9 MPa was implemented.

Overall, the model is constrained by a boundary condition of type Encastre, which constrains all displacements and rotations of the corresponding nodes, on the left side of the concrete prism to represent the counter holder. The load is applied, equally distributed on the front face of the CFRP tendon looking to the left in Figure 23, and directed along the longitudinal axes of the prism. In addition, the movement of the CFRP tendons front face is blocked in transverse directions. The concrete and the CFRP tendon are modelled as three dimensional linear brick elements with reduced integration of type C3D8R. The epoxy layer is modelled as fully integrated three dimensional linear brick elements of type C3D8. These linear brick elements are in general well suited for contact problems and thus were chosen here for good numerical convergence. To reach a good accuracy of the cohesive behaviour along the bond length, the mesh is refined locally. The elements along the bond interface are 0.5 mm long. All parts are assembled without any overclosure and shrinkage of the concrete during hardening is neglected.

For this task, the concrete material was assumed to be homogeneous and isotropic material with a linear elastic behaviour (Young's modulus $E = 40.59 \text{ GPa}$, see Table 1; Poisson ratio $\nu = 0.178$, following [39]). The epoxy layer (Huntsman 5052), was modelled to be isotropic linear elastic ($E = 2.63 \text{ GPa}$, $\nu = 0.35$) up to 30 MPa of stress. Afterwards, a nonlinear behaviour was implemented up to a failure stress of 70 MPa with the corresponding failure strain of 4.56%. The linear elastic as well as the nonlinear behaviour was gained by tensile testing of the related Hunstamn 5052 epoxy resin according to EN ISO 527-2:2012 (Determination of tensile properties).

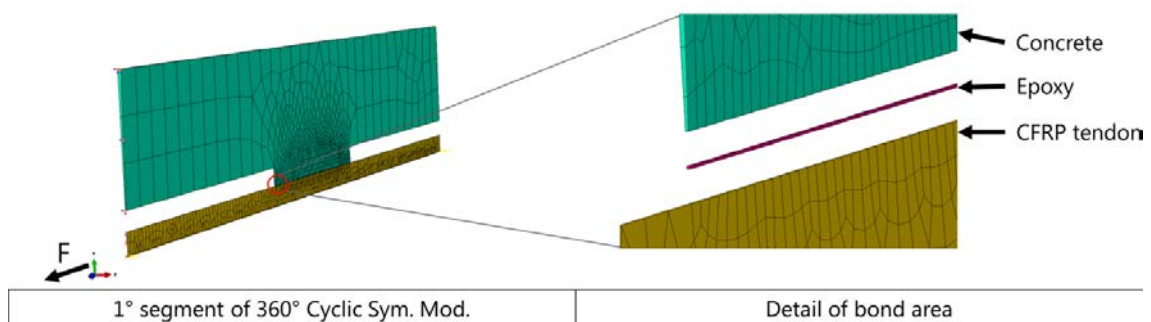


Figure 23: Overview of all components in the FEA.

2.3.5 FEM Validation

The validity of the implemented finite element (FE) model was checked in a simple comparison. The stresses, calculated values based on experiments inside the CFRP-tendon and the concrete-prism, were compared to their counterpart in the FEA. In both cases, a good agreement of model and experiment is present (Figure 24). However, it is important to notice that this simplified verification cannot cover and thus verify the influence of all input parameters. The

sensitivity of the simulation to two main input parameters such as the adhesive thickness and the cohesive stiffness are discussed in the summary section.

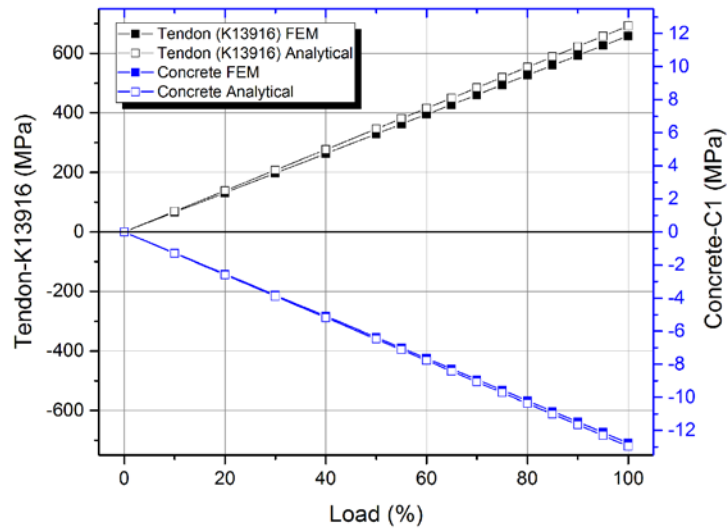


Figure 24: Validation of FE model. The calculated stresses inside the concrete as well as the CFRP tendon are compared. The blue graph indicates the concrete and the black graph represents the values of the CFRP tendon.

2.3.6 Results

Overall, the FEA showed good agreement with the experimental results. As seen before in the experiments, the tendon draw-in/-out starts nearly linear at low pull-out loads but increases rapidly thereafter, see A. As expected, the simulated draw-rate at the loaded end of the tendon is much higher compared to the unloaded end. The only noticeable difference between FEA and experiments was found in the early stage of the tendon draw-out at the loaded side of the tendon. Here, the experiments showed a slightly weaker s-shaped draw-out in the early stage up until 9 MPa of bond strength. Afterwards and logically at a certain off-set, the slope and the shape of both curves are again comparable. This effect is most likely due to settlement or orientation effects during loading, e.g., minimal local concrete crushing at the contact to the steel counter holder, loosening effects of small cement paste leftovers which were previously in contact with the tendon or slight tilting between the draw-out sensors and the counter holder. Based on this finding, it was suggested that the stress transfer in the bond area during a pull-out test should be more widespread at low loads for the UHM CFRP tendon in comparison to the UTS CFRP tendon. The visualization of the shear stresses inside the concrete prism, at different load levels and along the bond area confirmed this assumption (see Figure 27). Moreover, the transferred peak shear stress in the concrete is higher for the application of UTS CFRP tendons.

Furthermore, the FEA was used to investigate the origin of the experimentally-found differences in the tendon draw-in for UHM and UTS tendons. For this purpose, only the CFRP material was changed, from K13916 (UHM) to a UTS CFRP, in the simulation. Without adapting any other parameters, such as epoxy material, concrete type or adhesive layer thickness, the FEA result already indicated the same behaviour as found experimentally. This is visualized in Figure

25 A+B, in which the UHM CFRP tendon showed a higher tendon draw-in rate at low loads if compared to the UTS CFRP tendon. In addition, the experimentally-gained draw-in curve of the K13916 UHM CFRP tendon is plotted in the same graph as a reference.

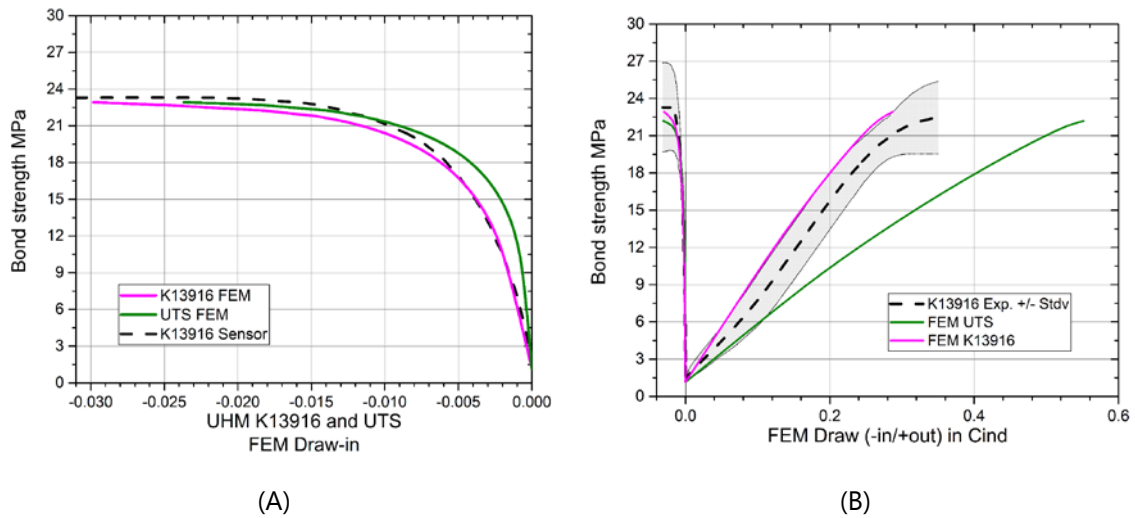


Figure 25: Tendon draw FEM compared to related Sensor measurements. (A) Draw in for FEM UTS and FEM UHMK13916. Results show the same trend as experiments in terms of the higher tendon draw in for the UHM tendon. Sensor data is shown as reference. (B) Draw-in and -out modelled using Cind, UTS and UHMK13916. Sensor 28d of UHMK13916 properties are shown as a reference.

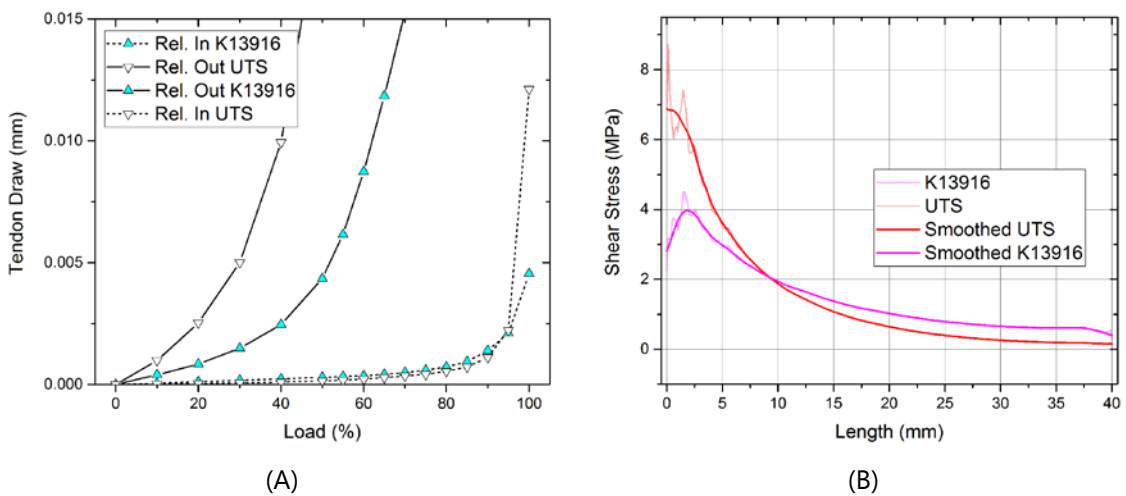


Figure 26: Influences on tendon draw-in and -out behaviour: (A) relative displacement between concrete and CFRP at the beginning (draw-out) and the end (draw-in) of the bond length; and (B) shear stress in the middle of the sand-epoxy segment, $t = 44 \mu\text{m}$, along the bond length for two CFRP materials at 10% load.

A deeper look into the modelled adhesive layer pointed in the same direction. Figure 26 A shows the relative displacement between the corresponding nodes at the concrete prism and the CFRP tendon, once at the loaded and once at the unloaded side. Here, it was found that the displacement for the UTS tendon was much larger and consequently, in the undamaged stage, the dependent shear stresses of the adhesive layer as well. Figure 26 B illustrates this fact, in which the shear stress in the middle of the adhesive layer is plotted along with the bond length for both tendon materials. The found results are in analogy to the shear stress analysis in adhesive layers as summarized by, e.g., da Silva et al. [90]. In [91], Tsai et al. showed for the

specific case of a double lap-shear-test that the shear stress in the adhesive layer is significantly dependent on the stiffness of the adhered parts. The same dependency was found in the presented FEA. Note, the found shear stress distribution does not necessarily correlate to a failure criterion as the failure initiation is most probably a local phenomenon. A subsequently performed sensitivity analysis, by separately changing every input material property of the CFRP tendon from UHM to UTS, revealed that only the change of the longitudinal stiffness from 137 to 509 GPa showed a significant influence on the tendon draw behaviour.

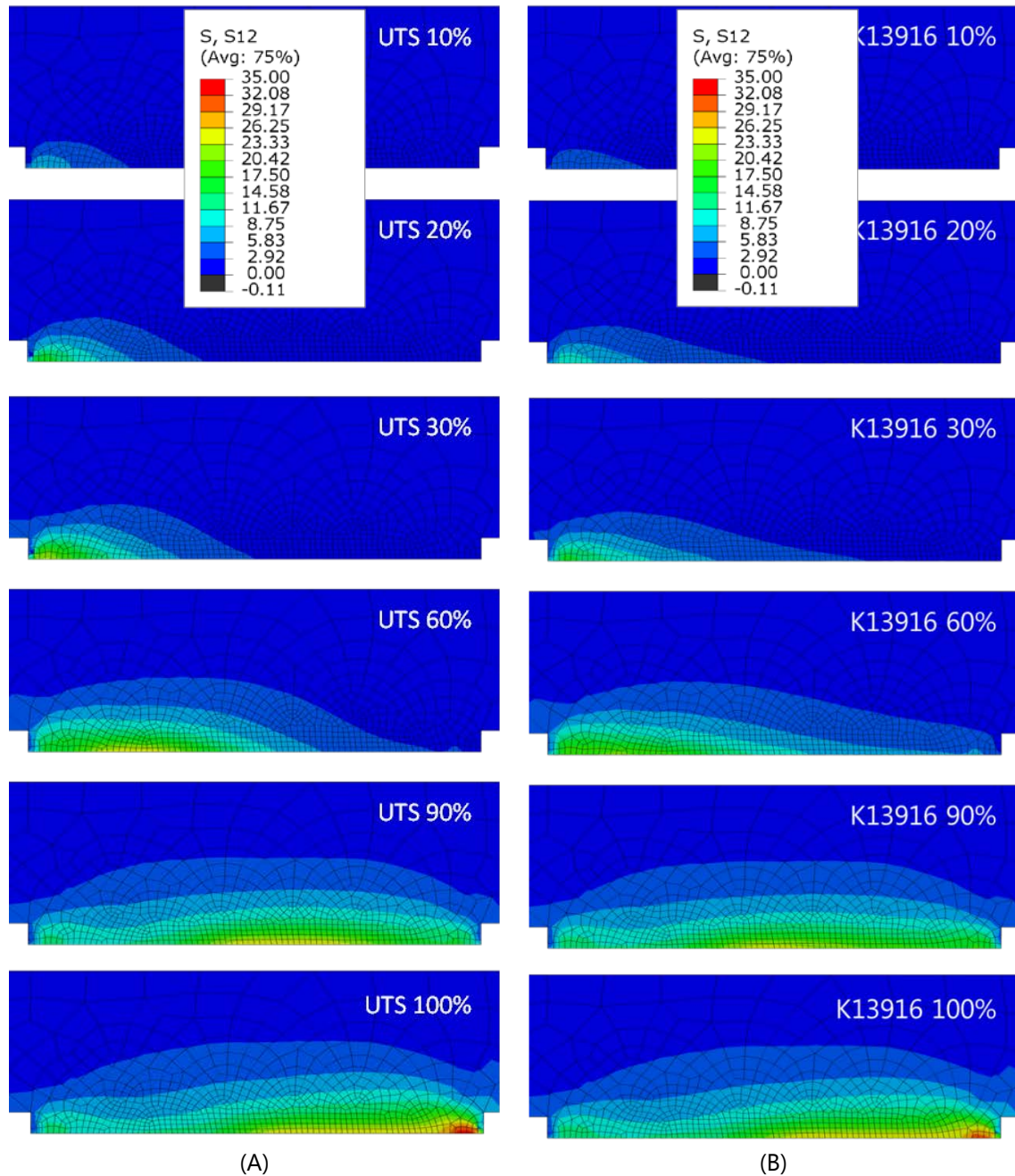


Figure 27: Shear stress distribution in longitudinal direction of the prism up to 22.39 MPa (100%) bond stress: (A) modelled using Cind and a UTS tendon in pull-out; and (B) modelled using Cind and UHMK13916 tendon in pull-out.

2.4 Summary and Discussion

The size of sand particles in the coating of the CFRP tendon has a significant influence on the bond failure mechanism. The tendons with either no coating or fine-sand coating showed a low bond strength but also a more continuous failure behaviour. However, if sufficiently coarse sand (>0.5 mm) and sufficiently high concrete strength (>85 MPa) were used, a sudden-slip failure at a much higher load values, as found for the two coarse coatings, was observed. In this case, the maximum pull-out strength reached values of 12–22 MPa and was limited by the bond properties of the corresponding epoxy-CFRP interface. This assumes that the bond between the coarse sand particles and the epoxy adhesive is much higher than the bond at the named interface. Both failure behaviours as well as the visual analysis of the failed surfaces confirm the experimental results shown in [77].

In addition, the applied different sand-epoxy combination used for the new-coarse coating showed an additional increase in the maximum bond strength. This effect is most probably related to the better adhesion to the tendon's surface of the Huntsman 5052 in comparison to the Bakelite epoxy resin. Furthermore, in the case of the brittle failure, the remaining load during further tendon pull out is slightly higher when compared to the load needed for the uncoated or fine-coated tendons. This effect was also found in [77], but was not further discussed. One explanation could be that this increase is related to the additional peel of the sand coating which is happening in these samples.

The tendons' longitudinal stiffness does not affect the maximum bond strength. This was shown over a broad range of longitudinal tendon stiffness (137 to 509 GPa). Restrictions may also apply for low strength concrete as well as for a pull-out failure different than the sudden slip-out. For instance, it was shown in [76] that for concrete compressive strength values around 15 MPa the bond failure will most probably appear inside the concrete prism. However, up to 60% of the max pull-out strength the tendon draw-in was influenced by the tendon's stiffness. Contrary to expectation, the stiffer tendon showed softer draw-in behaviour. This effect was investigated later in the FEA and found to be related to the longitudinal tendon stiffness only. This effect might also influence the transfer behaviour in a pre-stressed element and thus needs to be considered for the following work.

It was mentioned in the literature [76] that, above a certain minimum compressive strength of the concrete, the concrete strength does not influence the pull-out behaviour of CFRP tendons. However, these studies investigated mainly ordinary concrete mixtures and tendons of a much lower stiffness. Here, it was shown that this assumption is also valid for sand-coated UHM CFRP tendons in combination with a HPC.

Earlier, in [75, 76], the failure interface was already directed to be either inside the outer CFRP layers or in the coating of the tendon. For the sudden-slip failure of UHM CFRP tendons, it is shown in this work, by the aid of X-ray tomography, SEM and double notch shear (DNS) testing that the failure occurred directly at the interface between the coating epoxy and the tendon.

In general, the subsequently-performed FEA is based on this finding with the chosen position of the cohesive surface interaction between the ideal CFRP tendon and the adhesive layer. This implies that the FEA does not give any information about the local failure mechanisms. The FEA assumes that the local failure initiations, as most probably found in the experiments, act

together in a global manner. Furthermore, the FEA showed also a certain dependency from important input parameters such as the adhesive thickness and the cohesive stiffness, see Figure 28A,B respectively. In these graphs it was clearly shown that both values could possibly influence the draw-in behaviour significantly. With the performed 2D-Microscopy analysis of the sand coated tendon's cross-section, it was not possible to gain more precise information. For a complete description of the cohesive contact layer properties, a combination of 3D experimental and a finite element analysis would be necessary.

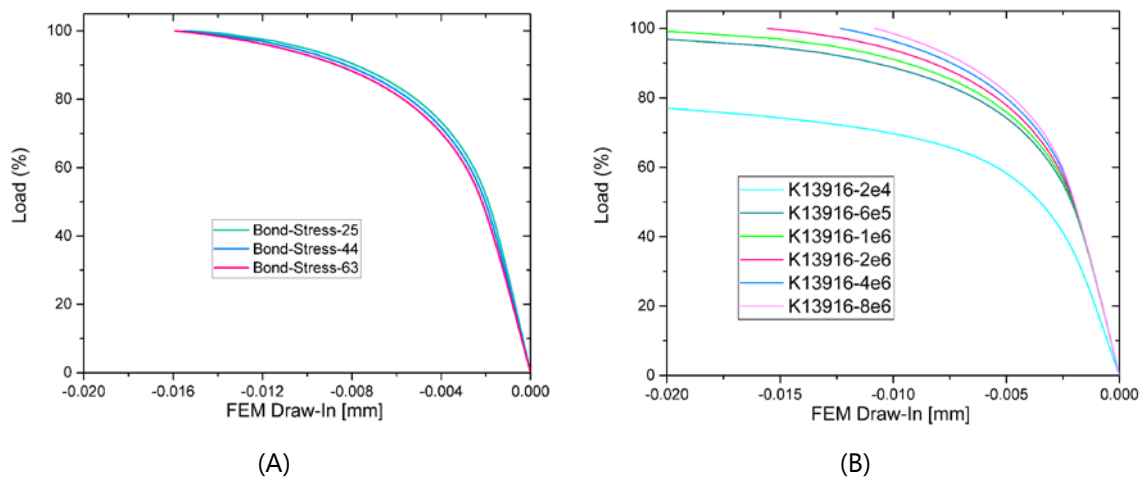


Figure 28: Sensitivity of FE model. (A) Thickness of the adhesive layer. In this visual, the adhesive thickness in μm is indicated by the number behind the label, e.g., Bond-Stress-25 represents an adhesive layer thickness of 25 μm ; (B) Variation of cohesive stiffness and their influence on the tendon draw-in behaviour.

2.5 Conclusions

Based on the test results of this study and the finite element analysis performed, the following conclusions can be drawn:

- The type of sand coating has a significant influence on bond for the used CFRP tendons. It is recommended to use a coarse sand (0.5–1.5 mm) to ensure the sudden-slip failure and thus the highest possible bond strength. Although this failure is brittle, it can be favoured over the soft behaviour due to the much higher level of absolute bond strength and the fact that a concrete element should not fail due to tendon pull-out.
- The highest bond strength in the given configuration seems to be dependent on the strength of the adhesive interface. The combination of X-ray, SEM, and visual analysis of the bond failure surfaces allowed locating the bond failure between CFRP tendon and the sand epoxy layer.
- The stiffness of a unidirectional CFRP tendon does not affect the maximum bond strength but it does influence the draw-rate in the corresponding τ - δ curve. In this case, the draw-in rate and the shear stress transfer behaviour between tendon and concrete are mainly controlled by the stiffness in pull-out direction of the related materials. Thereby, the most crucial condition of a good bond, according

to [70], for the design of load introduction areas is fulfilled for UHM CFRP tendons.

It can be summarized that the results of this work motivate a further investigation of the proposed beneficial material combination (UHM-CFRP and HPC). The focus of the following research will be the investigation of the prestress transfer behaviour. In addition, it will also be very interesting to see how these materials perform under long term and how creep effects will affect the performance.

Acknowledgements:

This research project is part of the National Research Programme "Energy Turnaround" (NRP 70) of the Swiss National Science Foundation (SNSF). Further information on the National Research Programme can be found at www.nrp70.ch. We gratefully acknowledge the financial support of SNSF and Empa. Part of this work has been performed by the use of the Empa Platform for Image Analysis, <http://empa.ch/web/s499/software/-/imaging-platform>, at Empa's Center for X-ray Analytics. We would like to thank Stefan Hartmann, Center for X-ray Analytics, Empa, for the installation of the X-ray source used for the X-ray tomography in this study. We are grateful to Iurii Burda for performing the SEM imaging and to Vanessa Rohr for executing the light microscopy measurements.

CHAPTER 3

Low clinker high performance concretes and their potential in CFRP-prestressed structural elements ^b

Abstract

Three novel low-clinker-high-performance concretes (LCHPC) with clinker replacement levels of 54, 58 and 70 % were developed to substitute high-performance concrete (HPC) in carbon-fibre-reinforced-polymer (CFRP) prestressed structural elements. The clinker substitution was achieved by a high amount of limestone filler and smaller amounts of metakaolin and silica fume. After 28 days, the LCHPCs reached high compressive strength values, between 77 MPa and 88 MPa, and Young's moduli between 35 GPa and 44 GPa. The LCHPCs showed self-compacting properties and low creep and shrinkage in comparison to a reference HPC.

A finite element analysis (FEA) of the internal stress development over time in CFRP-prestressed structural elements was performed, including creep and shrinkage. A higher prestress level was maintained in the LCHPCs compared to the reference concrete, thanks to their low shrinkage and creep. In contrast, the use of ultra-high-modulus CFRP prestressing tendons leads to increased pre-stress losses.

Keywords

Prestressed concrete; Low-clinker-high-performance-concrete; Concrete creep; Concrete shrinkage; CFRP; Finite element analysis.

^b This chapter was published as an original research paper. The format was adapted to fit the style of this thesis and hence does not necessarily reflect the exact published version. The full bibliography is given here: Lämmlein, T.D.; Messina, F.; Wyrzykowski, M.; Terrasi, G.P.; Lura, P. Low clinker high performance concretes and their potential in CFRP prestressed structural elements. *Cement and Concrete Composites*, 100 (2019) 130-138.

3.1 Introduction

In the last two decades, sustainability-oriented design of building materials has received increasing attention. Due to the large amounts of concrete that are currently employed to build and maintain the infrastructure and the built environment, it becomes paramount to reduce the emissions that are in particular associated with Portland cement clinker production. The production of cement is currently responsible for about 5% of the worldwide anthropogenic CO₂ emissions [92, 93]. An effective and promising approach to reduce the environmental impact of concrete structures is the reduction of the clinker content by optimizing the mixtures through supplementary cementitious materials (SCM) that are characterized by lower CO₂ emissions. Until a short while ago, the possible substitution levels of Portland cement with SCM were quite limited. Today, national and regional standards and guidelines (e.g., the recent SIA [60] guidelines in Switzerland or the EN-197 [61] in Europe) permit the use of concretes with significant amounts of cement replacement to allow the development of more sustainable concrete structures.

In Europe, the set of SCMs is generally given by the EN 197 [61] standard. In this framework, significant replacement levels of clinker are already possible. However, depending on the exposure classes, the required minimum cement content (MCC) of a mixture is defined by the standard EN 206-1 [94]. For example, in the case of XA3 and XS3 classes, the MCC can be as high as 360 kg/m³. In this case, the code-based approach poses effective limits to the design of sustainable low-clinker concretes (LCC). In 2009, Wassermann et al. [95] suggested a reconsideration of the concept of MCC. The authors argued that this parameter was a heritage of traditional concrete technology, when workability was not tunable by means of high range water reducing admixtures (HRWRA). They presented results related to durability such as carbonation and chloride ingress, demonstrating that the MCC was not a dominant parameter and that the service life was not negatively impacted by decreasing the cement content. In addition, other studies dealing with the influence of the code-based approach on the concrete compositions can be found in the literature, focusing on several aspects such as durability [96, 97], mechanical properties [98] and structural design parameters [99].

Calcined clays as SCM have started to receive substantial attention only in the last few years, even if the first systematic studies on the application of these pozzolans in concrete date back to the 1980s. Murat [100] reported a study on the hydration of metakaolin obtained by heating a commercial poorly-crystalline and fine-grained kaolinite (97-98% kaolinite) in a small fixed-bed electric furnace for six hours at about 730°C. This sample was mixed with water and activated by means of lime. The main reaction products were hydrated gehlenite, C-S-H and small quantities of tetra calcium aluminate hydrate (C₄AH₁₃ in cement chemistry notation). In subsequent studies [101-104], several dominant factors in calcined clays technology were discussed, such as the influence of raw material mineralogy, calcination technique and calcination conditions. The chemical and mineralogical properties of raw kaolin and the industrial processes for calcination are still the subject of research today. In [105], San Nicolas et al. investigated the properties of metakaolin obtained by means of flash calcination and compared them to those obtained by traditional rotary kiln calcination of the same kaolinite sources. The authors showed that flash calcination improved the rheological performance

without affecting the chemical composition. The workability improvement is determined by the morphology of the flash-calcined metakaolin (FCMK), which contains a fraction of spherical particles, while the typical morphology of metakaolin particles from rotary kilns is rather flaky.

More recently, it has been shown that the combined use of limestone and calcined clays allows achieving higher degrees of clinker substitution and a marked improvement in mechanical properties and durability. In [106], 45% Portland cement substitution (30% metakaolin, 15% limestone) resulted in better mechanical properties at 7 and 28 days than the pure Portland cement reference. The synergy between the two supplementary cementitious materials is explained by the fact that calcium carbonate reacts with alumina from the metakaolin, forming additional AFm phases and stabilizing ettringite [107].

SCM are often applied in high-performance concrete (HPC) [108]. This particular concrete type is characterized by dense packing of the aggregate, small maximum aggregate size, water-to-cement ratio (w/c) around 0.40-0.30 or lower (essential to obtain low porosity and high strength) and often addition of fine fillers or supplementary cementitious materials (usually silica fume [109], more recently also metakaolin [110]). Self-compacting concrete is obtained by appropriate grading of aggregates, cement and fillers and addition of superplasticizer and optionally viscosity modifiers [111]. By combining the high strength of HPC with self-compacting properties [112, 113], highly-optimized, thin-walled concrete elements become possible. To improve the particle packing and increase the compressive strength, typically 10 to 20% by cement mass of silica fume is used in HPC (e.g. [114]). However, besides increasing strength and reducing diffusivity [115], the refinement of the pore structure and especially the pozzolanic reaction of silica fume results in an increase of the autogenous shrinkage of HPC [116].

In HPC, due to the low w/c, complete hydration of cement cannot be reached. Cement hydration stops both due to lack of free water and lack of free pore space for forming new hydration products [117]. As a consequence, a substantial amount of cement (30-50%, depending on the w/c and on the amount and type of supplementary cementitious materials in the mixture) will remain unhydrated, ultimately wasting resources and energy invested in cement production [62]. By replacing the expensive particles of unhydrated cement with non-reactive fillers, cheaper and "greener" HPC can be produced. Bonavetti et al. [62] showed that in mixtures with w/c 0.30 and 0.34, almost the same compressive strength was obtained with 10% limestone substitution. At 20% substitution, the compressive strength was similar in the first 3 days and lower afterwards.

The substantial amounts of cement used in HPC mixtures highlight the necessity of making efficient use of the material, which is directly related to the degree of hydration of the cement at the given water-to-binder-ratio (w/b). Bentz and Conway [118] theoretically demonstrated the possibility to substitute coarser cement particles with inert fillers, without changing the mechanical performance at moderate substitution levels of up to 15%. These numerical results were successively confirmed in experiments with limestone filler [62, 63]. Recently, similar considerations allowed to develop static equivalent systems to study hydration-related early-age properties, shrinkage and creep, by substituting parts of the cement with inert quartz filler [119-122].

Based on the previous considerations, it can be assumed that in general the production of low clinker high performance concretes (LCHPCs) should be possible and that these mixtures could contribute to reduce the CO₂ emissions. The environmental impact of a structure using these LCHPC materials would be reduced additionally if the structure itself could be designed to fulfill only the structural (static and dynamic) requirements, while avoiding the durability regulations that would require a thick reinforcement cover, and hence a larger volume of concrete. An example for such a structure would be a CFRP-prestressed precast beam, façade or pole element [39, 43]. This technology allows benefiting from the outstanding mechanical properties of concrete in compression, while the CFRP do not need thick concrete covers to guarantee passivation and hence avoid corrosion of the reinforcement. In this particular application, the performance of prestressed structural elements is dependent on prestress loss, which is mainly related to creep, shrinkage and elastic shortening of the concrete [123]. Hence it would be beneficial, in terms of efficiency, if the used concrete would have a high elastic modulus in combination with low creep and shrinkage. A recent study already showed that a CFRP-prestressed structure should be able to reduce the environmental impact by up to 28% in comparison to an equivalent steel-prestressed structure [124]. Due to the low clinker content in LCHPC, carbonation is expected to be accelerated [125, 126]. However, this is again not expected to be a problem for the proposed application, as long as non-corrosive CFRP is used for prestressing.

Accordingly, the proposed combination of CFRP utilization, in terms of its mechanical design possibilities [127], and LCHPC in prestressed structural elements is expected to lead to lighter, more sustainable and finally more functional designs.

One main goal of this study is developing novel concrete recipes for structural applications with the mechanical performance of a HPC, but with significantly lower clinker contents. In addition, low shrinkage, low creep as well as a good bond between the CFRP prestressing tendon and the novel LCHPCs are essential to allow the application of these mixtures for manufacturing thin, prestressed structural elements.

Consequently, this work intends to show the potential impact of LCHPCs and of different CFRP materials to the remaining prestress level in a structure and hence to set the basis for an efficient structural design of prestressed concrete elements that takes into account also the material properties and the volume changes of the concrete.

3.2 Materials and Methods

Three new LCHPCs were developed, characterized mechanically and for their volume changes. Furthermore they were tested in bond pull-out tests with sand coated UHM CFRP tendons. The related materials, their characterization methods and the bond testing are described in this section.

3.2.1 Materials

Three LCHPCs (C2, C3 and C4) were designed to compete with an industrial reference (C1) in terms of their basic mechanical properties. The industrial reference itself was reproduced from a

mixture used in the Swiss precast industry for prestressed concrete elements (see Section 3.1); this mixture was used recently also in [127].

In general, all mixtures (C1-C4) contained ordinary, rapid hardening Portland cement CEM I 52.5 R (calculated modified Bogue composition by mass [128] C₃S 52.6%, C₂S 19.4%, C₃A 5.8%, C₄AF 11.2%), but in descending amounts. The specific surface of cement was equal to 5100 cm²/g and median particle diameter d₅₀= 10.3 μm (laser diffraction). The fly ash used in the mixture C1 had Blaine fineness equal to 2370 cm²/g. To compensate for the reduced cement content, the LCHPCs contained high volumes of limestone filler (sh_stone ash[®], sh minerals GmbH; density 2700 kg/m³, 98.5% by mass of CaCO₃, median particle size d₅₀= 6 μm). In addition, the mixtures named C2 and C3 contained also smaller amounts of calcined clay (flash-calcined metakaolin, Argeco), in the case of C3 in combination with silica fume (968-U[®], Elkem), as pozzolanic material. In the last mixture, named C4, only silica fume was used in addition to the filler. The oxide composition and the density of the cement, fly-ash, metakaolin and silica-fume are reported in Table 4. The sand (0/4 mm) and gravel (4/8 mm) quantity was kept constant in all mixtures considered (the volume fraction of the aggregates in the mixtures is approximately 0.60, while the volume ratio of sand to gravel is approximately 0.44). In comparison to C1 (w/b=0.35), the water to binder ratio of C2-C4 (w/b=0.17-0.2) was lowered to a minimum that still allowed good workability, in order to counteract the expected lower strength of these material due to substitution of the cement. To reach self-compacting properties, the amount of superplasticizer (SP) (ViscoCrete20HE, SIKA) had to be increased substantially in the mixtures with reduced cement content. Compared to the industrial reference (C1), the clinker reduction of the LCHPCs (C2-C4) reached values of 54 %, 58 % and 70 %, respectively. The mixture compositions are shown in Table 5, which includes the fresh concrete properties.

The final concrete compositions were mixed in a 75-l Eirich R08W mixer following the same mixing procedure for all four recipes. First, the dry components were tumbled for 60 s, afterwards water was added and finally the concrete was mixed for 120 s until a uniform mixture with good flow properties was achieved. Directly after mixing, the fresh concrete properties were measured according to EN 12350 and the different specimens were cast. Consequently, the experimental program of each investigated concrete was based on only one concrete batch. The mechanical properties of the developed concrete recipes, e.g. compressive strength and compressive Young's modulus, can be found in Table 6 of the results section.

The unidirectional CFRP tendons used in the pull-out tests consisted of Mitsubishi DIALED[™] K13916 ultra high modulus (UHM) carbon fibres (Mitsubishi Rayon Co. Ltd., Japan) in combination with a Huntsman XB3515/AD5021 hot-melt epoxy system. The tendons were produced by Carbolink AG (Fehraltorf, Switzerland) in a tape laying method at a fibre volume content of 67 %. To enhance the bond with the concrete, the cylindrical surface (d=5.3 mm) of the prestressing tendon was coated with quartz sand particles with size of 63-500 μm. It was shown earlier that sand in general [40, 42], and the chosen coating in particular, leads to an excellent and durable bond [127]. The described sand-coated UHM CFRP prestressing tendon was the same as already used in [127, 129] to study tendon pull-out and behavior of the tendons at high temperature, respectively. These tendons had a longitudinal elastic modulus of 509 GPa, a design tensile strength of 1400 MPa and a fibre volume content of 66 % [129].

Table 4: Oxide composition for cement, fly-ash, metakaolin and silica fume

	CEM I 52.5 R	Fly-ash	Silica fume	Metakaolin
SiO ₂ (mass %)	20.2	54.8	96.5	72.1
Al ₂ O ₃ (mass %)	5.3	24.5	0.7	22.3
Fe ₂ O ₃ (mass %)	3.3	8.5	0.3	2.2
MnO (mass %)	0.1	0.2	-	-
TiO ₂ (mass %)	0.3	1.0	-	1.1
P ₂ O ₅ (mass %)	0.2	0.3	0.1	-
CaO (mass %)	62.3	1.9	0.4	0.7
MgO (mass %)	1.7	3.0	-	-
K ₂ O (mass %)	0.9	3.2	0.9	0.2
Na ₂ O (mass %)	-	0.2	-	-
SO ₃ (mass %)	3.8	-	-	-
L.O.I. (mass %)	1.3	2.2	-	1.1
Particle density (kg/m ³) ^a	3150	2130	2200	2200

Table 5: Concrete composition and fresh concrete properties

Materials v	Concrete >	C1 ^c	C2	C3	C4
Cement (kg/m ³)		443.0	204.0	186.1	134.3
Fly ash (kg/m ³)		120.0	-	-	-
Limestone		-	412.7	372.1	511.7
Silica fume (kg/m ³)		20.0	-	93.0	67.2
Metakaolin (kg/m ³)		-	56.8	46.5	-
Aggregates 0/4 (kg/m ³)		1107.0	1105.6	1100.0	1097.9
Aggregates 4/8 (kg/m ³)		487.0	486.0	484.0	483.0
Water		204.0	135.6	118.6	121.2
Superplasticizer (kg/m ³)		5.2	25.6	25.1	16.4
w/b		0.35	0.2	0.17	0.17
w/c		0.46	0.66	0.64	0.92
Clinker reduction (%)		0	54	58	70
Bulk density (kg/m ³) ^a		2307	2388	2367	2368 ^b
Air void content (vol%)		3.6	3.9	4.8	3.2 ^b
Concrete flow (cm)		72.5	69	58	57.5 ^b

^a after 3 days^b measured on one additionally mixed batch^c same recipe as in [127]

3.2.2 Experimental program

The compressive strength of the concretes was tested on three 150 x 150 x 150 mm³ cubes after 3, 7 and 28 days, following standard EN12390 [13]. Until testing, the samples were stored in a climatic room at 20°C±0.3°C and RH > 95%.

Uniaxial creep in compression and shrinkage properties were measured on 120 x 120 x 360 mm³ prismatic specimens, generally following the standard SIA 262 at 20°C ±0.3°C and 70% RH ±3% RH. However, the experimental procedure for creep testing was modified compared to the standard. Instead of loading the sample after 28 days with a stress corresponding to 30% of the material's compressive strength, the samples were loaded in a sequence of increasing compressive stress applied at 3, 7 and 28 days after casting; at each loading step, the total stress was updated in order to correspond to 20% of the compressive strength at the time of loading. An overview of this specific loading procedure can be found in Figure 29.

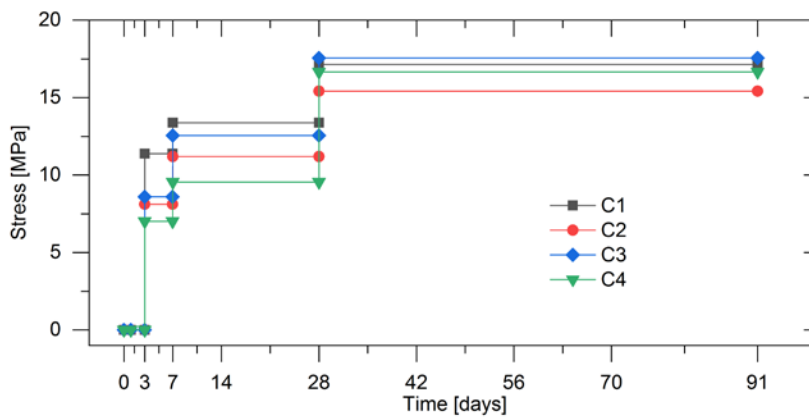


Figure 29: Scheme of the loading procedure – the stress applied on the samples at different ages is shown. The stress corresponded to 20% of the compressive strength (see Table 6) at the time of changing the load.

This procedure delivered valuable information about the creep behavior shortly after casting, which is of interest for the planned application to prestressed structural elements (pre-tensioning method for prefabrication). Furthermore, this allowed the calculation of the compressive Young's modulus by dividing the applied stress increase by the related strain increase for all considered concretes after 3, 7 and 28 days, respectively. The change of length of each sample was measured, both for shrinkage and creep, by a Ditast-250 mm high-precision distance meter (resolution 0.001 mm, gauge length 250 mm) on metal markers glued on two opposite sides of the prismatic specimens. All samples for creep and shrinkage measurements were cast from one batch per each concrete recipe and stored at a climate of 20°C±0.3°C and 90% RH±3% RH until demolding at 24 h after casting. The first measurement was done right after demolding. Next, the samples were exposed to drying at 20°C±0.3°C and 70%±3% RH. The total shrinkage measurements (performed on unloaded samples) were made at 1, 3, 7, 14, 28, 35, 42, 56, 70 and 91 d after casting. Creep and shrinkage were measured each on two prisms for all four recipes. The measured total shrinkage values included shrinkage due to self-desiccation and due to drying. Creep was obtained by subtracting shrinkage strain (measured

on unloaded samples) and the cumulative elastic strain from the total deformation measured on the two specimens under load.

In the pullout test program, five concrete prisms for each of the concrete recipes were cast. The prism geometry of 40 x 40 x 160 mm³ and the experimental setup was the same as used in an earlier study [127]. The sand-coated UHM-CFRP tendon, with a longitudinal stiffness of 509 GPa, was directed along the specimen's longitudinal axis. The bond area between tendon and concrete was limited by bond breakers to the inner 40 mm of the prism, allowing an unaffected load introduction. Detailed explanations and visualizations of the specimen's geometry and of the experimental setup can be found in [127]. The bond strength was obtained by pulling the whole specimen from one side of the CFRP tendon against a counter holder until failure and, at the same time, recording the applied force. The ultimate bond strength was calculated by dividing the measured maximum force by the initial bond area. The bond area was defined by calculating the CFRP tendons circumference based on its diameter after pullout failure. During loading, the tendon draw-in at the unloaded side of the specimen was recorded by a LVDT of type W2ATK HBM and the tendon draw-out at the loaded side of the test sample was monitored by two additional high-precision analogue sensors of type Baumer IPRM12I9505/S14. The bond strength pull-out tests were performed for all four mixtures after 7 and after 28 days. Until testing, the samples were stored at 20°C±0.3°C and 90% RH±3% RH.

3.3 Results

3.3.1 Mechanical properties

The main results presented here regard the LCHPC mixtures (C2-C4); more data on the reference mixture C1 can be found in [127].

Three days after casting the reference mixture C1 showed the highest compressive strength, followed by the systems C3, C2, which used metakaolin as a cement replacement, and last C4 which only used silica fume. The increase in strength between 3 and 7 days is most evident for C3. At 28 days of age, all tested mixtures reached high strength. Even the weakest LCHPC mixture C2 reached an average value of 77.1 MPa, only 10% lower than C1. The results of the strength measurements are shown in Table 6.

Table 6: Compressive strength and E-modulus of the LCHPCs and their reference HPC.

Recipe	f_{c3d} (MPa)	f_{c7d} (MPa)	f_{c28d} (MPa)	E_{c3d} (GPa)	E_{c7d} (GPa)	E_{c28d} (GPa)
N=	3	3	3	2	2	2
C1	56.9 ± 0.2	66.9 ± 0.4	85.7 ± 1.1 ^(a)	29.0 ± 0.9	29.4 ± 1.2	35.4 ± 0.4
C2	40.6 ± 0.1	56.0 ± 0.7	77.1 ± 0.7	27.9 ± 0.1	30.3 ± 1.3	35.7 ± 0.0
C3	43.0 ± 0.4	62.8 ± 0.4	87.8 ± 1.1	29.5 ± 0.5	33.6 ± 0.7	44.0 ± 1.5
C4	35.1 ± 0.2	47.8 ± 0.1	83.3 ± 1.0	26.8 ± 0.2	36.4 ± 0.9	38.8 ± 0.6

^(a)... Data from [127]

After 28 days, the compressive elastic Young's modulus (E_{c28d}) of all mixtures with reduced clinker content exceeded that of the reference mixture. In the most extreme case, the modulus of C3 was 24 % higher than the modulus of C1.

3.3.2 Shrinkage and Creep

The industry-based reference mixture C1 showed higher shrinkage than any of the tested cement-substituted mixtures (C2-C4). After 91 days, the measured values covered the range from 0.38 ‰ (C1) to 0.17 ‰ (C4).

The shrinkage rate for C1 was the highest during the first 28 days. Afterwards, the shrinkage rate of all mixtures was comparable (Figure 30-A).

The LCHPC mixtures (C2-C4) also showed much less overall creep. After 91 days, the mixtures C2, C3 and C4 reached creep levels of 59, 48 and 67 % of C1, respectively (Figure 30-B). To appreciate the creep reduction, it must be taken into account that 71% of the load of C1 was imposed on C2 at 3 d, 84% at 7 days and 90% at 28 days. For C3, these figures are 76% at 3 d, 94% at 7 days and 102% at 28 days. For C4, 62% at 3 d, 71% at 7 days and 97% at 28 days, see Figure 29. Despite lower loads (especially at early ages), the overall creep reduction is still evident (in other words, the reduction of creep in the LCHPC mixtures is larger than the ratio of loads between the LCHPC and C1), in particular for C3.

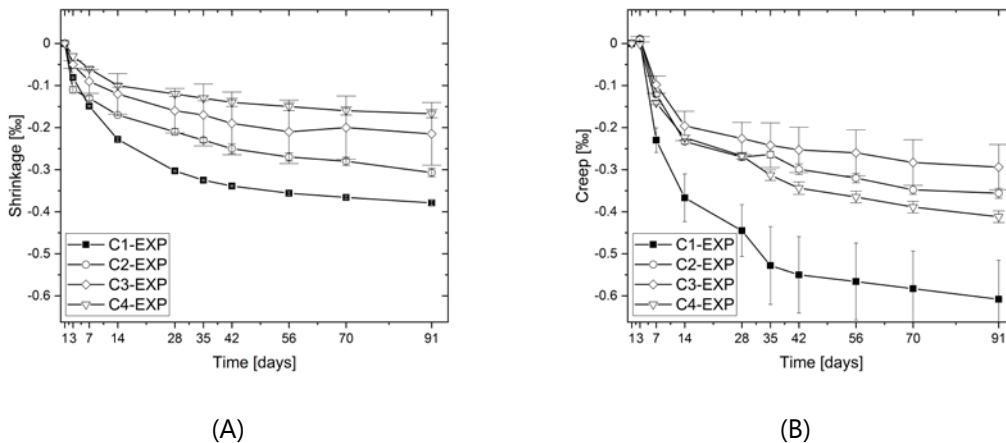


Figure 30: Shrinkage (left) and creep (right). In creep measurements, the load was increased to correspond to 20% of compressive strength at 3, 7 and 28d. C1 represents an industrial self-compacting HPC as it is currently used in the Swiss precast industry. C2-C4 correspond to the newly-developed LCHPCs.

3.3.3 Bond of reinforcement in LCHPC

The LCHPC mixtures showed bond strength values to sand-coated UHM-CFRP pre-stressing tendons similar to bond strength with conventional HPC reported in previous work [127]. Already after 7 days, the maximum bond strength for C2-C4 was in the range 17-21 MPa, not significantly different from C1.

As for the reference recipe C1, the tendon draw-in and –out was found to be linear approximately up to 75 % of the maximum bond strength. At the loaded end, the draw-out rate of the tendon reached values between 11.1 and 12.5 [$\mu\text{m}/\text{MPa}$], while at the unloaded end the tendons draw-in rate reached values between 3.4 and 4.3 [$\mu\text{m}/\text{MPa}$]. Afterwards, the tendon draw-in rate increased significantly until a sudden failure occurred. The failure occurred for all LCHPC samples in the same sudden manner of tendon slip-out failure and was comparable to the failure behaviour found for C1 in [127]. In particular the tendon slip-out failure could be proved to be a shear failure occurring between the CFRP tendon`s surface and the sand coating layer. It is noticed that the scatter in bond strength is large but typical for such kind of pull out tests; see e.g. [130].

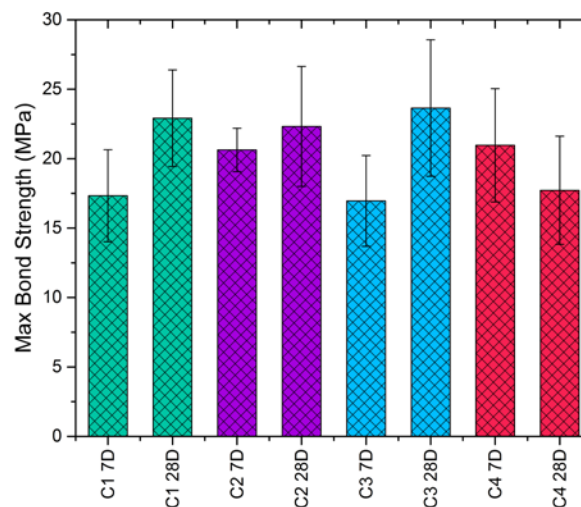


Figure 31: Bond performance of UHM-CFRP to LCHPC (C2-C4) and the reference concrete C1; data of C1 taken from [127].

3.4 Discussion

3.4.1 Mechanical properties and volume changes of LCHPC

The newly-developed LCHPCs reached high levels in their 28 d compressive strength and were comparable to the selected industrial reference. The cement reduction in the LCHPCs was compensated by a substantial decrease of the w/b and corresponding low initial porosity and an increase in the solid fraction, which resulted in comparable or even higher elastic modulus already at early ages (Table 6). The LCHPCs generally showed a slower strength and slightly slower elastic modulus development in comparison to C1 (Table 6). This was mostly caused by the high amount of superplasticizer (see Table 5), that delayed setting and hardening [131]. While the reference C1 contained $5.2 \text{ kg}/\text{m}^3$ of superplasticizer, C2 and C3 had about 5 times this amount and C4 3 times.

As expected (see e.g., [132]), the elastic modulus development was faster than the concrete strength development for all investigated mixtures and this was much more pronounced for the LCHPCs, see Table 7. A possible explanation is that the elastic modulus depends on the

establishment of a percolated solids network through the microstructure [133], while the strength is known to be governed by the size of the largest defects present in the material. Cement hydration products connect quickly the solids (unhydrated cement and aggregates), while filling of the pores is a slower mechanism [133].

Table 7: Development of compressive strength and elastic modulus in compression over time in respect to their 28d properties (100%)

Time	C1 f_c [%]	C1 E [%]	C2 f_c [%]	C2 E [%]	C3 f_c [%]	C3 E [%]	C4 f_c [%]	C4 E [%]
3d	66	82	53	78	49	67	42	69
7d	78	83	73	82	71	76	57	94

In bond tests between sand-coated UHM-CFRP tendons and LCHPCs, the results (i.e. maximum bond strength, tendon draw-in and mode of failure) were practically independent of the concrete mixture. The only detected bond-failure behavior for sand-coated UHM-CFRP tendons in LCHPCs was a slip-out failure as described previously for C1 [127]. Hence it can be assumed that, as for C1, also for LCHPCs C2-C4 the failure mechanism is mainly related to the applied sand coating on the prestressing tendon. This is proposed to be valid at least for LCHPCs that reach strength and stiffness levels comparable to those of standard HPCs.

Creep was successfully reduced in the new LCHPCs, most likely due to C-S-H (resulting from hydration of cement) with elastic fillers. In fact, C-S-H is supposed to be the major phase experiencing viscoelastic behaviour among different phases in hydrated cement paste [134, 135]. On the other hand, the LCHPCs mixtures contain high volume of fillers that should be intrinsically elastic. Furthermore, the higher solids fraction and lower porosity of the LCHPC mixtures should further correspond to lower creep [136]. Examining closely the creep curves in Figure 30-B, a slight decrease in creep could be observed for the mixture C2 between 28 d and 35 d. Considering that these values are based on the total deformation of only two tested specimens and that creep was calculated by subtracting the shrinkage of two additional shrinkage specimens, this drop can be explained mainly by natural variation between specimens.

The lower total shrinkage of the LCHPCs (C2-C4) compared with the reference C1 can be explained on one hand by the higher solid fraction (resulting in higher bulk modulus) [137]. The content of inert material by volume (aggregates and limestone filler, disregarding the limited reactivity of the limestone) is: 60.2% for C1 (65.8% if we consider also fly ash as non-reactive), 75.3% for C2, 73.6% for C3 and 78.6% for C4. On the other hand, the lower shrinkage of the LCHPCs can be also explained by their lower C-S-H content, since shrinkage can be considered as the viscoelastic response to the internal pore pressure [138, 139]. If we assume that only the cement reacts in all mixtures (fly ash, metakaolin and silica fume are not expected to react completely), a simplified calculation based on Powers' model [117] yields an amount of hydration products by volume of concrete of 21.4% for C1, 9.8% for C2, 8.9% for C3 and 6.5% for C4. This is in any case an underestimation because part of the SCMs will also react. In any case, the differences between C1 and the LCHPC mixtures will remain large.

In addition, the autogenous shrinkage is reduced in the LCHPCs because, while the w/b (considering limestone filler) is lower, the actual w/c of these mixtures is higher than in the reference (see Table 5) and less self-desiccation occurs [140, 141]. A low w/b also results in a limited drying front penetration (due to lower porosity, permeability and diffusivity) and thereby in reduced rate of drying shrinkage [142]. It is noticed that the shrinkage reductions observed in the LCHPC mixtures depend on the mixture compositions that were used and on the reference C1. When substituting high amounts of cement with SCMs, the creep and shrinkage reduction is expected to vary both with w/c and with paste content.

3.4.2 Effects of LCHPCs in CFRP prestressed structures

The new LCHPCs fulfilled the requested properties in terms of strength, stiffness, bond to sand-coated CFRP tendons and workability for their proposed application to prestressed structures. In a pre-stressed structure, it is important to know how much prestress is transferred and how the prestress changes over time. The main causes of prestress losses in prestressed concrete elements are elastic shortening, shrinkage and creep of concrete. Hence, the novel LCHPC recipes developed in this study, especially in combination with UHM-CFRP prestressing tendons, may significantly influence the prestress level that is maintained in the long term in such elements. It can be anticipated that the mechanical performance during the whole service life of a structural element manufactured according to this method might strongly depend on the chosen material combination.

An Abaqus FEA model, including concrete creep and shrinkage, was used to estimate the losses corresponding to the mentioned three main contributors. Generally, the measured drying shrinkage of a concrete specimen can be considered to be the combined response of higher skin shrinkage and lower core shrinkage [143]. Upon drying, an internal RH and water saturation gradient is established in the specimen. These gradients induce higher shrinkage close to the surface (skin concrete) and lower shrinkage in the core of the specimen. Differential shrinkage results in self-induced stresses (the skin is in tension and the core is compressed) and the global shrinkage of the specimen at any time during drying is between that of the skin and that of the core. The shrinkage evolution depends further on the specimen's geometry, in particular on the surface to volume ratio. It is also known that the creep behavior is also strongly coupled with drying, see e.g. Pickett's effect [144]. For simplification and because the modelling of this complex behavior is not the focus of the present study, the implemented FEA model used the same geometry of $120 \times 120 \times 360 \text{ mm}^3$ for the prestress-loss model beam geometry as used in the experimental creep and shrinkage testing. In this special case, the experimental results can be directly used as input for creep and shrinkage of the concrete in the model, at the cost of disregarding the shrinkage gradients within the specimens. It is noticed that while the shrinkage gradient may have initially some effect on the prestress losses, it is expected to show less influence as it becomes less steep with the progress of drying. In the case of specimens of relatively small cross section as examined here, the prestress loss of the tendon is expected to reflect mostly the global shrinkage/creep of the concrete specimen.

While the FEA model presented in the following has by necessity a number of simplifications, it is essential to quantify the effects of UHM-CFRP tendons and LCHPCs on the prestress losses. In

particular, one may expect to obtain lower prestress losses as a result of the lower creep and shrinkage of LCHPCs. On the contrary, the high stiffness of UHM-CFRP tendons is expected to result in higher prestress losses than for conventional tendons. However, based on the mechanical properties of concrete and tendons and on the volume changes of the tendons, without an FEA model it is hardly possible to quantify the impact of each of the different phenomena on the prestress losses.

To apply the prestress on the chosen geometry, a total of four prestressing tendons ($d=5.3$ mm) were placed symmetrically, as *beam elements (Type B31)*, at one third of the sample's height and width along its longitudinal axes. A prestress could be applied to the tendons by a *PREDEFINED FIELD* of *TYPE=STRESS* and released after three days. The surrounding concrete was modelled using linear brick elements with reduced integration and hourglass control (*Type C3D8R*). As a simplification the tendons were superimposed on the concrete and a perfect bond between the tendon and the concrete was assumed. This restricts the validity of the prestress loss calculation on a fully prestressed and un-cracked beam section. Further this simplification does not include a detailed bond-slip modelling approach which would be needed for further analysis of ultimate loading in prestressed members. In the respective case of investigating prestress losses without additional structural loads, bond slip can be assumed to be irrelevant and hence it was neglected during this modelling. The sample beam was only restricted by a *symmetry boundary condition* at one side. This choice of boundary condition allows visualizing the prestress drop at the free end of the specimen and also shows the stress situation in the fully prestressed section. A visual overview of the FEA model is given in Figure 32.

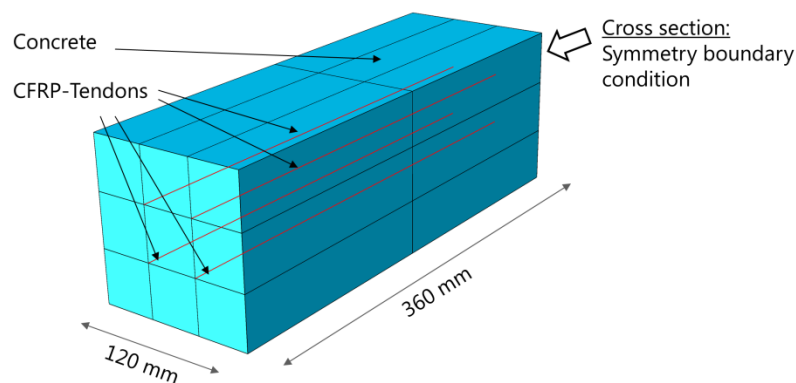


Figure 32: Overview of the Abaqus FEA-model. The concrete prism is visualized in blue, the four prestressing tendons in red colour.

The elastic behaviour of the CFRP tendon and the concrete was modelled using **ELASTIC* of *TYPE=ENGINEERING CONSTANTS* and **ELASTIC* of *TYPE=ISOTROPIC* respectively. In addition, Abaqus allows defining a temperature-dependent elastic modulus. This approach was used to model the time dependence of the four concrete mixtures by linking their tested 3 d, 7 d, 28 d elastic modulus to the corresponding fictitious temperatures used for shrinkage modelling (see details below). To assess the full range of CFRP tendon materials influence on prestress, an industry standard (UTS $E_{11}=138$ GPa) tendon and a new ultra-high modulus tendon (UHM-K13916 $E_{11}=509$ GPa) were chosen; their mechanical properties were taken from [127]. Based on [35], stress relaxation of the tendons is expected to reduce the prestress by less than 1.4 % in

the case of UTS-CFRP and around 1.1 % for UHM-CFRP tendons. This loss was not considered in the FEA and would show no significant effect on the results presented in Figure 34, Figure 35 and Figure 36.

Shrinkage was modelled by a thermal expansion coefficient analogy after [145]. In Abaqus 6.14, the shrinkage was implemented by the **EXPANSION* function in combination with a predefined fictitious temperature field. The applied temperature was homogeneous throughout the complete model at each calculated time point but changed its absolute value over time to simulate the shrinkage. The final results of shrinkage modelling were evaluated and compared to the experiments. As expected, due to the strict numerical fit, the shrinkage behavior was found for all four mixtures to be very well represented by the applied model (see Figure 33A).

The creep of concrete was modelled in Abaqus using **VISCOELASTIC*. In principle, this modelling approach can be expressed by a parallel arrangement of several Maxwell elements and a spring element. In this case a Prony series of the bulk relaxation modulus $k_R(t)$ and the shear relaxation modulus $g_R(t)$ describes the viscoelastic material behavior. For modelling the creep behaviour using creep test data, Abaqus requires the input of the normalized shear compliance. This shear compliance can be calculated by dividing the actual shear stress by the constant shear stress applied in shear creep tests [146].

To represent the creep behavior of all four recipes, the experimentally-gained uniaxial creep data was assumed as shear creep data in Abaqus and normalized. To provide support values in the area of low experimental data coverage, the normalized creep data was fitted to a logarithmical curve and finally added into Abaqus for material fitting. In addition, Abaqus allows defining the long term normalized shear compliance, which was set to best represent the creep curves in the long term. This procedure was applied to all four recipes and added into the FEA based on the results of the creep test program. In particular the creep load applied in the previous experiments after 3 days, 7 days and 28 days respectively was used when implementing the creep model in Abaqus. The results of this fit are summarized in Figure 33 B. The load variation over time was not further considered during the prestress loss assessment in the FEA.

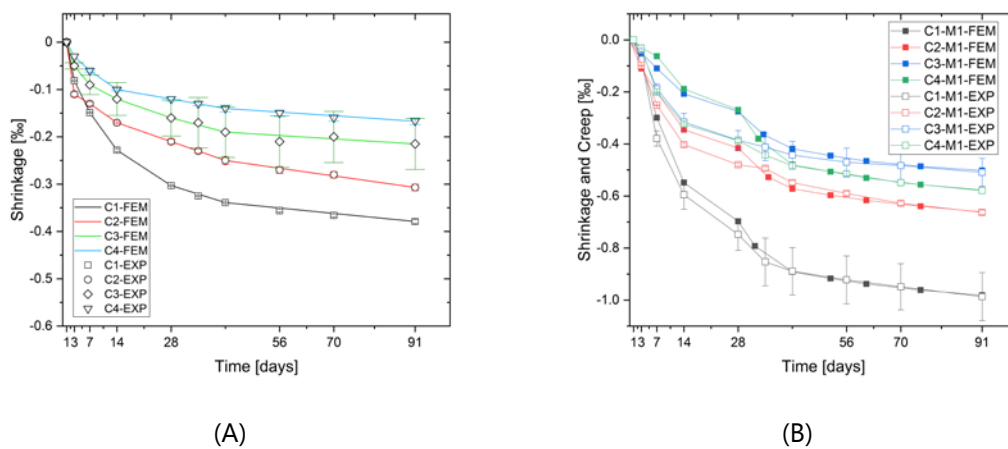


Figure 33: Validation of the FEA creep and shrinkage material models. The left graph (A) shows the results of the shrinkage modelling as colored lines in comparison to the experimental shrinkage data. The experimental shrinkage data is shown as symbols including their standard deviations. The right graph (B) shows the results including creep and shrinkage.

The simulation was performed for the two most extreme concrete mixtures (C1 and C3) in combination with the two CFRP materials at two tendon prestress levels (800 MPa and 1200 MPa). The prestress levels were chosen according to recent publications in the field of CFRP prestressed concrete [42, 147]. To investigate the prestress losses related to different processes, the longitudinal stress within one CFRP prestressing tendon was analysed once considering both shrinkage and creep, once without creep and once without shrinkage. This allowed assigning specific amounts of prestress loss to the different mechanisms and to analyze their evolution over time, up to until 91 d after casting. The results of the stress development inside the CFRP tendon are shown exemplarily for the combination C1-UHM-K13916 in Figure 34 B. All other combinations showed, at their level of transferred prestress, a comparable behavior. The longitudinal stress distribution inside the concrete prism was visualized over time to show the influence of creep and shrinkage on the specimen's internal stress distribution (Figure 34 A). The prestress level inside the CFRP tendons was plotted as a function of time for both CFRP tendon materials in the concrete recipes C1 and C3 at the 800 MPa prestress level, see Figure 35. For all combinations, most of the losses were predicted by the FEA to appear within the first five weeks after casting. In the eight weeks thereafter, the increase in prestress loss was reported to be very low for all investigated material combinations. For example, the largest additional loss in the last eight weeks occurred for the UHM-CFRP prestressing tendon in C1 concrete and amounted only to 2.2 %.

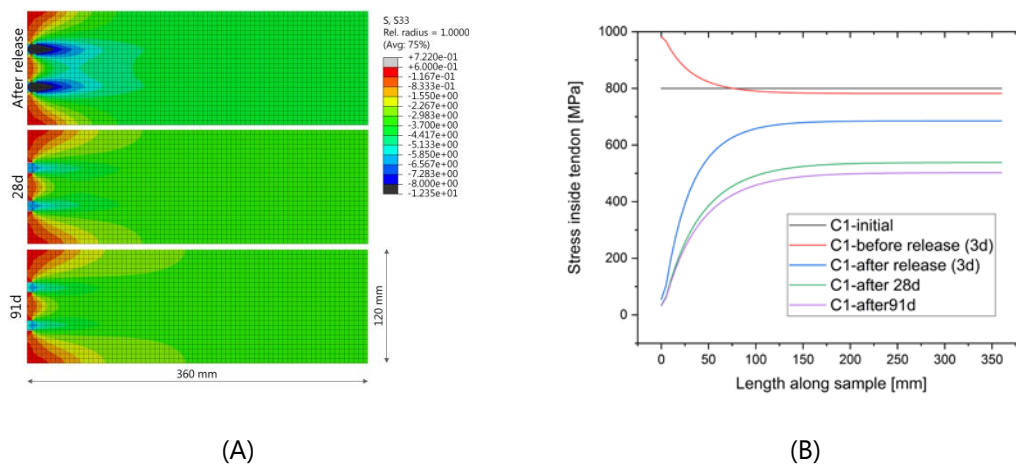


Figure 34: FEA results of the prestress transfer behaviour. The left graph (A) shows the longitudinal stress distribution inside the concrete prism for specified time points. After the prestress release, this visualization shows the redistribution of the stresses inside the concrete prism due to concrete creep. As expected, the stresses in the higher loaded areas of the concrete prism were reduced. The right graph (B) shows the tendon stress along the specimen's longitudinal axis evaluated at critical time points during the FEA analysis, with and without creep and shrinkage. Here, the results are exemplarily shown for C1 and a UHM-K13916 prestressing tendon. The general behaviour of the LCHPCs prestressed with UHM-K13916 CFRP prestressing tendons was comparable. However, differences were present due to the different levels of prestress transfer, concrete creep and concrete shrinkage.

Not surprisingly, due to their very high longitudinal stiffness of 509 GPa, the largest total prestress losses were also found for the UHM-CFRP tendons and reached values of 37 % prestress loss in C1 and 24 % loss in C3. The lower shrinkage and creep of LCHPCs compared to the reference reflected in lower prestress losses for both tendon materials (e.g. UTS @800 MPa=12 % in C1 and 7 % in C3). Hence, the low shrinkage and creep in the

LCHPCs were able to reduce the prestress loss for UTS-CFRP tendons by 35% and for UHM-CFRP tendons by 42% respectively. Creep, shrinkage and elastic shortening were found all to contribute noteworthy amounts to the final prestress loss. The contribution of the different mechanisms was subdivided into parts and visualized in Figure 36 .

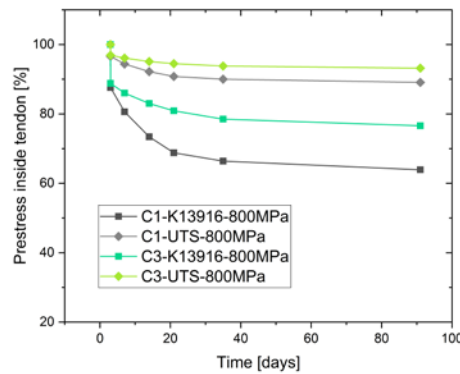


Figure 35: Calculated prestress inside the CFRP tendon from the time point of prestress release until 91 days after casting. In the FEA, the prestress was released 3 days after casting; the value of 100% prestress corresponds to the prestress inside the CFRP tendon right before the prestress release. Due to shrinkage, this value was already slightly lower than the initial 800 MPa. The presented curves include all modelled sources of prestress losses; shrinkage, creep and elastic shortening. The labeling of the lines expresses the chosen concrete in first position, then the CFRP material and the CFRP prestress level, in MPa, in third position.

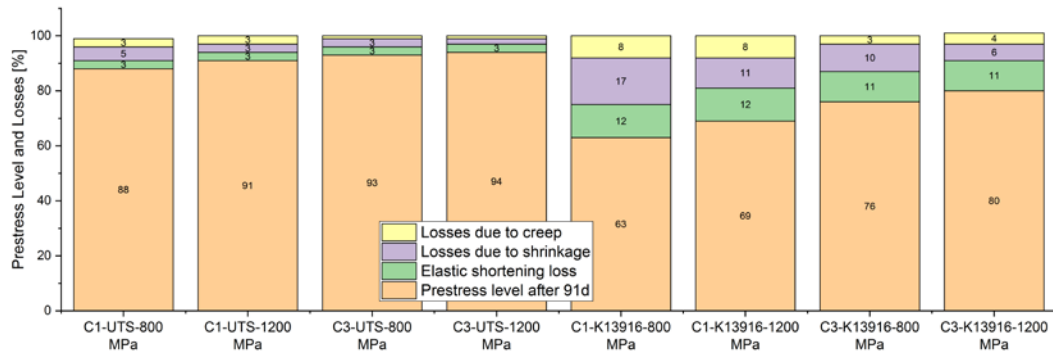


Figure 36: Prestress losses related to shrinkage, creep and elastic shortening after 91 d based on FEA analysis. The labelling of the columns expresses the chosen concrete in first position, then the CFRP material and the CFRP prestress level, in MPa, in third position.

3.5 Conclusions

Based on the laboratory work during concrete design, the mechanical testing and the modelling of concrete creep and shrinkage in Abaqus 6.14, the following conclusions can be drawn:

- By using limestone and metakaolin as SCMs, it is feasible to design and cast LCHPCs with self-compacting properties and clinker reduction levels of up to 54–70%. These novel LCHPCs showed very good general mechanical properties, e.g. a high compressive strength between 77 – 88 MPa, and a good bond to sand-

coated CFRP tendons. In fact, the bond strength of UHM-CFRP tendons reached 17-21 MPa, not significantly different from the reference concrete C1 typical for precast prestress applications. Hence, they are considered to be good candidates to be used in CFRP-prestressed structures.

- Prestress losses are significantly dependent on the chosen material combinations. The prestress of a UHM-CFRP prestressing tendon will react very sensitively to small changes in creep and shrinkage, due to the high longitudinal stiffness of these tendons. Low creep and shrinkage of the LCHPC mixtures in combination with a low longitudinal elastic modulus of the CFRP prestressing tendons contribute to a high remaining prestress level in a prestressed structure.

The results of this work show very good potential for improving the current CFRP prestressing technology on structural level. However, these results still focus mainly on the short term behaviour of a prestressed structure. Now, data about the structural behaviour and its integrity over a longer period of time (years) in harsh environmental conditions would be needed. This would bring confidence in industry about these new material trends and finally bring this technology into construction.

Acknowledgements:

This research project is part of the National Research Programme "Energy Turnaround" (NRP 70) of the Swiss National Science Foundation (SNSF). Further information on the National Research Programme can be found at www.nrp70.ch. Mateusz Wyrzykowski was supported by an SNSF Ambizione grant (project 161414, "Role of water redistribution in creep of concrete"). We gratefully acknowledge the financial support of SNSF and Empa. We are grateful to Daniel Käppeli, Marcel Käppeli, and Daniel Völki for their strong support during sample production and testing.

CHAPTER 4

Prestressing low clinker structural concrete elements by ultra-high modulus carbon fibre reinforced polymer tendons ^c

Abstract

Low clinker high performance concrete (LCHPC) and ultra-high modulus (UHM) carbon fibre reinforced polymer (CFRP) tendons were recently introduced and proposed for application to prestressed structural elements. The 70 % reduction in cement content and the very high CFRP tendon stiffness (>509 GPa) were expected to impact the mechanical behaviour of such structures. This study follows 3 m-long beam specimens during prestressing, concrete hardening and in 4 point-bending experiments. After 28 days, the LCHPC recipe did not show measurable differences in their prestress loss behaviour in comparison to a conventional HPC. The UHM-CFRP prestressing tendons showed higher prestress losses. However they increased the beam's maximum load bearing capacity by 21% and showed significantly less deflection in comparison to the current industry standard.

Keywords

Finite element analysis (FEA), Creep, Carbon fibre, Mechanical testing

^c This chapter is intended to be submitted with small supplements as an original research paper for consideration as publication in the Elsevier Journal "Composites Part B: Engineering". The current bibliographic information is given here: Lämmlein, T.; Justs J.; Terrasi, G.P.; Lura, P. Prestressing low clinker structural concrete elements by ultra-high modulus carbon fibre reinforced polymer tendons. Intended to be submitted in Composites Part B: Engineering, planned submission Spring 2019.

4.1 Introduction

Sustainable and innovative designs in construction can make a significant contribution for improving the carbon footprint of structures in the future. In terms of structural design, there are two main approaches to tackle this challenge. The first approach consists in reducing the environmental impact of the employed materials. The second approach is based on optimizing the structures from the point of their mechanical performance and hence the effectiveness in the use of materials.

Already in the 1990s, one first step for improving the structural design on building facades was the development of slender carbon fibre reinforced polymer (CFRP) prestressed elements [39, 148]. However, for nearly two decades, the space for further developments in this field was constricted by both the high price of the materials and existing standards. Currently, standard modulus CFRP costs about 20 €/kg. Ultra-high modulus (UHM) carbon fibre reinforced polymers have become recently more affordable with a cost of about 50 €/kg [129]. In addition, new guidelines [61, 83] are allowing the development of novel low clinker high performance concretes (LCHPC) with clinker replacement levels of up to 70% [149]. The combination of both materials results in a very promising composite system that satisfies both the sustainability aspects and the technical improvement objectives.

Prestressing of concrete became technically feasible with the invention of high strength steels and was first realized by Freyssinet in the 1920s [21]. By counteracting tensile stresses in concrete, the prestressing technique allowed the manufacturing of lighter structural elements at much lower cost. Later in the 1970-80s, fibre reinforced polymers were first brought to use in concrete structures [150]. Due to their excellent strength, their low weight and their corrosion resistance these materials gained international attention and were widely investigated for strengthening, retrofitting and prestressing of structures. In particular CFRP, having the highest strength and stiffness among all fibre reinforced polymers, can be seen as the technically ideal material for prestressing applications [151]. In contrast to glass-fibre and aramid-fibre reinforced polymers, CFRP is not subjected to stress corrosion [36] or creep [151, 152], respectively. Since the invention of the prestressing technique, the load deflection behaviour of a prestressed concrete structure was linked with the level of prestress and hence dependent thereon. In consequence, it was crucial for the designers and engineers to assess the amount of prestress loss over time which needed to be considered in their designs. First investigated by Magnel [21, 25], this finally resulted in numerous codes and recommendations, e.g. [153-156]. In the case of internal prestressing by CFRP tendons, the main contributors to prestress losses can be seen as elastic shortening, shrinkage and creep of concrete. The measurement and monitoring of prestress losses was performed by different approaches. In [157], Maaskant et al. implemented fibre-optic Bragg grating (FBG) sensors on steel and CFRP prestressing tendons to monitor the prestress losses. They concluded that prestress losses were significantly lower for CFRP compared to steel, mostly due to the 25% lower stiffness of the CFRP tendon. In a later study [158], detachable mechanical strain gauges were placed at a 50 mm distance on the sidewall of prismatic concrete specimens, to evaluate prestress losses without disturbing the bond between tendon and concrete. Direct application of strain gauges on the surface of the tendons was also employed [159], which neglected possible effects of bond disturbance. Recently, a prestressed

concrete strand with an integrated FBG sensor to allow prestress measurements in concrete structures was developed [160]. The center wire of the strand was exchanged with a CFRP wire and a FBG sensor was inserted into the CFRP wire during production.

The prestress needs a certain distance starting from a structure's boundary to be transferred by bond to the concrete. The distance needed to reach the fully prestressed section in a prestressed concrete element is commonly referred to as the prestress transfer length. Knowing precisely where a structural component is fully prestressed and hence external loads could safely be introduced is indispensable. In [66], published in 1999, all major steps to describe transmission of prestress by bond are outlined. Up to that paper, no realistic model had been developed that was able to describe the context of prestress transfer as a whole. This theoretical feat has not been accomplished in the last two decades after the publication of [66]. On the other hand, numerous experimental studies investigating the prestress transfer length of FRP tendons were conducted in the last 20 years. The main outcome in [68], a study of the transmission mechanism of prestress to concrete by FRP, was that the transfer length is mainly affected by the surface characteristics and the size of the tendons. Furthermore, in [68], it was shown that the mechanism of load transfer is different in FRP compared to classic steel tendons. A study about the force transfer of FRP bars in concrete [40] showed that a sand-coated FRP bar had a stress transmission length limited to only $16\varnothing$ and stated this length was smaller in comparison to steel tendons.

The tensile behaviour of CFRP is linearly elastic until failure. In contrast, steel is well known to have an elastic-plastic material behaviour. It is therefore to be expected that brittleness of the CFRP will affect the structural behaviour of a prestressed concrete structure. The structural behaviour requires further investigation and the development of new guidelines. Several institutions around the world were involved in this process for FRP materials since the 1980s. Their findings and approaches have first been reviewed in [161] and more comprehensively in [162]. Both reviews commented that the used FRPs had a lower elastic modulus in comparison to steel and hence they would increase the deflection and the crack width in loaded concrete structures. Additionally, in a study about the rational use of advanced composites in concrete, it was stated that the structural use of FRPs is generally feasible [33]. Later, Bakis concluded that FRP applications would probably be restricted to cases where their properties of low weight, high strength or corrosion resistance are crucial [162].

The short-term and long-term flexural behaviour of FRP prestressed concrete elements were studied experimentally and modelled analytically [38, 43, 56, 57, 148]. This topic is still of recent interest. For instance, Rezazadeh et al. proposed a new simplified approach to predict the flexural behaviour of CFRP-prestressed, simply-supported beams [58]. The new method, based on strain compatibility and on the principle of static equilibrium, showed a good predictive performance for the load deflection behaviour. In terms of prestress transfer length, prestress loss and load bearing behaviour, all of the discussed studies used CFRP tendons with longitudinal stiffnesses lower than 200 GPa [38, 43, 56-59]. The new UHM-CFRP tendons considered here are considerably stiffer than classic CFRP materials and even stiffer than steel. It could be anticipated that this difference in stiffness will have significant influences on the structural behaviour. It must also be remarked that the reduced clinker content in the novel LCHPCs would cause faster carbonation and hence would be a limitation for the use of classic

prestressing steel. The proposed UHM-CFRP tendons, not unlike other CFRP materials, are practically immune to corrosion and hence ideal for the proposed implementation in LCHPCs.

The goal of this work was to provide a first structural characterization of LCHPC beams prestressed with UHM-CFRP prestressing tendons. To support the design of efficient and sustainable structures, the effects of the new LCHPCs and of the UHM CFRP tendons on the prestress behaviour were of particular interest. This study identifies the amounts of each individual contributor to the total prestress loss and discusses approaches for improving the ultimate load bearing capacity of CFRP-prestressed beam elements.

4.2 Materials and Methods

New materials for prestressing of structural concrete elements, UHM-CFRP and LCHPCs, were tested to observe their behaviour during prestressing and during 4-point bending tests of such elements. In addition, the structural behaviour of these beams was also characterized. The related materials, their characterization methods and the experimental program are described in this section.

4.2.1 Raw Materials and Composites

A high performance self-compacting concrete (HPSCC) was selected to investigate the influence of the CFRP prestressing tendon's stiffness on the structural performance of a prestressed concrete beam. This concrete recipe ($w/b = 0.35$), named C1, contained a large amount of ordinary Portland cement CEM I 52.5 R, fly ash, silica fume, sand 0/4, gravel 4/8 and superplasticizer (SP) (ViscoCrete20PlusN, Sika AG). This is the same recipe as recently employed as a reference mix during the development of LCHPCs [149]. It was previously developed, see [163], based on a HPC which was employed by the Swiss precast industry in CFRP prestressed structural elements. In addition, to evaluate the potential of LCHPCs for prestressing applications, the recipe C4 ($w/b = 0.17$) was chosen from three recently developed LCHPCs [149]. This recipe substituted large amounts of cement with limestone filler and an increased amount of silica fume. The amount of sand and gravel was the same as in C1. The clinker reduction between the recipe C4 and the recipe C1 was calculated to be 70%, both mixtures were presented in detail recently in [149].

All concrete compositions were mixed in a 250-l Eirich RV11 mixer. For the recipe C1, all dry components were tumbled for 60 s, afterwards water was added and finally the concrete was mixed for 120 s until a uniform mixture with good flow properties was achieved. The LCHPC mixture C4 was mixed in a slightly adapted manner. Tumbling of the dry components was performed but with a reduced amount of only 100 kg sand 0/4. Then water was added and the recipe was mixed until the superplasticizer started functioning. Finally the remaining aggregates of sand 0/4 and gravel 4/8 were added and the recipe was mixed for another 120 s until a uniform mass with good flow properties was achieved.

The fresh concrete properties were measured according to EN 12350 (2009) directly after mixing. Subsequently a total of nine $150 \times 150 \times 150 \text{ mm}^3$ cube specimens and five beam specimens were cast for each concrete/CFRP combination.

The compressive strength of the concretes was tested on three 150 x 150 x 150 mm³ cubes after 3 and 28 days, following standard EN 12390 (2009). In addition, the static E-modulus of the concretes was measured after 28 days on cylinder specimens (d=50 mm, h= 150mm), following the standard EN 12390 (2013) Method B. Until testing, the samples were stored in a climatic room at 20°C±0.3°C and RH > 95%. The storage conditions of the beam specimens are specified in the general part of section 4.2.2. The test results of all investigated concretes can be found in Table 8.

Table 8: Properties of Concretes

Concrete recipe	Compressive Strength 3 days		Compressive Strength 28 days		Compressive E-Modulus 28 days		Tensile Strength 28 days		Density	Air void content
	[MPa]	Stdv	[MPa]	SD	[GPa]	Stdv	[MPa]	Stdv	[kg/m ³]	[%]
C1-reference*	56.9	0.5	85.7	1.1	35.4	0.4	6.6	0.8	2307	3.6
C1-UTS-Mix	61.8	0.3	87.5	1.6	35.2	0.6	n.a.	n.a.	2272	3.5
C1-UHM-Mix	62.8	0.3	87.9	1.8	35.1	0.8	n.a.	n.a.	2274	3.9
C4-reference*	35.1	0.1	83.3	1.0	38.8	0.6	4.7	0.6	n.a.	n.a.
C4-UHM-Mix	32.9	0.5	88.3	1.2	41.7	0.2	n.a.	n.a.	2368*	3.2*

*data equivalent to [149]

n.a. means not available

In this study, two significantly different CFRP-tendon materials were investigated. The first tendon type represented a standard-modulus CFRP material (UTS-CFRP) and consisted of Tenax®-J/E-UTS50 carbon fibres (Teijin Carbon Europe GmbH, Germany) in combination with a Huntsman XB3515/AD5021 hot-melt epoxy system. The second tendon type was made out of Mitsubishi DIALEDTM K13916 ultra high modulus (UHM) carbon fibres (Mitsubishi Rayon Co. Ltd., Japan) also in combination with the Huntsman XB3515/AD5021 hot-melt epoxy system; hereafter named UHM-CFRP.

The tendon materials were characterized in tensile tests following the standard EN 2561. The longitudinal elastic modulus of the UTS-CFRP tendon was E_{11} of 145 ± 3 GPa and the one of the UHM-CFRP tendon was E_{11} of 509 ± 13 GPa [129]. Both tendon types were produced by Carbolink AG (Fehraltorf, Switzerland) in a tape laying method with a cylindrical surface and a diameter of $d=5.3$ mm. After curing, the tendons were coated with quartz sand particles (63-500 μ m) to enhance the bond between the tendons and the concrete. The chosen sand coating showed its effectiveness recently not only due to its strong bond to concrete but also due to its concrete bond durability [38, 147]. The sand-coated UHM-CFRP tendon was the same tendon type as previously used in [127, 129] but produced in another batch.

4.2.2 Prestressed concrete beam elements

To evaluate the structural behaviour of UHM-CFRP prestressed LCHPC elements, a slender beam geometry was chosen. The beam length was set to 3000 mm, with a height of $h=157.5$ mm and a width of $w=90$ mm. This geometry followed, albeit scaled down to $\frac{3}{4}$, an earlier work in the field of "Pretensioned prestressed concrete members" by Nanni and Tanigaki [69]. The

prestressing tendons were positioned at a distance of 22.5 mm to the bottom and the sidewalls of the beam respectively. The resulting low concrete cover and the chosen prestress level of 800 MPa inside the CFRP prestressing tendons were based on recent literature [42].

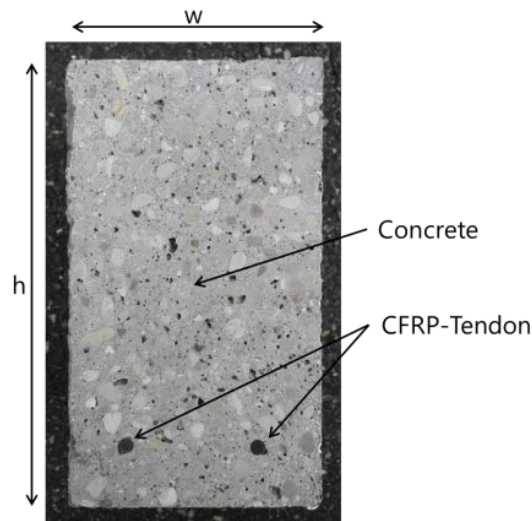


Figure 37: Cross section of CFRP prestressed concrete beam.

The beam elements were produced at Empa by the aid of a specially-designed prestressing rig. This rig allowed the production of up to five beam specimens and the application of the prestressing force to all employed prestressing tendons at once by using two hydraulic cylinders. In addition, to reach a consistent prestress level of $800 \text{ MPa} \pm 5\%$, each tendon could be adjusted individually by a thread mechanism. The prestress level was monitored for each tendon by the aid of a strain gauge which was applied in the free length of the tendon between the formwork and the tendon clamping mechanism. The prestress was released three days after casting. Afterwards the samples were stored in a climate chamber at $20^\circ\text{C} \pm 0.3^\circ\text{C}$ and $90\% \text{ RH} \pm 3\% \text{ RH}$ until 21 days after production. Then the beams were transported into the mechanical testing laboratory and stored until 28 days after casting in controlled climate conditions of $23^\circ\text{C} \pm 2^\circ\text{C}$ and $50\% \pm 5\% \text{ RH}$.

In total, 15 concrete beam elements were cast, 5 beams each for the following combinations; UHM-CFRP and C1, UTS-CFRP and C1, UHM-CFRP and C4.

4.2.2.1 Optical fibre strain measurements

The tape-laying production method of the CFRP tendons allowed for the implementation of fibre optic sensors in the centre of the CFRP prestressing tendon along the tendon's longitudinal axis. The very thin fibre optic sensor ($d=125 \mu\text{m}$) had no significant influence on the diameter of the CFRP prestressing tendon but allowed strain measurements inside the tendon without affecting the tendon's sand-coated surface. Each sensing point inside the fibre optic sensor was represented by a 5 mm-long fibre Bragg grating (FBG). A FBG is in principle a periodic microstructure with a varying refractive index which can be written into the core of the optical fibre by intense ultraviolet light. When strained, the FBG elongates, the fibre index changes and hence the reflected Bragg wavelength of the FBG shifts. The measurement of this shift can be

analysed and correspondingly the strain at the position of the FBG can be calculated [164]. A detailed summary of the FBG measurement principle, their possible applications and variations can be found in [165].

The fibre optic sensors used in this work were DTG-A3A4-A01 fibres produced by FBGS International NV (Geel, Belgium) and supplied by Com&Sens bvba (Eke, Belgium). To preserve the sensitive optical fibre from damage a thin Teflon tube of $d=0.9$ mm covered the optical fibre until 0.32 m ahead of the first sensing point. In addition, to safely protect the optical fibre when outside the CFRP tendon and until reaching the connector to measurement device, a robust Teflon tube of $d=3$ mm was additionally employed.

The available 15 FBG sensing points in the optical fibre were positioned to be able to best record the prestress transfer length. Their detailed positions along the 3 m-long concrete beam specimen can be found in Table 9. The final positioning of the sensing points in the respective prestressed concrete beam element were determined by the aid of a reference marking which was placed on the 3 mm protective Teflon between the end of the concrete beam and the optical fibre connector. Based on the distance measured between the reference point and the concrete beam, the exact position of the first FBG was evaluated and used as reference during the analysis.

Table 9: Specified FBG sensing point position along the concrete beam.

Sensing point #	1	2	3	4	5	6	7	8	9	10	11	12	13	14	15
Position along beam length [mm]	0	12	24	36	60	84	108	156	204	300	996	1248	1752	2004	2760
Group	A	A	A	A	A	A	A	A	A	A	B	B	B	B	A

Before casting, the optical fibres were connected to an FBG SCAN 804D high precision measurement device and the reference zero strain level was set in the analysis software Illumisense V2.2.

The prestress transfer length was measured based on the sensing points of Group A and the measurement of the prestress level was based on the sensing points of Group B. As proposed in literature [166], the prestress transfer length calculation was based on reaching 95 % of the full prestress measured in Group B. The final prestress length was calculated by linear interpolation in between two sensing points of Group A where the 95 % criterion was reached.

The prestress level after casting was calculated for all time points and beam configurations in relation to the first strain measurement taken three days after casting right before the prestress release. This first measurement was considered to correspond to 100% prestress and the subsequent prestress levels were calculated based on this point.

4.2.2.2 Digital image correlation

A LIMESS-Q400 two-camera digital image correlation system (LIMESS Messtechnik u. Software GmbH, Germany) was set up for monitoring the beam elements during loading. In combination with the analysis software Istra4D (Dantec Dynamics A/S, Denmark), this arrangement allowed

measuring the concrete beam's deflection and the strain distribution on the vertical face in the beam's middle third.

The two cameras, each with a 1" sensor and 6 MP resolution, were mounted in a stereoscopic setup on one tripod and placed approximately 1.8 m in front of the experimental setup. The lenses of the cameras had a focal length of 16 mm. The field of view (FOV) in this arrangement was about 1.5 m wide. The camera set up was calibrated with an AL_35_WMB_9x9 calibration target using the implemented procedure in the analysis software Istra 4D. On the vertical surface of the concrete beams, facing the cameras, a randomly-distributed contrast pattern (speckle pattern) was applied. Pictures were taken during the 4 point bending experiments every 2 s. The local surface pattern was automatically assigned in the camera images and the strain distribution as well as the beam's deflection could be evaluated.

4.2.3 Four point bending experimental setup

To investigate the influence of a LCHPC and a UHM-CFRP prestressing tendon on the load bearing capacity of prestressed concrete beams, a simple 4 point bending test configuration was chosen. The distance between the beam support points was set to 2500 mm. This allowed an overhang of 250 mm on each side of the beam and avoided interaction between the prestress transfer area and the loaded beam section. The load was applied by a servo hydraulic cylinder and transferred to the beam by means of a spreader beam. The range of constant bending moment was set to 840 mm in this configuration. All contact points to the concrete beam were steel cylinders with a diameter of $d=50$ mm. An overview of this 4 point bending set up is shown in Figure 38.

Moreover, the mid beam deflection was measured by a linear variable differential transformer (LVDT) of type W20TK HBM (Hottinger Baldwin GmbH (HBM), Germany) to validate the DIC measurement. All beams were loaded continuously at a velocity of 1 mm/min until failure.

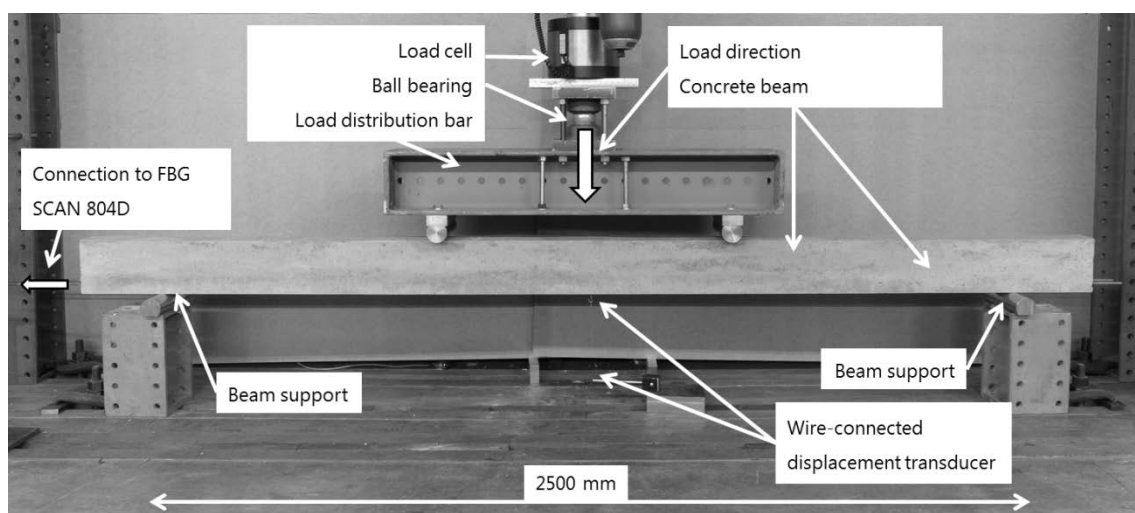


Figure 38: Four point bending test configuration: Overview of mounted sample in experimental set-up.

4.3 Results

4.3.1 Prestress length and loss

The first strain measurements inside the CFRP prestressing tendons were taken three days after casting, right before and after the prestress release. The measurement was repeated for all beams at 7, 14, 21 and 28 days after casting. One additional measurement was performed for C4-UHM-CFRP beams 4 days after casting.

All five beams of type C1-UTS-CFRP were equipped with one sensing and one non-sensing CFRP tendon. In the beam configurations of type C1-UHM-CFRP and C4-UHM-CFRP, four of the five beams were initially equipped with one sensing and one non-sensing CFRP tendon. In these groups of beams, the remaining beam was equipped with two non-sensing CFRP tendons. However, for the C4-UHM-CFRP beams, the very brittle material behaviour of the UHM-CFRP led to the loss of one sensor cable during demolding and the loss of another during transport after the 21 day measurement.

The average prestress transfer length in the beams C1-UHM-CFRP was found to be 173 mm with a standard error of the mean (SEM) of ± 11 mm. The same behaviour was found for the beams C4-UHM-CFRP with a prestress transfer length of 183 mm and a SEM of ± 17 mm. The beams using a standard modulus CFRP tendon, C1-UTS-CFRP showed a significantly shorter prestress transfer length of only 88 mm and a much smaller SEM of ± 2 mm. Over time, between prestress release and until 28 days after casting, no significant change in the prestress transfer length could be observed for any of the investigated beam types. The detailed results of the prestress transfer length measurement can be found in Figure 39. In this Figure, the obvious drop in the prestress transfer length for C4-UHM beams after 28 days was caused by the loss of one sensing tendon. As a consequence, the last calculation of the averaged prestress transfer length for C4-UHM-CFRP beams, see Figure 39, was based only on two beams.

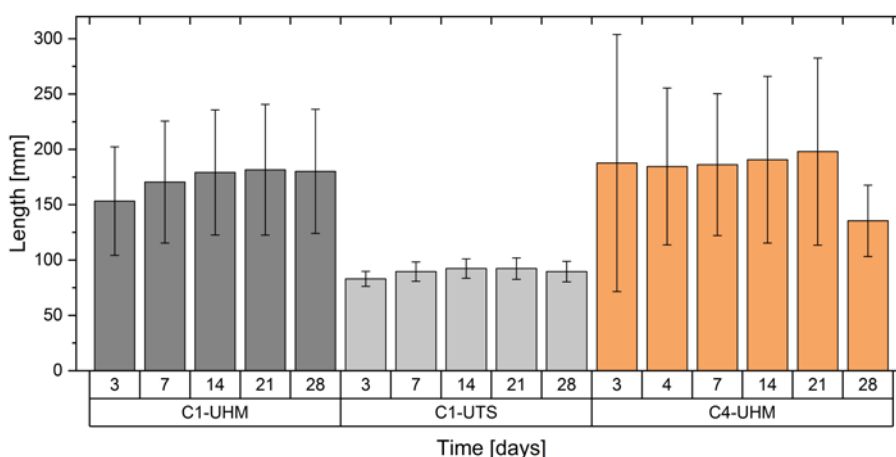


Figure 39: Prestress transfer length development over time. The bars show the averaged value of the beams investigated including their standard deviations. The drop in prestress transfer length for the C4-UHM-CFRP beams after 28 days is caused by the loss of one sensing tendon after the 21 day measurement.

The initial prestress level after release was measured on average with 75 % for C1-UHM-CFRP beams, 96 % for C1-UTS-CFRP beams and 75 % for C4-UHM-CFRP beams respectively. Afterwards, the prestress level of all investigated beams showed a clear decrease over time. The total loss was most pronounced in the beams C4-UHM-CFRP measured with 42 % in relation to the initial prestress. The C1-UHM-CFRP beams showed also a high loss of 40 % while the C1-UTS-CFRP beams showed significantly smaller losses of only 11 % when measured 28 days after casting. A detailed overview of the prestress level and its behavior over time for each configuration can be found in Figure 40.

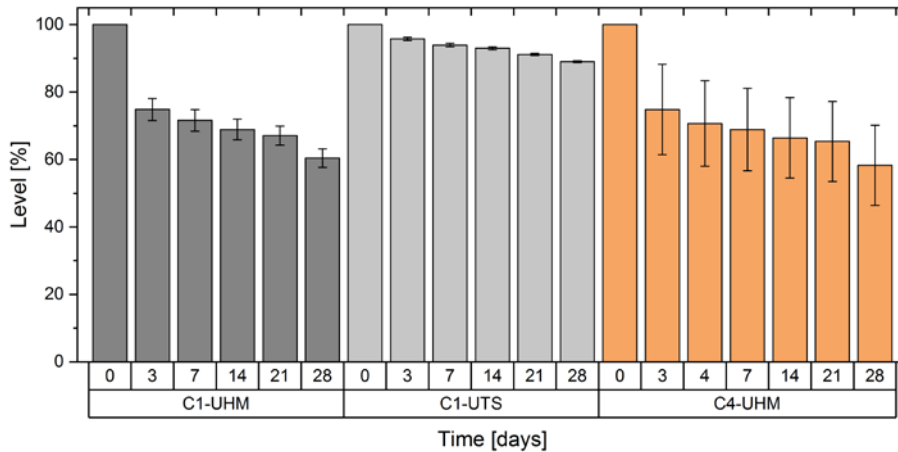


Figure 40: Prestress level development over time. The bars show the averaged value of the beams investigated including their standard deviations.

4.3.2 Concrete beam deflection and maximum load bearing capacity

The aim of this experimental program was to investigate the influence of UHM-CFRP prestressing tendons and LCHPC on the structural behaviour of prestressed concrete elements. For this purpose, three beams of type C1-UHM-CFRP and C4-UHM-CFRP as well as two beams of type C1-UTS-CFRP were tested in 4-point bending tests. All samples were loaded continuously at a constant velocity of 1 mm / min.

A similar deflection behaviour was observed in all beam types in the first branch of loading. In contrast to this first branch, where all beams showed a very similar constant load increasing rate of about 3.40 kN / mm, this was different in the second branch. The beam types C1-UHM-CFRP and C4-UHM-CFRP showed a load increase rate of 0.88 kN / mm and 0.97 kN / mm respectively. The beam type C1-UTS-CFRP deflected faster and had a load increase rate of 0.23 kN / mm, see Figure 41 A. In the transition zone between the first branch and the second branch, the rate of increase of the load decreased progressively.

All beams failed in a sudden and complete breakdown due to CFRP tendon rupture. The averaged maximum failure load is shown for all beam types in Figure 41 B. The C1-UTS-CFRP beams had clearly the lowest load carrying capacity of 21.68 kN. The beams C1-UHM-CFRP and

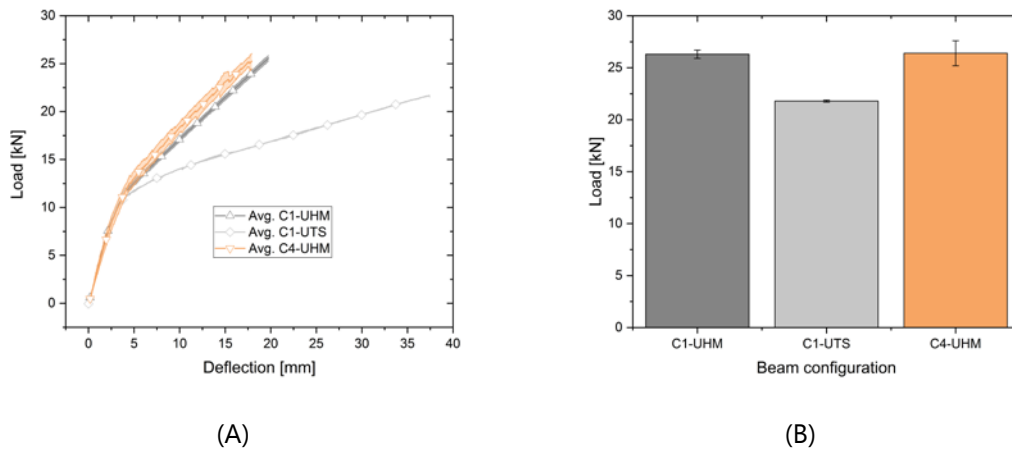


Figure 41: Results of 4p-bending tests performed, 28 days after casting, on CFRP prestressed beam specimens. Orange indicates the new C4-UHM-CFRP beam type, dark grey the C1-UHM-CFRP beams and light grey the current industry standard C1-UTS-CFRP type. All beams were initially prestressed to the same level of 800 MPa. The averaged bi-linear load deflection behaviour for the different beams is shown in (A), including their standard deviations. The corresponding maximum load bearing capacity is visualized in (B), also including their respective standard deviations.

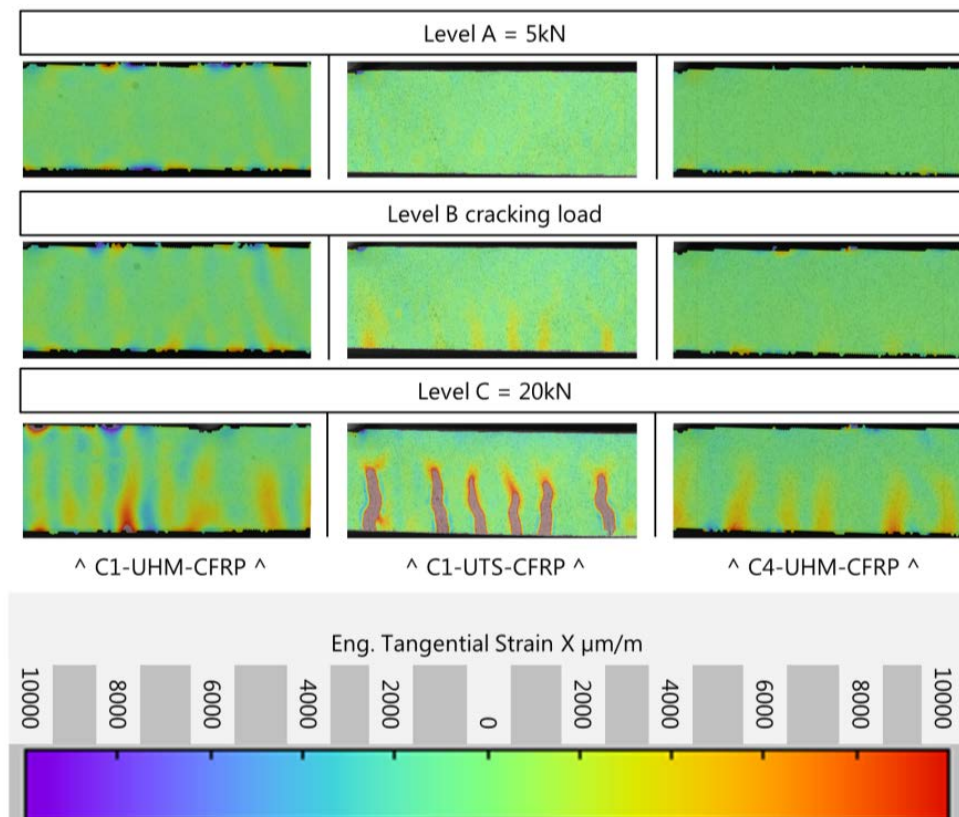


Figure 42: Visualization of the surface strain pattern along the horizontal direction of the beam's vertical face at selected load levels. Level A corresponds to a load of 5 kN, level B to the cracking load and level C to 20kN. The left column represents a beam of type C1-UHM-CFRP, the middle column an industry standard type C1-UTS-CFRP and the right column the new C4-UHM-CFRP beam type. The distance between the cracks in the pattern of the different beam types was similar; all showed about 6 cracks in the same field of view. The crack width was visually larger for beams prestressed with C1-UTS CFRP tendons. A precise crack width analysis was not performed.

C4-UHM-CFRP reached on average maximum loads of 26.31 kN and 26.37 kN respectively. The corresponding maximum beam deflections at the middle of the span were measured for C1-UTS-CFRP beams with an average of 37.85 mm. The beams C1-UHM-CFRP and C4-UHM-CFRP deflected less and reached an average of 20.76 mm and 19.18 mm respectively. At the point of failure, the ultimate strain inside the CFRP prestressing tendons was on average 1.08 % in the case of UTS-CFRP tendons and 0.38 % in the case of UHM-CFRP tendons.

Furthermore, the strain distribution on the vertical face of the concrete beams was measured with the DIC system. Typical results for each type of beam are shown in Figure 42. In this visualization, it is clearly visible that the cracks in the C1-UTS-CFRP beams open more in comparison to both UHM-CFRP prestressed beam types. The beams which are not shown in this graph had very similar strain patterns within their respective group of beams.

4.4 Discussion

4.4.1 Effects of UHM-CFRP tendons in prestressed concrete

The implemented UHM-CFRP tendons were 3.5 times stiffer in comparison to their UTS CFRP counterparts. Not surprisingly, their response to the beam's strain changes (shrinkage and creep, see Chapter 3), after the prestress release, were found to be more significant and resulted in much lower tendon stress levels. In addition, the measurement of the prestress transfer length and the prestress level revealed a large scatter for beams prestressed with UHM-CFRP tendons; see results in and . Both of these values are generally dependent on the effective strain distributions inside the beams that are reached after prestress release (when elastic shortening of the concrete happens) but also over time (due to creep and shrinkage of the concrete). In this context, local concrete material variations, geometrical beam imperfections and prestress tendon positioning tolerances seem likely to affect the prestress related parameters in UHM-CFRP prestressed beams more significantly than in UTS-CFRP prestressed beams. Due to the higher longitudinal stiffness of UHM-CFRP, this effect is proposed to be resulting in the larger scatter found in the experiments. In other words, beams prestressed with UHM-CFRP can be expected to be more sensitive in their resulting prestress force and this uncertainty should be considered when designing such beams in practice.

4.4.2 Effects of UHM-CFRP tendons on the structural behaviour of prestressed concrete beam elements

In 4-point bending, the scatter in the load-deflection behaviour was found to be much smaller within each group of beams if compared to the analysis of the prestress level and length. In the case of deflection, the overall beam geometry was dominant for the investigated behaviour. Within the given beam dimensions, the influence of the local material variations, the geometrical imperfections and the tendon positioning tolerances were of minor importance and likely to have resulted in only small deviations within each respective group of beams.

The tested prestressed concrete beams showed the expected bi-linear moment deflection behaviour; see [35, 167] and . This bi-linear behaviour could be described by the flexural stiffness in the respective section. The flexural stiffness follows the gross moment of inertia (I_g) in the first branch ($M < M_{cr}$), the cracked moment of inertia (I_{cr}) in the second branch ($M > M_{cr}$) always in combination with the elastic modulus (E) of the concrete [167]. For the beams used in this study, I_g is affected little by the presence of the CFRP tendons, see Table 10. Consequently, the behaviour until cracking should be comparable for all investigated beam configurations, which was indeed confirmed by the experimental results. When using the transformed area diagram to calculate I_{cr} , see [168], it is obvious that I_{cr} must be smaller than I_g . In this case the contribution of the rectangular cross section of the concrete beam decreases while the contribution of the CFRP tendons, due to Steiner's theorem, increases. Moreover, the contribution of the CFRP tendons to I_{cr} is proportional to the modular ratio between tendon and concrete ($n = E_{cfRP}/E_c$) which would logically result in a stiffer deflection behaviour in the cracked state for UHM-CFRP tendons in comparison to their UTS-CFRP counterparts. Both expectations were confirmed by the experimental results. In fact, the relation between the cracked moments of inertia $I_{cr,UHM}/I_{cr,UTS}$ was calculated to be 2.9, which corresponds well to the ratio of 3.0 found in the experimental deflection of both beam types.

Table 10: Moments of inertia of cracked and un-cracked beams and the modular ratio between CFRP and concrete

Beam configuration	I_g [mm ⁴]	$I_{cr,exp}$ [mm ⁴]	$I_{cr,cal}$ [mm ⁴]	n [-]
C1-UTS-CFRP	$2.97 \cdot 10^7$	$2.59 \cdot 10^6$	$2.65 \cdot 10^6$	4
C1-UHM-CFRP	$3.11 \cdot 10^7$	$7.75 \cdot 10^6$	$7.66 \cdot 10^6$	14
C4-UHM-CFRP	$3.08 \cdot 10^7$	n.a.	n.a.	12

n.a. means not available

However, the load bearing capacity of beams prestressed by UHM-CFRP tendons exceeded the capacity of beams prestressed by UTS-CFRP tendons. This was unexpected considering the results of the tensile tests on the respective materials, see Table 11 . In these characterization tests, UTS-CFRP showed a significantly higher tensile strength when compared to UHM-CFRP. Based on these results, in combination with the analytical beam deflection model of Rezazadeh et al. [58], the maximum load carrying capacity of UTS-CFRP prestressed beams was calculated to be 11.34 kNm and for UHM-CFRP beams 11.10 kNm. Both calculations assume a tendon tensile failure. This could be assumed based on calculating a critical amount of CFRP. A value smaller than the critical value would yield towards a tendon's tensile failure and a value larger to concrete crushing. For the investigated beams, following [58], the critical amount of CFRP was calculated to be 2.01 % for C1-UHM-CFRP prestressed beams and 0.61 % for C1-UTS-CFRP prestressed beams. The real amount of CFRP in the tested beams reached only 0.36 %. Accordingly, the assumption in the model to have tendon tensile failure in both cases could be verified.

Table 11: Longitudinal properties of CFRP tendons

Tendon material	Tensile Strength S_{11u} [MPa]	Young's Modulus E_{11} [GPa]	Design Tensile Strength S_{11uD} [MPa]	Ultimate tendon stress in beams S_{11u_beams} [MPa]
UHM-CFRP	1562 ± 68 *	509 ± 22 *	1426 *	1924 ± 146
UTS-CFRP	2031 ± 31	145 ± 4	1969	1561 ± 34

*data equivalent to [129]

The employed model of Rezazadeh et al. described the experimental load-deflection behaviour with accuracy, see Figure 43 A. The observed differences in the load bearing capacity could be based on multiple reasons. Two of them are discussed in the following.

First, the concrete properties itself could be affected and hence the critical ratio between the CFRP tendons and the concrete could have been changed and so the failure mode of the beams. The beam's top-fibre compressive strain was analysed after the 4 point bending experiments with the help of the DIC system, Figure 43 B. These results indicate clearly that the maximum compressive strain in UTS-prestressed beams reached a value of 0.0018 and in UHM-prestressed beams 0.0012 respectively. Both values are significantly lower than the suggested peak strain of 0.003 given by ACI [35]. Hence it could be concluded that the concrete was far from crushing and is not expected to be the cause of the beam's early failure.

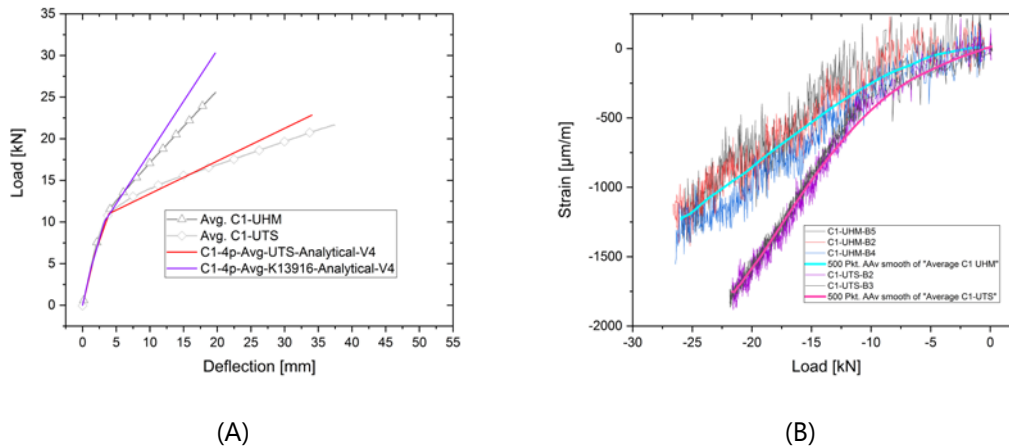


Figure 43: Influences on a prestressed beam's deflection behavior: A: Analytical deflection modelling, based on the approach of Rezazadeh et al. [58], in comparison to the experimental results. B: Development of the concrete's top fibre strain for C1-UHM-CFRP beams and C1-UTS-CFRP-beams during loading.

Secondly, the stress distribution inside the CFRP tendons in a cracked section of the beam could be different to the assumed ideal tensile stress condition. This case would be reasonable if large transverse stresses were introduced either by the large deflections of the UTS-CFRP prestressed beams or due to the different CFRP material properties. Hence, the tendon would show an unexpected early failure.

The respective situation in the investigated beams was analysed by a simplified finite element analysis using a quarter model of a beam's cut-out section. In this model the materials were

modelled with a linear elastic behaviour. The beam's concrete geometry was cut to represent the crack until the position of the neutral axis as observed in the experiments. After releasing the prestress from the CFRP tendon, the different beam types were continuously loaded with the bending moment corresponding to the ultimate bending moment found in the experimental program. To account for possible damage of the bond interface between tendon and concrete, the first 3 mm on the side of the crack were modelled with a high tangential friction ($\mu=0.8$) contact behaviour. The remaining contact of the tendon was ideally bonded to the surrounding concrete. The initial prestress was chosen so that the remaining prestress after the release was the same as in the experiments. Time-dependent properties of the concrete, such as creep and shrinkage, were not included in the model. This simplification was based on the short time frame of the investigated cracked beam situation shortly before failure. In this short term situation it can be assumed that shrinkage and creep would not influence the structural behaviour. For validation of the model, the curvature at the ultimate bending moment as well as the prestress inside the tendon after release were analysed and compared. At the experimental failure load, the UTS-CFRP prestressed beams showed a tensile stress in the tendon's vertical direction (S_{22}) of >50 MPa and the UHM-CFRP tendons of around 20-25 MPa, Figure 44. Both are critical values in the transverse direction, e.g. in [169] a comparable unidirectional CFRP material reached a transverse tensile strength of only 24 MPa. It can be concluded that the low load bearing capacity of the UTS-CFRP beams was due to the unfavourable stress situation in the limit state. According to the FEA this was found to be more critical for the UTS-CFRP beam than for the UHM-CFRP beam, see Figure 44.

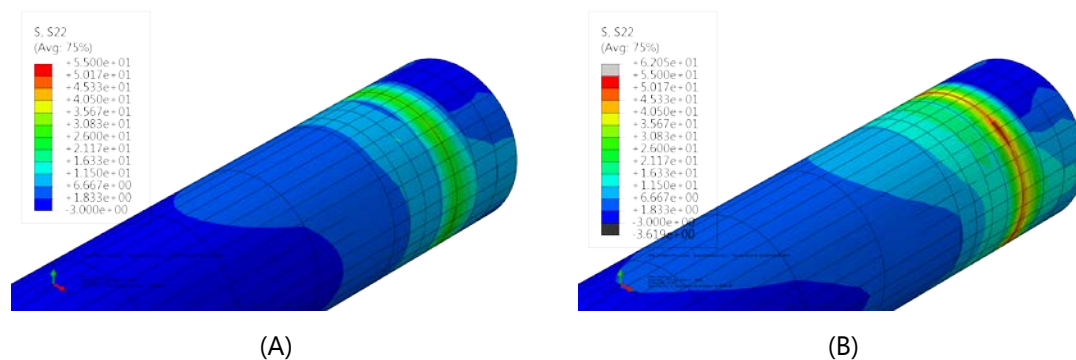


Figure 44: FEA results showing the vertical stress component (S_{22}) in the CFRP tendons at ultimate load condition. A: For a C1-UHM-CFRP beam. B: For a C1-UTS-CFRP prestressed beam.

4.4.3 Effects of LCHPC on CFRP prestressed structural elements

The tested LCHPC recipe (C4) had both Young's modulus and compressive strength very close to the current industry standard C1, see Table 8. Hence, the deflection behaviour was mainly controlled by the UHM CFRP prestressing tendons and not by the LCHPC, -A. In addition, effects on the prestress loss based on the lower shrinkage and creep of LCHPC (C4) in comparison to HPC (C1) were expected but could not be identified in the experimentally investigated prestressed concrete beams. This was mostly caused by the high scatter in the experimental results observed in the C4-UHM-CFRP beam specimens, see .

Recently, in [149], the effects of shrinkage, creep and elastic shortening on prestress losses in LCHPC prestressed elements were estimated based on an idealized and simplified finite element

analysis. Their element's geometry was based on a shrinkage and creep test specimen to reduce geometrical effects of the specimen on modelling shrinkage and creep and hence to allow a comparison between modelling and the respective experiments. The beams used in this study did not have the same dimensions as the specimens examined in [149]. The cross-sectional area of the employed beams was 1.97 times larger than the creep and shrinkage specimens in [149]. In a first step, the FEA model, developed in [149], was adapted in geometry and applied to the beam specimens tested in this study. For validation, the results of prestress losses after 28 days were compared to the measured prestress losses, see Figure 45 A. Within a small tolerance, the values measured experimentally were very well predicted by the FEA. The contribution of the elastic shortening, shrinkage and creep on the prestress loss were analysed based on the FEA, Figure 45 B. As in [149], it was found that all three contributors deliver noteworthy amounts of prestress loss to the investigated beam specimens. Based on the FEA, the prestress loss in LCHPC beams was calculated to be only around 3% less in comparison to their HPC beam counterparts, see Figure 45 A and B. Considering the large scatter in the experimental prestress loss measurements, this effect could neither be disproved nor confirmed by the experiments.

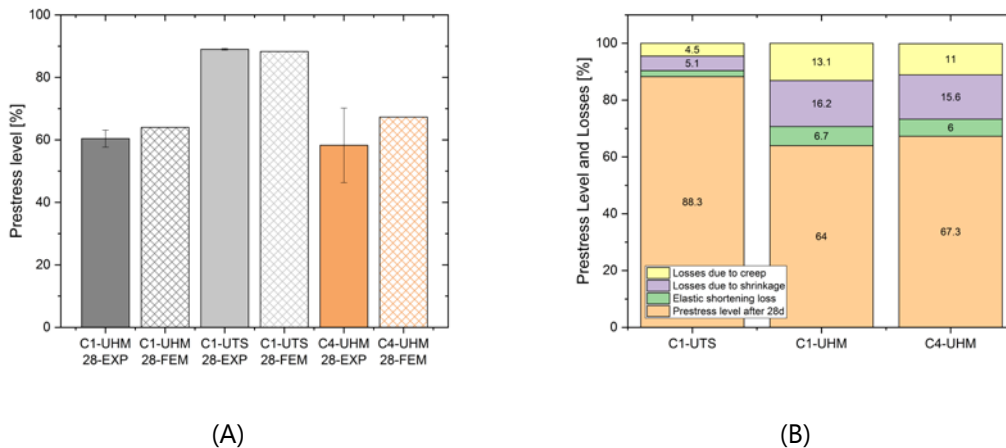


Figure 45: Prestress loss assessment. A: Comparison of experimental results with FEA predictions. B: Breakdown of prestress losses into the three main contributions of shrinkage, creep and elastic shortening based on the FEA.

As a result, the theoretical benefit of a higher remaining prestress in the structure due to the lower creep and shrinkage was not significant, not even in the case when the tensile-wise very sensitive UHM-CFRP tendons were used for prestressing. However, the experiments described in this paper confirm that the LCHPC, with their clinker reduction of up to 70 %, could be used as a replacement for the current HPC in CFRP prestressed structural elements without compromising their short term mechanical performance. These results are considered to be valid for the specific case investigated in this study. The effects of creep and shrinkage might be different in structures of other dimensions, which would need further investigations that are beyond the scope of this work.

4.5 Conclusions

Based on monitoring the prestress inside beam specimens up to 28 days after casting, full scale 4-point bending beam tests and additional upscaling of a small scale FEA model to structural level in Abaqus 6.14, the following conclusions can be drawn:

- The prestress transfer length is affected by tendon stiffness. Here, the shear stress transfer between the prestressing tendon and the concrete is dependent mainly on the stiffness of the materials in the direction of the applied prestress. Hence, in the same concrete recipe, the stiffer tendon has the longer transfer length.
- UHM-CFRP prestressed structures showed less deflection, narrower cracks and also an increased load bearing capacity in comparison to their UTS-CFRP prestressed opponents. When using UHM-CFRP, the structure could be used more efficiently in terms of its structural performance.
- LCHPC, with much lower clinker content than traditional HPC, is well suited for prestressing applications. In particular, the flexural behaviour of prestressed beams was not that different from the reference HPC. While LCHPC has lower creep and shrinkage, in the particular structure investigated in this study no benefits in term of reducing prestress losses was observed, possibly due to the high scatter of these measurements.

The results of this work show very good potential for improving the current CFRP prestressing technology at the structural level by using UHM tendons. However, these results still focus mainly on the short-term behaviour of a prestressed structure. Critically, also data about the structural behaviour and its integrity over a longer period of time (several years) in harsh environmental conditions would be needed. This would give confidence into the industry about these new material trends and finally bring this technology into construction.

Acknowledgements:

This research project was part of the joint project "Concrete Solutions" within the framework of the National Research Programme "Energy Turnaround" (NRP 70) of the Swiss National Science Foundation (SNSF). Further information on the National Research Programme can be found at www.nrp70.ch. We are grateful to Daniel Käppeli, Sebastiano Valvo, Marcel Käppeli, and Daniel Völki for their strong support during sample production and testing.

CHAPTER 5

Life Cycle Analysis of CFRP prestressed LCHPC ^d

Abstract

UHM-CFRP prestressed LCHPC beam elements were recently developed with the aim of reaching the same mechanical performance as classic CFRP-prestressed HPC elements but at a much lower cost of embodied energy and CO₂ emissions. A previously-performed environmental assessment promised a large energy and emission saving potential when using classic CFRP prestressed elements instead of a steel reinforced concrete structure. In this study, the considered measures were the global warming potential (GWP), the cumulative energy demand (CED) and the ecological scarcity method (UBP). In this study, the saving potential was calculated to be around 83% for the UBP, 75 % for the GWP and about 61% for the CED measure. After finishing the development of the CFRP prestressed LCHPC beam elements (see Chapters 2-4), this evaluation was repeated and adapted to the new materials. The additional saving potential for using LCHPCs was found to be 9%, 15 % and 20 % for the UBP, GWP and CED measure respectively. However, these results also revealed a high sensitivity of the results to the chosen functional unit. Hence, for assessing the full potential of the new technologies, additional investigations would be needed to gain more robust results.

Keywords

Low clinker high performance concrete (LCHPC), high performance concrete (HPC), CFRP, prestressing, Life cycle assessment (LCA), Environmental savings potential (ESP), Ecoinvent 3 database, SimaPro

^d This chapter is in part based on a paper by Zingg et al. presented at the Sustainable Built Environment (SBE) conference in Zurich in 2015 [129]. Among other topics dealt with in this paper, one aspect were slender prestressed concrete elements. In particular, the possible advances in reducing emissions due to the use of LCHPCs and CFRP prestressing tendons. Some of the content presented in this chapter, in particular the gained results about the initial calculation of the saving potential of CFRP prestressed structural elements, the employed methods and conclusions were either directly taken, adapted or rewritten based on [129]. Thereafter, based on the model of Zingg et al. [129], additional knowledge was created by evaluating the environmental saving potential of the novel LCHPCs which were developed in Chapter 3 and the CFRP-prestressed LCHPC beam elements which were developed in Chapter 4. This additional knowledge was combined with the work of Zingg et al. to form this chapter. The full bibliography of the work of Zingg et al. is given here:

S. Zingg, G. Habert, T. Lämmlein, P. Lura, E. Denarié, A. Hajiesmaeili, *Environmental assessment of radical innovation in concrete structures, Sustainable Built Environment (SBE) Regional Conference, Zurich, Switzerland, June 15-17, 2016, vdf Hochschulverlag AG, G. Habert, A. Schlueter (Eds.) 2016, p. 687.*

5.1 Introduction adapted after [124]

The Swiss energy market is likely to change within the next decades. This change is seen to be mainly caused by the introduction of new technologies but also due to economic changes and for political reasons. To best prepare the Swiss economy for this expected change the Federal Council developed the Energy Strategy 2050 with the goal to reduce the energy related environmental impact and hence to secure the current energy supply standard [170]. To support this strategy and to develop new construction materials and techniques with low embodied energy and low carbon emissions, the Swiss National Science Foundation (SNSF) launched the National Research Project (NRP) 70 "Energy Turnaround". As mentioned earlier in this thesis, see Chapter 1, the production and use of building materials, in particular of concrete, is energy intensive and responsible for large amounts of CO₂ emissions. The joint project "Concrete Solutions" was setup in the framework of the NRP70 to investigate low energy construction materials and techniques to finally support the Energy strategy 2050.

The presented development of novel UHM-CFRP prestressed LCHPC elements, see Chapters 2–4, was part of the joint Concrete Solution project and aimed to reduce the environmental impact of such elements without compromising the element's mechanical performance. On the one hand, the motivation for this approach was based on recent guideline developments in 2014 (SIA Merkblatt 2049), which allowed clinker substitution in concretes of up to 65% [60]. This is significantly more than the current allowances in the European standard EN 197-1 of 35 % [61]. On the other hand, the material development in CFRPs progressed since they were first introduced for prestressing of concrete in the 1990ies [39]. New -CFRP materials with ultra-high modulus (UHM) became recently affordable but their potential in prestressed concrete elements had not yet been evaluated. The particular advantage of using CFRP for prestressing of concrete elements is its low-weight and corrosion resistance [171]. This allows the production of slender prestressed concrete elements without the need of additional concrete cover to prevent possible corrosion. Even though the production of CFRP is known to be more energy intensive than steel, as found by Griffing et al. [172] and stated in Zingg et al. [124], the benefit from reducing the concrete volume was expected to dominate. The goals in terms of the mechanical performance were reached during the development of sustainable second generation CFRP-prestressed concrete elements and presented in Chapter 4 of this thesis.

The aim of this Chapter is to put the potential environmental saving of this new technology in the context of well-established technologies such as reinforced concrete and steel-prestressed concrete. Therefore, the saving potential was evaluated before, during and after the development of the novel UHM-CFRP prestressed LCHPC elements. This approach allowed the potential savings due to the prestressing technique in general, the use of LCHCPs and finally on the CFRP-prestressed concrete elements to be isolated.

5.2 Material and Methods taken from and adapted after [124]

To evaluate the environmental impact and hence to assess the sustainability of UHM-CFRP prestressed LCHPC elements, a life cycle assessment (LCA) was performed. The LCA was based

on the ISO standard 14040 [173] and used the Swiss Ecoinvent 3 database [174] in combination with the SimaPro 8.0.5 LCA software.

The analysis was done in two separate parts. First, the current state of the art CFRP prestressed element technology was analysed and compared to reinforced concrete and classic steel prestressed structures. This first stage also included a future prospect for CFRP prestressed structural elements with an estimate for potential use with novel low clinker concretes. In the second part, the novel LCHPCs were analysed to their environmental impact separately but also in the context of the recently developed UHM-CFRP prestressed LCHPC beam elements, see Chapter 3 and Chapter 4. For simplification only one type of CFRP material was considered during the analysis in this chapter. As shown in Chapter 4 both tendon materials, UHM-CFRP and UTS-CFRP, showed a comparable load-deflection behaviour until crack initiation in a concrete beam. During the design of such beams in Switzerland the commonly used criteria is to not decompress the prestressed concrete and hence to avoid cracking in the long term. Therefore, the simplification to use only one CFRP material can be seen to be reasonable.

The employed methods, the material data and the chosen functional units are described in the following.

5.2.1 Impact assessment methods ^{taken from [124]}

The impact assessment methods were the same as used by Zingg et al. [124]. Hence, their description is directly applicable to this work and was described previously in [124] as follows:

“The LCA methods used in this study are harmonized with the methods employed in the KBOB list, a well-established LCA dataset of buildings and constructions in Switzerland [175]. In particular, these methods are: the IPCC 2013 100a method for the calculation of the Global Warming Potential (GWP) or greenhouse gas emissions (also termed as carbon emission in this paper) [176]; the Cumulative Energy Demand (CED) for the calculation of primary energy demand [176]; and the Ecological Scarcity Method 2013 for the calculation of total environmental impacts (UBP) or eco-points [177]. UBP integrates different environmental factors into one indicator. It is an indicator particularly applicable for Switzerland as the method employs eco-factors based on Swiss environmental targets and legislation.”

5.2.2 Functional unit and system boundary ^{adapted after [124]}

Three different functional units (I-III) were defined for the assessment of the different stages in the LCA. The state-of-the-art CFRP prestressed HPC elements were analyzed based on one linear meter of a reference prestressed concrete beam, see [178] and Table 12. The novel LCHPCs were analysed first on one cubic meter of concrete to see the direct concrete material's influence and afterwards on one linear meter of a UHM-CFRP prestressed structural beam element, see Chapter 4 and Table 12.

All functional units were chosen accordingly, so that the mechanical performance and the service life of the investigated technology were comparable to their respective reference.

In all cases, the LCA was based on a cradle-to-gate approach. This approach includes all emissions from material extraction up to the final production. It does not include emissions due to further transportation apart from the production plant nor for set-up or infrastructure on the construction site. The chosen functional units are summarized in Table 12.

Table 12: Overview of the functional units I-III as they were used in the LCA. In particular the relevant data of the functional unit I was taken from [124]. The data for functional units II and III were calculated based on the model developed in [124].

Functional unit	I			II	III	
	Conventional reinforced concrete ^a	Steel prestressed HPC slab ^b	CFRP prestressed HPC slab ^c	Concrete (HPC vs. LCHPC)	CFRP prestressed HPC beam	CFRP prestressed LCHPC beam
Tensile load, kN	270	270	270	n. a. ^e	n. a.	n. a.
Concrete strength, MPa	30	90	90	86, 77, 88, 83	86	77, 88, 83
Cross section, cm ²	900	429 ^d	189	n. a.	142	142
Volume, m ³	0.09	0.043	0.019	1	0.14	0.14

^a 1.12% vol. steel; ^b 0.85% vol. steel; ^c 0.84% vol. CFRP;

^d Additional concrete cover for steel protection is included; ^e n.a. means not available

5.2.3 Data sources and acquisition ^{adapted after [124]}

The main data source for the LCA analysis on all levels was the Swiss Ecoinvent 3 database [174]. Unavailable material data which was not included in the database, e.g. CFRP, was modelled using data from relevant literature.

5.2.4 Environmental savings potential ^{adapted after [124]}

The applied LCA methods had different environmental factors as their objective. For instance, the calculation of the GWP factor indicates the global warming potential of a technology, the CED factor indicates the primary energy demand and the UBP factor integrates different environmental factors in one point-based indicator which is in particular valid and hence interesting for Switzerland.

The impact of a new technology is not necessarily the same for all three indicators. For a better comparison the environmental savings potential (ESP) was calculated after [124] as a percentage using an adapted formula from [179], see Formula (1).

$$ESP = \frac{Impact_{ref} - Impact_x}{Impact_{ref}} \times 100 \quad (1)$$

In this formula, $Impact_{ref}$ corresponds to the environmental impact (GWP, CED or UBP) of the reference technology and $Impact_x$ to the environmental impact of the improved technology respectively. In this context, a positive ESP indicates a reduced environmental impact of the

assessed technology in comparison to their reference. In contrast, a negative *ESP* would logically indicate a larger environmental impact in relation to the reference.

5.3 Results and Discussion

This section presents the results of the environmental assessments performed in the context of the development of novel UHM-CFRP prestressed LCHPC beam elements. Three different calculations were performed. First, the potential of CFRP-prestressed concrete elements was evaluated in comparison to a reinforced concrete structure and to the alternative of a steel-prestressed concrete element. These results were taken from [124] and the calculation was based on the functional unit I (see Table 12). Furthermore, in the second evaluation set, the novel LCHPCs (Chapter 3), were analysed individually and their *ESP* was compared to the reference HPC recipe C1 based on the functional unit II (see Table 12). Finally, in the third evaluation, the novel CFRP-prestressed LCHPC beam elements were analysed and their *ESP* was compared to a reference beam produced by using the reference concrete C1 and the functional unit III (see Table 12).

5.3.1 Pre Assessment of CO₂ saving potential taken from and adapted after [124]

Relative to a reinforced concrete structure, the environmental assessment of CFRP prestressed HPC element showed a saving potential in energy of around 60% and in emissions of about 70%. This large saving potential is thanks to almost a fivefold reduction in volume of the beam (Table 12). However, a more reasonable evaluation of the *ESP* in terms of functional structural units would be the comparison between steel-prestressed HPC and CFRP prestressed HPC. In this case, the *ESP* calculation still shows a saving of around 10% in energy and more than 20% in emissions (Table 12).

Prior to the development of the LCHPC (Chapter 3), the potential of substituting cement in a CFRP prestressed HPC element was estimated by using a fictitious cement with only 40% clinker content. This potential clinker replacement was calculated to give an additional 5% to 8% *ESP* in comparison to the CFRP prestressed HPC elements. These results are also presented in Figure 46 and indicated by the label HPC-CFRP optima.

The saving potential of CFRP prestressed structural elements, however, is less than anticipated when only the volume reduction and hence concrete saving of about 56% (Table 12) for these elements would be considered. The main reason for that lower difference in saving potential could be directed to the high impact of the CFRP prestressing tendons, in particular visible in the CED measure, see Figure 46.

In the Ecoinvent 3 database, the life cycle inventory of CFRP was not yet included. The production process of the employed CFRP prestressing tendons needs several steps. First the two components of the CFRP, the carbon fibres themselves and the epoxy resin need to be produced. In particular, the production of the carbon fibres is highly energy intensive due to high temperatures (up to 3000°C) needed in the carbonization process of the fibres. After the production of the fibres and of the epoxy resin, the CFRP material can be formed in a subsequent manufacturing step. In the case of prestressing tendons with a circular cross section

and a longitudinal fibre direction the pultrusion process would be best suited. For assessing the life cycle inventory these steps were considered and modelled following Griffing and Overcash [180] for the carbon fibre production, Suzuki and Takahashi [181] for the pultrusion process, and Terrasi [178] for the carbon fibre epoxy mix. From a sustainability perspective, further improvements would be most needed in the process of carbon fibre production. If this could be optimized and less energy would be consumed, the sustainability would improve effectively. As for many materials, the efficiency in the carbon fibre production is largely dependent on the technology and the used facilities [172]. The production scale of carbon fibre is not yet large enough to result in high efficiency as the large-scale carbon fibre production industry is still relatively young [181].

The results presented in Figure 46 are based on a cradle-to-gate approach. A further reduction of the environmental impact of CFRP-prestressed HPC could be expected during the construction phase. Additional savings due to the low weight and slender dimensions of such elements would occur during transportation and set-up (smaller and less machinery). In addition, they would need smaller foundations and linkages. In combination with recycling of the related materials this could bring further savings when the process would be looked at in a cradle-to-grave or cradle-to-cradle approach. However, this goes beyond the scope of this chapter, which is focused on evaluating the sustainability of CFRP-prestressed concrete elements.

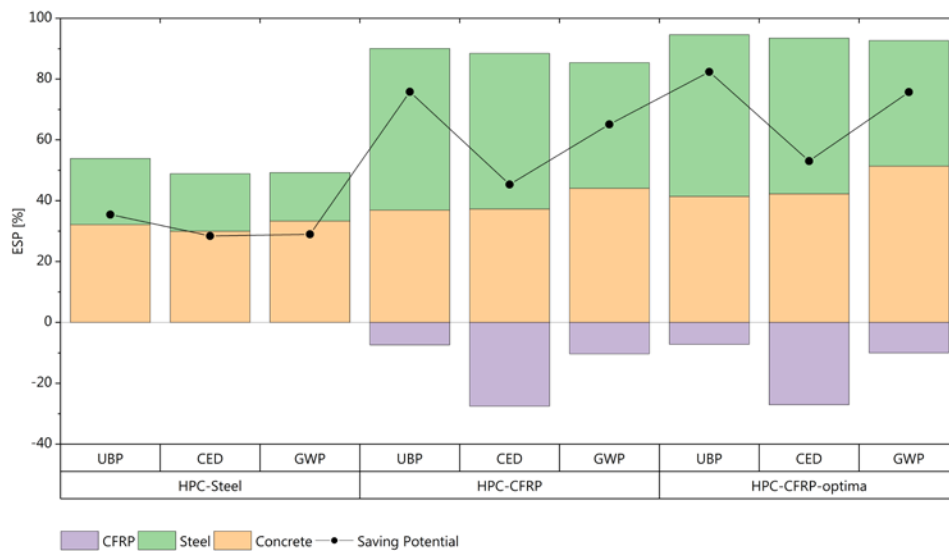


Figure 46: Environmental saving potential for different prestressed concrete elements in comparison to a conventional reinforced concrete structure. This comparison is based on one linear meter of the functional unit I, see Table 12. For steel-prestressed and CFRP-prestressed HPC elements, the recipe of C1, see Chapter 3, was considered; for the estimation of CFRP prestressed HPC-optima a concrete with a fictitious 40% clinker content was used. The data was taken from and the graph redrawn after [124].

5.3.2 Savings in LCHPCs and CFRP prestressed LCHPC beam elements

After the development of the LCHPCs (Chapter 3) and the CFRP-prestressed LCHPC beam elements (Chapter 5) thereafter, the initial LCA was extended to evaluate the sustainability potential of these new composite materials.

When comparing all three measures (UBP, CED and GWP) of the LCHPC related LCA, it is obvious that a direct substitution of a HPC (C1) would lead to substantial savings in the ESP of between 40% and 70%, depending on the chosen concrete recipe and the selected measure, see Figure 47. Furthermore, the visualizations of the different measures in Figure 47 clearly show that almost all of this saving is caused by the substitution of the cement by fillers and supplementary cementitious materials (SCMs). The large amount of limestone filler which was used in the LCHPCs (C2-C4) results in a direct ESP saving due to the very small environmental burden of the limestone, which is a locally-available material in Switzerland [124]. This cannot be considered to be always the case when cement is substituted by fillers and SCMs, as described by Zingg et al. [124]:

"It is noted however that a higher clinker substitution does not necessarily mean better savings as presented in the study of Pushkar and Verbitsky (2016) [181]. The choice of supplementary cementitious material (SCM) is critical to optimizing the concrete mix. Depending on the environmental burden allocation of secondary material used as SCM, e.g. fly ash, slag or BOS^e, the resulting concrete mix could have a lower or a higher environmental impact [181]. LCA modelling of low energy concrete will be improved to consider the allocation impact from secondary material particularly BOS, in parallel with the optimization of concrete."

The LCA on the LCHPCs confirmed this statement. In particular, in the CED measure, where metakaolin and the superplasticizer contribute significant amounts to the embodied energy of the LCHPCs, see Figure 47. To a minor extent, this effect was also noticeable in the UBP and the GWP measure. It needs to be noted that the aggregates contribute a significant impact on the point based Ecological Scarcity Method (UBP), see top diagram in Figure 47. During the design of the LCHPCs, the amount of aggregates was intentionally kept constant. Consequently, the relative contribution on the UBP measure was increased as the total amount of cement was decreased in the LCHPCs. However, a direct reduction or replacement of the aggregates to improve UBP balance is not easily possible. This would affect the mechanical properties as well as the workability of the concretes and thus it would require completely new recipes.

The new LCHPCs were now further evaluated in their application in a CFRP-prestressed beam element. As expected, the reduced environmental impact due to the use of the LCHPCs is practically the same as found in the LCA on the LCHPCs. In addition, the CFRP prestressing tendons added an extra 2% in the UBP and GWP measure and about 20-25% in the embodied energy (CED). The total ESP of the CFRP-prestressed LCHPCs was however much higher in comparison. This proposed application attains up to 90% of savings in the UBP and GWP measure and around 80% in the CED measure in comparison to reinforced concrete structures, see Figure 48. For simplification, it was assumed in this evaluation that the saving potential of CFRP prestressed HPC (C1), was the same in the functional unit I and III. The saving potential of the CFRP-prestressed LCHPCs was calculated thereon.

^e BOS...Burnt Oil Shale

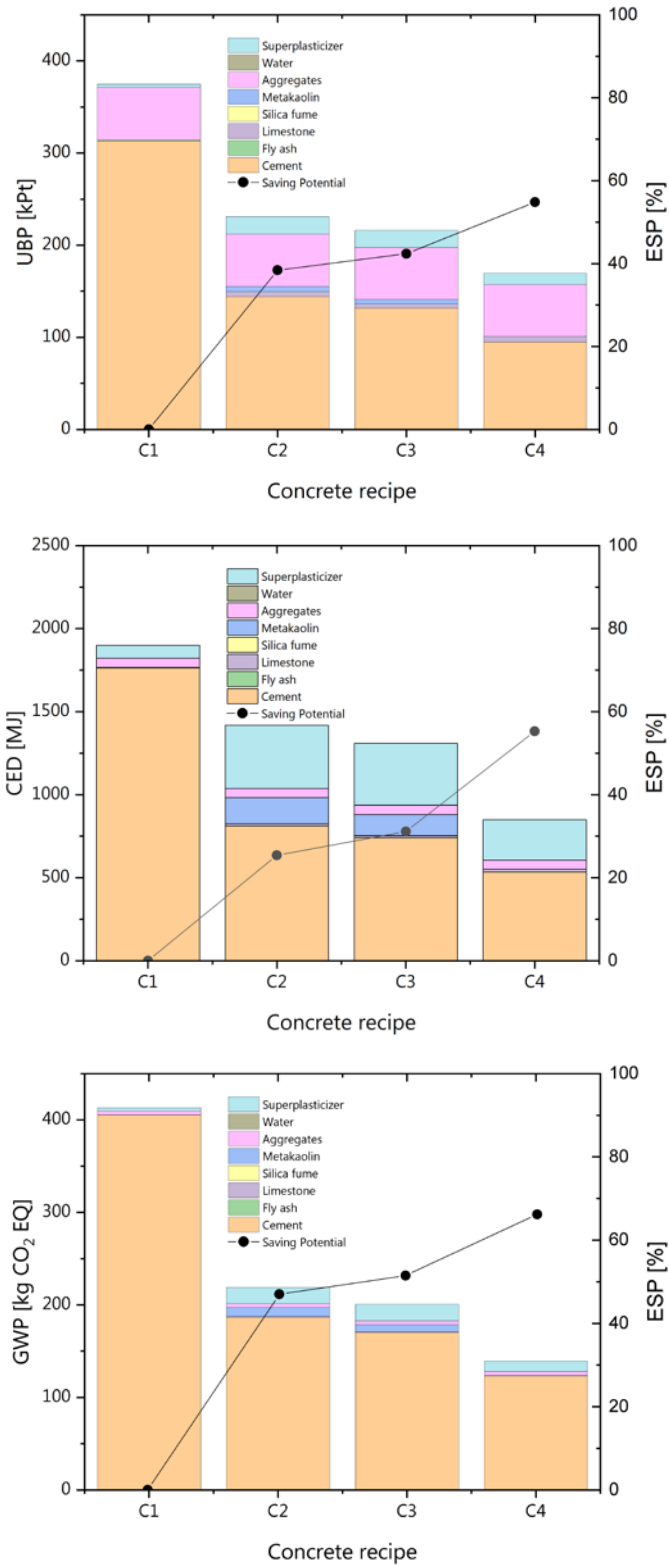


Figure 47: Assessment of the LCA measures, UBP, CED and GWP for the developed LCHPCs C2-C4 and their reference mixture C1. The environmental saving potential (ESP) was calculated for the LCHPC recipes in comparison to C1. All results presented above are based on one cubic meter of concrete, which corresponds to the functional unit II, see Table 12.

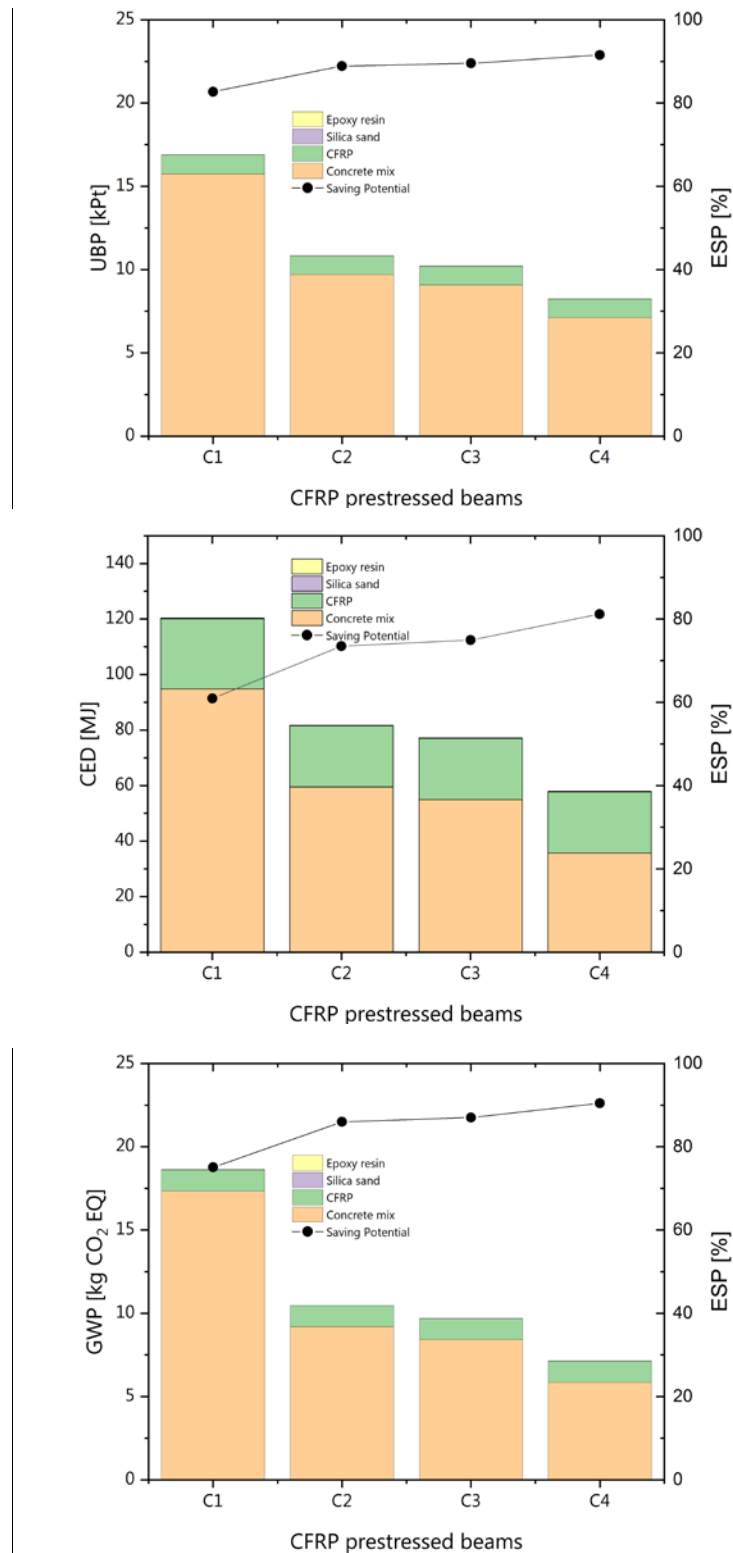


Figure 48: Assessment of the LCA measures, UBP, CED and GWP for the developed CFRP prestressed LCHPC beam specimens, see Chapter 4. This assessment was based on one linear meter of the CFRP-prestressed beam elements, which corresponds to the functional unit III given in Table 12. The environmental saving potential (ESP) was calculated in comparison to a conventional reinforced concrete structure. This calculation was simplified by assuming the ESP of the CFRP-prestressed HPC, see Figure 46 to be equal to the ESP of the CFRP prestressed C1 beam element. The ESP calculation of the CFRP prestressed LCHPC beams was finally based thereon.

5.4 Conclusions

The LCA performed on different stages during the development of the CFRP prestressed LCHPC elements presents huge potential for saving energy and emissions. This technology can be seen to strongly support the energy turnaround in Switzerland and contribute to a successful energy strategy 2050. In particular the following conclusions can be drawn at the current state of investigation:

- The direct substitution of cement in an industry based HPC, using SCMs and significant amounts of limestone filler, enabled an environmental-saving potential between 25 and 50% for recipes containing metakaolin (C2-C3) and even up to 55-70% when only limestone and silica fume was used (C4).
- Prestressing of HPC (C1) structures enables a large environmental-saving potential in comparison to classic reinforced concrete. When steel is used for prestressing, the saving potential can be around 55% and this potential saving even increases for CFRP prestressed elements up to 60-80%, depending on the chosen LCA measure.
- The combination of CFRP prestressing and the use of LCHPC further increased the environmental saving potential. In the specific case of the prestressed beam elements, the saving potential reached 73-80% in embodied energy and even up to 90% in carbon emissions and eco points.

5.5 Outlook

The current results of the LCA on CFRP prestressed LCHPC elements show high environmental saving potential if these elements were implemented in construction. However, the amount of potential saving needs to be judged carefully. Currently, three different functional units, see Table 12, were employed during different stages of the LCA analysis and used for the conclusions presented in Section 5.4. The saving potential for CFRP-prestressed HPC was assumed to be equal for the functional units I and III. In addition, the possible increase in saving potential due to the higher load bearing capacity in UHM-CFRP prestressed LCHPC beams, see Chapter 4, was not taken into account during this LCA.

For a final conclusion on the saving potential of UHM-CFRP prestressed LCHPC elements the following steps are suggested to be performed:

- Definition of one consistent functional unit, for a specific case close to a real application in construction based on reinforced concrete technology and a limitation in height of about 250 mm to be able to be placed in ceilings.
- Design of steel, CFRP and UHM-CFRP prestressed beam elements with a maximum height of 250 mm which are able to withstand the same loads as the defined functional unit of reinforced concrete. In addition, in these elements the concrete should not become decompressed to avoid cracking and guarantee the performance in the long term.

- Variations in cross section for CFRP and UHM-CFRP prestressed concrete elements within the given maximum height of 250 mm with the goal of additional material saving, e.g. I beam design.

With a consistent study based on the points proposed above, the saving potential could be analysed in the context of one specific but realistic application and finally a well-founded conclusion could be drawn.

Subsequently, the results of this proposed further study could be developed into a “road map” of sustainability for structural concrete elements in construction. For instance, a matrix could be built showing in one dimension the different strengthening techniques (reinforced concrete, steel prestressed concrete, CFRP-prestressed concrete, UHM-CFRP prestressed concrete, UHM-CFRP prestressed concrete with varied cross section) and in the other dimension the different concrete mixture (Ordinary concrete 30 MPa strength, Low clinker concrete 30 MPa strength, Ordinary concrete 80 MPa strength, Low clinker concrete 80 MPa strength). This matrix would allow an easy and quick assessment of the best technology to be used from a sustainability aspect.

The consideration of additional life cycle assessment approaches, e.g. cradle-to-grave or cradle-to-cradle, would finally complete this analysis and would add a third dimension into the proposed roadmap.

Acknowledgements:

I would like to thank the Swiss National Science Foundation (SNSF) for funding “Concrete Solutions” in the framework of the NRP 70 “Energy Turnaround”. In addition, I would like to acknowledge the whole team working in the joint research project from Empa, EPFL and ETHZ. In particular I would like to thank Sharon Zingg for the fundamental work [124] on which this chapter was based on and parts of the content and the results were taken from. Moreover, I would like to thank F. Pittau and G. Habert for the fruitful discussions and for running the calculations in the SimaPro LCA software.

CHAPTER 6

Summary and Conclusions

In this thesis, a 2nd generation of slender CFRP prestressed concrete elements with reduced environmental impact and an enhanced ultimate load bearing capacity was developed. This was achieved by substituting the two main components in the prestressed concrete elements, the CFRP-tendons and the HPC, by novel alternatives, in particular UHM-CFRP tendons and LCHPCs. In the past decades, CFRP tendons were used as alternatives to steel prestressing tendons in prestressed concrete elements. Research was primarily directed to improve certain weaknesses of the system; e.g. different approaches for increasing the bond between prestressing tendon were studied [81] and the high temperature stability of CFRP-prestressed systems was improved [42, 129]. Up to a short while ago, sustainability was not a principal interest in the applications of CFRP-prestressed structural elements. As a consequence, hardly any research was directed in reducing or even assessing the environmental impact of such elements. In the field of concrete technology this was different. Here, the need for sustainability was recognized early on and approaches were developed to produce cements with low CO₂ emissions [52]. With the introduction of the energy strategy 2050 in Switzerland, novel technology for reducing the energy requirements and environmental impact of future infrastructure became needed and practical solutions were demanded.

Aside the development of the 2nd generation of prestressed concrete elements, another aim of this thesis was to expand the current state of the art knowledge in CFRP-prestressed concrete into two new directions. At first, into the effects of using ultra-high modulus carbon fibres inside the CFRP-prestressing tendons and secondly into substituting un-hydrated cement by fillers and SCMs in HPC to reduce their environmental impact. Thereby, it was the ambition to give a fundamental overview of the two new areas and their principles to researches and engineers so that they could make use of these findings for their particular application or research.

The main steps of this development process are summarized and the main conclusions are presented in the following.

The crucial criteria for prestressing tendons in prestressed concrete are their high strength and their good bond to concrete. Consequently, the determination of strength and modulus of the proposed sand-coated UHM-CFRP tendons was of interest first. Afterwards, these tendons were tested in pull-out tests for their bond to HPC and the related bond failure was studied thoroughly by X-ray tomography, SEM and visual analysis. The gained knowledge was consolidated and developed into a finite element model describing the tendon pull-out behaviour up until failure. With this model it was possible to study the dependence of the tendon pull-out on its longitudinal stiffness and on the thickness of the adhesive layer which bonds the sand particles on the CFRP tendon's surface. Bond pull-out tests using a reference tendon and diverse sand coatings (different in sand particle size), showed a significant

dependence of the bond strength between CFRP tendon and concrete on the respective sand coating. Based on these results it can be recommended to coat the CFRP tendons with coarse sand (0.5 - 1.5 mm), albeit the failure of this sand coating was found to be brittle. Tendons coated with this coarse coating reached an absolute bond strength of around 19 MPa, which was more than twice as high as any other tested sand-coating. Consequently, the risk of bond failure during loading of such a sand coated CFRP-prestressed member is unlikely. In comparison to other failure mechanisms such as concrete crushing or tendon rupture the bond failure would occur at much higher loading and hence can reasonably be neglected. The bond failure in the pull-out tests was observed between the CFRP tendon and the sand-epoxy layer by X-ray tomography and confirmed by SEM and visual analysis. Accordingly, it could be experimentally demonstrated that the maximum bond strength was not affected by the stiffness of the unidirectional CFRP tendon but only by the adhesive strength between CFRP tendon and sand coating layer. In contrast to that, the tendon draw-in rate on its unloaded end and the corresponding τ - δ curve were majorly controlled by the longitudinal tendon stiffness. Here, the stiffer tendon (UHM-CFRP) showed a greater tendon draw-in in comparison to the current industry standard (UTS-CFRP).

With their good bond to concrete, the novel sand-coated UHM-CFRP tendons accomplish the most critical criteria, namely a good bond to concrete, in accordance to Bruggeling [70], for their application in prestressed concrete elements.

In CFRP-prestressed concrete elements, the use of self-compacting HPCs, with their low porosity and high strength, was reasonable and well-established in industry praxis. However, recent energy-related guidelines demand new environmental-friendly technologies. It has been shown that replacing unhydrated cement particles in HPCs (w/c 0.30 and 0.34) by limestone did not significantly affect the compressive strength of these recipes [62]. In addition, theoretical considerations about the replacement of coarse cement particles by inert fillers in HPCs indicated no significant influence on the mechanical performance for replacement levels lower than 15% [62]. Considering these previous results and starting from an industry reference HPC, environmental-friendly LCHPCs were developed in Chapter 3. Large fractions (54-70 %) of cement were replaced by metakaolin, limestone and silica fume. A high strength could be reached by reducing the w/b ratio to as low as 0.2 and 0.17, respectively. Furthermore, self-compacting properties could still be achieved by substantially increasing the amount of superplasticizer. The final LCHPCs were characterized mechanically (compressive strength and modulus) but also investigated for their bond to sand coated UHM-CFRP prestressing tendons. In all cases, the LCHPCs were able to compete against the industry reference, reaching compressive strength of about 80 MPa and bond strengths to sand coated CFRP-tendons of around 20 MPa. Shrinkage and creep were likely expected to be reduced in the LCHPCs due to their lower C-S-H content and their higher solid fraction. This expectation was validated by experiments and transferred into a finite element model to finally estimate their effect on prestress losses in UHM-CFRP prestressed concrete elements. The results of this model showed that the low shrinkage and creep of the LCHPCs contributed to a high remaining prestress in a fictitious prestressed concrete element. In contrast to that, with their longitudinal stiffness of 509 GPa, the UHM-CFRP tendons are very sensitive to volumetric changes. This led to a contradictory result of a reduced prestress for all investigated concrete recipes but in particular

relative to in the industry reference HPC with high creep and shrinkage. With these properties, the new concretes were considered to be ideal candidates for applications in prestressed concrete elements. The UHM-CFRP tendons, even though higher prestress losses need to be considered, were seen to have possible benefits in reducing a loaded element's deflection and limiting the width of cracks.

It was the final goal of this thesis to make a proof of concept and hence to develop a UHM-CFRP prestressed LCHPC beam element based on the results of Chapter 2 and Chapter 3. This beam, using the recipe C4 and UHM-CFRP prestressing tendons, was compared in its load vs. deflection behaviour in 4-point bending tests to beams using the reference concrete recipe (C1) and two different types of prestressing tendons, UHM-CFRP and UTS-CFRP, respectively.

Based on an adapted FEA of Chapter 3, the prestress loss was modelled for the three specific beam configurations in Chapter 4 considering shrinkage, creep and elastic shortening. The simulation showed a clear reduction in the remaining prestress for beam specimens using the stiffer tendons (UHM-CFRP). Optical fibre strain measurements, inside the CFRP prestressing tendons, allowed the experimental measurement of the prestress loss and confirmed the FEA predictions. The potentially decreased prestress loss due to the low shrinkage and creep of the LCHPCs was predicted by the FEA to be very limited in the chosen beam design and could not be experimentally validated nor rejected due to the high scatter in the experimental results.

Considering the experimental and numerical results presented in Chapter 2 about the tendon pull-out behaviour a significantly longer transfer length in beams prestressed with UHM-CFRP tendons was expected. This behaviour was experimentally confirmed and it could be concluded that the transfer length was only related to the tendon's longitudinal stiffness.

In 4 point bending tests, significant differences were foreseen by an analytical model of the load-deflection behaviour between beams prestressed by UHM-CFRP tendons and beams using the current industry standard UTS-CFRP tendons. In the cracked state, when in particular the UHM-CFRP tendons contribute to the actual moment of inertia, the load-deflection behaviour was predicted to be significantly higher for beams prestressed with UTS-CFRP tendons. This behaviour was verified in the experimental program. Accordingly, the beams prestressed with UHM-CFRP tendons showed smaller crack widths, smaller ultimate deflections but higher maximum load bearing capacities. According to the previous results on bond (Chapter 2 and Chapter 3) and the mechanical characterization of the LCHPCs, see Chapter 3, no differences in the load deflection curves between beams made of either of the two concrete recipes (C1 or C4) were expected. The measurement of the beam's mid-span deflection and the analysis of the compressive strain development in the concrete beam's top section by digital image correlation confirmed the expectations and found no significant difference between the two concrete recipes.

In conclusion, using UHM-CFRP prestressing tendons helped to improve the serviceability of the investigated prestressed beams and resulted in a higher maximum load bearing capacity, in lower deflections and a smaller crack width. In addition, the LCHPCs with their significantly reduced clinker content of up to 70% did not change the load deflection behaviour and hence can be seen as ideally suited for their application in prestressed concrete elements.

It can be summarized that, from a structural perspective, the developed UHM-CFRP prestressed LCHPC beams performed well and were in many areas superior in comparison to their classic HPC reference beams. However, beside the structural performance, one main goal of this development was the reduced environmental impact of the new beams. To allow classification and evaluation in terms of sustainability, a comprehensive LCA was carried out. Up to 70 % environmental saving potential could be realized by substituting parts of the cement with limestone and metakaolin (see Chapter 5 and recipe C4). Prestressing of concrete, in particular prestressing with CFRP-tendons, allowed the saving potential to increase in comparison to a reinforced concrete structure by up to 80 % in embodied energy and even up to 90 % in carbon emission.

This is a huge saving potential, especially when considering the fact that the LCA, due to the lack of an appropriate design criterion, did not further consider the increased load-bearing capacity of UHM-CFRP prestressed beam elements.

CHAPTER 7

Outlook

Novel UHM-CFRP structural beam elements were successfully developed and they fulfilled all the desired and set criteria. With small adaptations, the gained knowledge could be directly transferred into praxis and help to improve the CO₂ footprint of future infrastructure. In particular, a first implementation of the new UHM-CFRP prestressed structural elements could be included as a subcomponent in current state-of-the-art infrastructure. This approach would help to gain visibility to the public but also to generate confidence about this new technology in the civil engineering industry.

One critical matter worthy of further investigation is the fact that all current results presented in this thesis are based on short-term material and structural behaviour. The used epoxies are polymers that are expected to creep under load with time. Some studies exist which investigated the long-term stability of the bond between sand coated CFRP tendons and HPC in prestressed concrete elements [38, 41]. However, none of them used UHM-CFRP prestressing tendons. It has been found in this thesis that the UHM-CFRP tendons reacted very sensitively to small strain variations of shrinkage and creep in concrete. It could be anticipated that possible creep at the bond interface may also significantly affect the prestress transfer in the long term. Furthermore, the trend in the results presented about the prestress loss over time showed neither significant slowdown nor stabilization. In this context, when using UHM-CFRP tendons, the long-term remaining prestress level needs further investigation. To address all the above-mentioned points, it is proposed to set up long term 4-point bending tests in which the different beam types are loaded once at their concrete decompression point and once at about 60% of their short-term failure load. Ideally, these tests should run for several years in outdoor weather conditions. Over these years, the beam deflections and the prestressing tendon strain variations could be studied and analysed to give further guidelines for practical applications of this technology. Based on such guidelines, the optical fibre strain measurement system, which was employed during this thesis, could be further developed into a self-standing system to be implemented at the critical section of novel elements. It then could be used for monitoring and to report critical conditions at an early state and independently from man-based surveillance. Such a system would not only help to gain more data of long term applications, it would also give property owners and engineers confidence and hence reduce the barriers for possible applications.

Another topic, with potentially promising benefits, could be the applications of the UHM-CFRP materials as sand-coated, short-length reinforcing tendons. In the presented thesis, the UHM-CFRP tendons ($d=5.3$ mm) were able to significantly reduce the crack width in 4-point bending tests, mainly due to their very high longitudinal stiffness of 509 GPa. This characteristic could potentially be very successful when applied without prestressing only for reinforcement

purposes. In particular, CFRP tendons with a much smaller diameter (e.g. 0.5 mm) could be used in small amounts (e.g. 1-2% in volume), cut into 1-3 cm long sections and homogeneously distributed in the concrete matrix. Such reinforced concretes may show significant strength increase due to the hindered crack network development. The UHM-materials are about 2.4 times stiffer than steel and hence their effectiveness could be anticipated to outperform those of steel fibres which are typically used in such applications.

Recently, the implementation of UHM-CFRP tendons enabled the development of self-prestressed reinforced concrete elements [159]. A totally new class of concrete materials could potentially be formed by combining the expansive concretes mentioned in this patent [159] with the above proposed thin, sand-coated, short-length UHM-CFRP reinforcing tendons. This combination would potentially form a reinforced concrete which would be additionally prestressed in all directions. This would not only result in higher strength and stiffness, it would also have the potential advantage of increasing in particular the tensile strength of this new composite material significantly and beyond those of the current technology.

The future perspectives listed above range from mandatory investigations to ensure the long-term behaviour of UHM-CFRP prestressed beam elements towards the formation of new and undiscovered composite materials. This widely open perspective shows today's interconnectivity of different engineering and research disciplines. It will be thrilling to see the future evolution of such technology and in particular how far the implementation of this thesis' results are realized in praxis ten or more years from now.

Bibliography

- [1] L. Rodgers, Climate change: The massive CO₂ emitter you may not know, 2018. <https://bbc.in/2UTRunN>. (Accessed 17.01.2019).
- [2] E.M. Gartner, D.E. Macphee, A physico-chemical basis for novel cementitious binders, *Cement and Concrete Research* 41(7) (2011) 736-749.
- [3] Ein neues Mass zur Klassifizierung von Gipfeln, 2014. <https://bit.ly/2TImA0L>. (Accessed 08.02.2019).
- [4] C. Thöni, Theorie III - Weitere Kriterien. <https://bit.ly/2WUeqEA>. (Accessed 08.02.2019).
- [5] M. Huss, Ein Jahr der Extreme für Schweizer Gletscher, 2018. <https://bit.ly/2tnERFj>. (Accessed 21.01.2019).
- [6] S. Ulmer, Eisvolumen der Schweizer Gletscher neu bestimmt, 2009. <https://bit.ly/2RSvPcT>. (Accessed 21.01.2019).
- [7] Ö. Kirca, Ancient binding materials, mortars and concrete technology: history and durability aspects, IVth Int. Seminar on Structural Analysis of Historical Constructions, Padova, Italy, 2004.
- [8] R. Mark, P. Hutchinson, On the structure of the Roman Pantheon, *The Art Bulletin* 68(1) (1986) 24-34.
- [9] J.F. Ryan, The story of Portland cement, *Journal of Chemical Education* 6(11) (1929) 1854-1868.
- [10] S. Macdonald, *Concrete: building pathology*, John Wiley & Sons New York, 2008.
- [11] R.H. Bogue, *The chemistry of Portland cement*, Reinhold, New York, 1955.
- [12] A.M. Neville, J.J. Brooks, *Concrete technology*, Pearson Education Limited, Harlow, England, 1987.
- [13] EN 12390-3 Testing hardened concrete, Part 3: Compressive strength of test specimens, European Committee for Standardization (CEN), Brussels, 2009.
- [14] P. Lura, *Autogenous Deformation and Internal Curing of Concrete*, Doctoral dissertation, TU Delft, Delft University of Technology, Delft University Press, 2003.
- [15] A.A. Griffith, M. Eng, VI. The phenomena of rupture and flow in solids, *Phil. Trans. R. Soc. Lond. A* 221(582-593) (1920) 163-198.
- [16] G.B. Neville, G. Neville, *Concrete Manual: Based on the 2015 IBC and ACI 318-14*, International Code Council, 2015.
- [17] K.L. Scrivener, A.K. Crumbie, P. Laugesen, The Interfacial Transition Zone (ITZ) Between Cement Paste and Aggregate in Concrete, *Interface Science* 12(4) (2004) 411-421.
- [18] N.J. Carino, J.R. Clifton, *Prediction of cracking in reinforced concrete structures (NISTIR 5634)*, US Department of Commerce, National Institute of Standards and Technology, Gaithersburg, 1995.
- [19] E.G. Nawy, *Prestressing Systems and Anchorages*, *Prestressed concrete a fundamental approach*, Prentice Hall, Upper Saddle River, 2010, pp. 61-69.
- [20] N. Rajagopalan, *Prestressed concrete*, Alpha Science Int'l, Oxford, 2005.
- [21] T. Dinges, *The history of prestressed concrete: 1888 to 1963*, Department of Architectural Engineering and Construction Science, Kansas State University, Manhattan KS, 2009.
- [22] P.H. Jackson, *Construction of artificial-stone or concrete pavements*, U.S. Pat.No. 375999, United States, 1888.
- [23] E. Freyssinet, J. Séaillesfile, *Fabrication process for reinforced concrete elements*, The invention of prestressed concrete and precast segmental construction, Patent No. 640547, France, 1930.

- [24] T.Y. Lin, N.H. Burns, Design of prestressed concrete structures, John Wiley & Sons, New York, 1981.
- [25] G. Magnel, Prestressed Concrete, McGraw-Hill, New York, 1954.
- [26] R.I. Gilbert, N.C. Mickleborough, Design of prestressed concrete, Unwin Hyman, London, 1990.
- [27] V. Gouda, W. Halaka, Corrosion and corrosion inhibition of reinforcing steel: II. Embedded in concrete, British Corrosion Journal 5(5) (1970) 204-208.
- [28] U. Nürnberger, Corrosion induced failure mechanisms of prestressing steel, Materials and Corrosion 53(8) (2002) 591-601.
- [29] J. Walraven, High performance concrete: exploring a new material, Structural Engineering International 5(3) (1995) 182-187.
- [30] N. Gowripalan, H. Mohamed, Chloride-ion induced corrosion of galvanized and ordinary steel reinforcement in high-performance concrete, Cement and Concrete Research 28(8) (1998) 1119-1131.
- [31] Z.I. Mahmoud, S.H. Rizkalla, E.E.R. Zaghoul, Transfer and development lengths of carbon fiber reinforced polymers prestressing reinforcement, ACI Struct J 96(4) (1999) 594-602.
- [32] J.M. Lees, C. Burgoyne, Transfer bond stresses generated between FRP tendons and concrete, Magazine of Concrete Research 51(4) (1999) 229-239.
- [33] C. Burgoyne, Rational use of advanced composites in concrete, Proceedings of the 3rd International Symposium on Non-Metallic (FRP) Reinforcement for Concrete Structures, Japan Concrete Institute, 1997, pp. 75-88.
- [34] G.P. Terrasi, U. Meier, Design with Polymers and Advanced Composites, 2008.
- [35] ACI440.3R-04 Guide test methods for fiber-reinforced polymers (FRPs) for reinforcing or strengthening concrete structures, Farmington Hills (MI) : American Concrete Institute 2004.
- [36] F. Micelli, A. Nanni, Durability of FRP rods for concrete structures, Construction and Building Materials 18(7) (2004) 491-503.
- [37] A. Puck, Einführung in das Gestalten und Dimensionieren, Konstruieren und Berechnen von GFK-Teilen (1969) 44-66.
- [38] G.P. Terrasi, U. Meier, C. Affolter, Long-Term Bending Creep Behavior of Thin-Walled CFRP Tendon Pretensioned Spun Concrete Poles, Polymers 6(7) (2014) 2065-2081.
- [39] G.P. Terrasi, Mit Kohlenstoffasern vorgespannte Schleuderbetonrohre, Diss. Techn. Wiss. ETH Zürich, Nr. 12454, Ref.: H. Bachmann; Korref.: U. Meier, 1998.
- [40] L. Taerwe, I. Pallemans, Force Transfer of AFRP bars in concrete prisms, Non-Metallic (FRP) Reinforcement for Concrete Structures: proceedings of the Second International RILEM Symposium (FRPRCS-2), Ghent, 1995, pp. 154-163.
- [41] T.D. Lämmlein, G.P. Terrasi, Bending creep behaviour of CFRP prestressed slender concrete elements, in: J. Lees, S. Keighley (Eds.) Proceedings of the 7th Biennial Conference on Advanced Composites in Construction, NetComposites Limited, St. John's College, University of Cambridge, UK, 2015, pp. 56-61.
- [42] G.P. Terrasi, L. Bisby, M. Barbezat, C. Affolter, E. Hugli, Fire Behavior of Thin CFRP Pretensioned High-Strength Concrete Slabs, Journal of Composites for Construction 16(4) (2012) 381-394.
- [43] G.P. Terrasi, Prefabricated thin-walled structural elements made from high performance concrete prestressed with CFRP wires, Journal of Materials Science Research 2(1) (2013) 1.
- [44] B.B. Agyei, J.M. Lees, G.P. Terrasi, Fatigue of high strength concrete beams pretensioned with CFRP tendons, in: K.H. Tan (Ed.) Proceedings of the Sixth International Symposium on FRP

Reinforcement for Concrete Structures (FRPRCS-6), World Scientific, Singapore, 2003, pp. 935-944.

[45] E. Hawkins, P. Ortega, E. Suckling, A. Schurer, G. Hegerl, P. Jones, M. Joshi, T.J. Osborn, V. Masson-Delmotte, J. Mignot, P. Thorne, G.J.v. Oldenborgh, Estimating Changes in Global Temperature since the Preindustrial Period, *Bulletin of the American Meteorological Society* 98(9) (2017) 1841-1856.

[46] M. Joshi, E. Hawkins, R. Sutton, J. Lowe, D. Frame, Projections of when temperature change will exceed 2 °C above pre-industrial levels, *Nature Climate Change* 1 (2011) 407.

[47] X. Guo, J. Huang, Y. Luo, Z. Zhao, Y. Xu, Projection of precipitation extremes for eight global warming targets by 17 CMIP5 models, *Natural Hazards* 84(3) (2016) 2299-2319.

[48] X. Guo, J. Huang, Y. Luo, Z. Zhao, Y. Xu, Projection of heat waves over China for eight different global warming targets using 12 CMIP5 models, *Theoretical and Applied Climatology* 128(3) (2017) 507-522.

[49] The State of Greenhouse Gases in the Atmosphere Based on Global Observations through 2017, WMO Greenhouse Gas Bulletin, World Meteorological Organization, 2018.

[50] S. Callery, Global Temperature, 2019. <https://climate.nasa.gov/vital-signs/global-temperature/>. (Accessed 23.01.2019 2019).

[51] B. Afkhami, B. Akbarian, N. Beheshti, A. Kakaee, B. Shabani, Energy consumption assessment in a cement production plant, *Sustainable Energy Technologies and Assessments* 10 (2015) 84-89.

[52] E. Gartner, Industrially interesting approaches to "low-CO₂" cements, *Cement and Concrete Research* 34(9) (2004) 1489-1498.

[53] K.L. Scrivener, V.M. John, E.M. Gartner, Eco-efficient cements: Potential economically viable solutions for a low-CO₂ cement-based materials industry, Report of the United Nations Environment Programme, 2016.

[54] R.M. Andrew, Global CO₂ emissions from cement production, *Earth System Science Data* 10(1) (2018) 2213-2239.

[55] P.-C. Aitcin, S. Mindess, Sustainability of concrete, Spon Press, Milton Park, 2011.

[56] G.P. Terrasi, J.M. Lees, CFRP prestressed concrete lighting columns, *ACI Special Publication* 215 (2003) 55-74.

[57] C.W. Dolan, Flexural design of prestressed concrete beams using FRP tendons, *Prestressed Concrete Institute Journal* 46(2) (2001) 76-87.

[58] M. Rezazadeh, J. Barros, I. Costa, Analytical approach for the flexural analysis of RC beams strengthened with prestressed CFRP, *Composites Part B: Engineering* 73 (2015) 16-34.

[59] A.Z. Fam, S.H. Rizkalla, G. Tadros, Behavior of CFRP for prestressing and shear reinforcements of concrete highway bridges, *ACI Struct J* 94(1) (1997) 77-86.

[60] SIA 2049:2014 Anforderungen an Neue Zemente, Schweizerischer Ingenieur und Architektenverein (SIA), Zürich, 2014.

[61] EN 197-1 Cement-Part 1: Composition, Specifications and Conformity Criteria for Common Cements, European Committee for Standardization (CEN), Brussels, 2011.

[62] V. Bonavetti, H. Donza, G. Menendez, O. Cabrera, E.F. Irassar, Limestone filler cement in low w/c concrete: A rational use of energy, *Cement and Concrete Research* 33(6) (2003) 865-871.

[63] D.P. Bentz, Replacement of "coarse" cement particles by inert fillers in low w/c ratio concretes: II. Experimental validation, *Cement and Concrete Research* 35(1) (2005) 185-188.

[64] P. Lura, G.P. Terrasi, Reduction of fire spalling in high-performance concrete by means of superabsorbent polymers and polypropylene fibers: Small scale fire tests of carbon fiber

reinforced plastic-prestressed self-compacting concrete, *Cement and Concrete Composites* 49 (2014) 36-42.

[65] D. Chung, *Carbon fiber composites*, Butterworth-Heinemann 2012.

[66] A.S.G. Bruggeling, *Controlling transmission of prestress by bond in progress*, Düsseldorf : VBT Verlag Bau + Technik, Düsseldorf, 1999.

[67] E. Cosenza, G. Manfredi, R. Realfonzo, Development length of FRP straight rebars, *Composites Part B: Engineering* 33(7) (2002) 493-504.

[68] A. Nanni, T. Utsunomiya, H. Yonekura, M. Tanigaki, Transmission of prestressing force to concrete by bonded fiber reinforced plastic tendons, *ACI Struct J* 89(3) (1992) 335-344.

[69] A. Nanni, M. Tanigaki, Pretensioned prestressed concrete members with bonded fiber reinforced plastic tendons: development and flexural bond lengths (static), *ACI Struct J* 89(4) (1992) 433-441.

[70] A.S.G. Bruggeling, Übertragen der Vorspannung mittels Verbund, *Beton- und Stahlbetonbau* 96(3) (2001) 109-123.

[71] Y. Guyon, E. Freyssinet, *Béton précontraint : Étude théorique et expérimentale*, Eyrolles, Paris, 1958.

[72] T.Y. Lin, N.H. Burns, *Design of prestressed concrete structures*, John Wiley & Sons, New York, 1981.

[73] R. Tepfers, L. De Lorenzis, Bond of FRP reinforcement in concrete - A challenge, *Mech. Compos. Mater.* 39(4) (2003) 315-328.

[74] A. Nanni, M. Al-Zaharani, S. Al-Dulaijan, C. Bakis, I. Boothby, Bond of FRP reinforcement to concrete-experimental results, *Non-Metallic (FRP) Reinforcement for Concrete Structures: Proceedings of the Second International RILEM Symposium*, CRC Press, 1995, p. 135.

[75] F. Sayed Ahmad, G. Foret, R. Le Roy, Bond between carbon fibre-reinforced polymer (CFRP) bars and ultra high performance fibre reinforced concrete (UHPC): Experimental study, *Construction and Building Materials* 25(2) (2011) 479-485.

[76] Z. Achillides, K. Pilakoutas, Bond behavior of fiber reinforced polymer bars under direct pullout conditions, *Journal of Composites for Construction* 8(2) (2004) 173-181.

[77] F. Al-mahmoud, A. Castel, R. François, C. Tourneur, Effect of surface pre-conditioning on bond of carbon fibre reinforced polymer rods to concrete, *Cement and Concrete Composites* 29(9) (2007) 677-689.

[78] A. Stark, J. Hegger, Bond Behaviour of Pre-tensioned CFRP Tendons in UHPC, in: J. Barros, J. Sena-Cruz (Eds.) 11th international symposium on fiber reinforced polymer for reinforced concrete structures, University of Minho, Guimaraes, Portugal, 2013.

[79] A. Katz, Bond to Concrete of FRP Rebars and Tendons, *Composites in Construction*, American Society of Civil Engineers 2001, pp. 121-129.

[80] Bond of reinforcement in concrete, fib Bulletin No. 10, State-of-art Report, International Federation for Concrete, Lausanne, Switzerland, 2000.

[81] G. Portnov, C.E. Bakis, E. Lackey, V. Kulakov, FRP Reinforcing bars - Designs and methods of manufacture (Review of Patents), *Mech. Compos. Mater.* 49(4) (2013) 381-400.

[82] K.M.A. Hossain, D. Ametrano, M. Lachemi, Bond strength of standard and high-modulus GFRP bars in high-strength concrete, *J. Mater. Civ. Eng.* 26(3) (2014) 449-456.

[83] SIA 2052:2016, Ultra-high performance fiber reinforced concrete (UHPC) –Materials, design and execution, Schweizerischer Ingenieur und Architektenverein (SIA), Zürich, 2016.

[84] SIA162-1, Betonbauten Materialprüfungen, Schweizerischer Ingenieur und Architektenverein (SIA), Zürich, 1989.

- [85] A. Losberg, Anchorage of beams reinforcement shortened according to the moment distribution curve, IABSE congress report (1964).
- [86] J. Banhart, Advanced tomographic methods in materials research and engineering, Oxford University Press, Oxford, UK, 2008.
- [87] L. Feldkamp, L. Davis, J. Kress, Practical cone-beam algorithm, *JOSA A* 1(6) (1984) 612-619.
- [88] P. Lura, G. Plizzari, P. Riva, 3D finite-element modelling of splitting crack propagation, *Magazine of Concrete Research* 54(6) (2002) 481-494.
- [89] K. Song, C.G. Dávila, C.A. Rose, Guidelines and parameter selection for the simulation of progressive delamination, *ABAQUS User's Conference*; Newport, RI; United States (2008).
- [90] L.F.M. da Silva, P.J.C. das Neves, R.D. Adams, J.K. Spelt, Analytical models of adhesively bonded joints—Part I: Literature survey, *International Journal of Adhesion and Adhesives* 29(3) (2009) 319-330.
- [91] M.Y. Tsai, D.W. Oplinger, J. Morton, Improved theoretical solutions for adhesive lap joints, *International Journal of Solids and Structures* 35(12) (1998) 1163-1185.
- [92] G. Habert, N. Roussel, Study of two concrete mix-design strategies to reach carbon mitigation objectives, *Cement and Concrete Composites* 31(6) (2009) 397-402.
- [93] M.C.G. Juenger, F. Winnefeld, J.L. Provis, J.H. Ideker, Advances in alternative cementitious binders, *Cement and Concrete Research* 41(12) (2011) 1232-1243.
- [94] EN206–1, Concrete–Part 1: Specification Performance, Production and Conformity, European Committee for Standardization (CEN), Brussels, 2000.
- [95] R. Wassermann, A. Katz, A. Bentur, Minimum cement content requirements: a must or a myth?, *Materials and Structures* 42(7) (2009) 973-982.
- [96] R. Wasserman, A. Bentur, Effect of concrete composition on durability in natural acidic environment, *Advances in cement research* 18(4) (2006) 135-143.
- [97] N. Buenfeld, E. Okundi, Effect of cement content on transport in concrete, *Magazine of Concrete Research* 50(4) (1998).
- [98] B.L. Damineli, F.M. Kemeid, P.S. Aguiar, V.M. John, Measuring the eco-efficiency of cement use, *Cement and Concrete Composites* 32(8) (2010) 555-562.
- [99] R. Muigai, M. Alexander, P. Moyo, A novel framework towards the design of more sustainable concrete infrastructure, *Materials and Structures* 49(4) (2016) 1127.
- [100] M. Murat, Hydration reaction and hardening of calcined clays and related minerals. I. Preliminary investigation on metakaolinite, *Cement and Concrete Research* 13(2) (1983) 259-266.
- [101] J. Ambroise, M. Murat, J. Pera, Hydration reaction and hardening of calcined clays and related minerals V. Extension of the research and general conclusions, *Cement and Concrete Research* 15(2) (1985) 261-268.
- [102] J. Ambroise, M. Murat, J. Pera, Hydration reaction and hardening of calcined clays and related minerals. IV. Experimental conditions for strength improvement on metakaolinite minicylinders, *Cement and Concrete Research* 15(1) (1985) 83-88.
- [103] M. Murat, C. Comel, Hydration reaction and hardening of calcined clays and related minerals III. Influence of calcination process of kaolinite on mechanical strengths of hardened metakaolinite, *Cement and concrete research* 13(5) (1983) 631-637.
- [104] M. Murat, Hydration reaction and hardening of calcined clays and related minerals.: II. Influence of mineralogical properties of the raw-kaolinite on the reactivity of metakaolinite, *Cement and concrete research* 13(4) (1983) 511-518.
- [105] R. San Nicolas, M. Cyr, G. Escadeillas, Characteristics and applications of flash metakaolins, *Applied Clay Science* 83 (2013) 253-262.

- [106] M. Antoni, J. Rossen, F. Martirena, K. Scrivener, Cement substitution by a combination of metakaolin and limestone, *Cement and Concrete Research* 42(12) (2012) 1579-1589.
- [107] T. Matschei, B. Lothenbach, F.P. Glasser, The role of calcium carbonate in cement hydration, *Cement and Concrete Research* 37(4) (2007) 551-558.
- [108] P.-C. Aïtcin, *High-performance concrete*, E & FN Spon, London, 1998.
- [109] V. Yogendran, B. Langan, M. Haque, M. Ward, Silica fume in high-strength concrete, *Materials Journal* 84(2) (1987) 124-129.
- [110] C.S. Poon, S.C. Kou, L. Lam, Compressive strength, chloride diffusivity and pore structure of high performance metakaolin and silica fume concrete, *Construction and Building Materials* 20(10) (2006) 858-865.
- [111] Å. Skarendahl, Ö. Petersson, *Self-Compacting Concrete, State-of-the-Art Report 23*, Rilem Technical Committee 174-SCC, RILEM publications, 2000.
- [112] B.S.M. Persson, Shrinkage and Creep of High-Performance Self-Compacting Concrete (HPSCC), *ACI Special Publication 220* (2004) 155-180.
- [113] H. Okamura, Self-compacting high-performance concrete, *Concrete international* 19(7) (1997) 50-54.
- [114] M. Mazloom, A. Ramezaniapour, J. Brooks, Effect of silica fume on mechanical properties of high-strength concrete, *Cement and Concrete Composites* 26(4) (2004) 347-357.
- [115] D.P. Bentz, O.M. Jensen, A. Coats, F.P. Glasser, Influence of silica fume on diffusivity in cement-based materials: I. Experimental and computer modeling studies on cement pastes, *Cement and Concrete research* 30(6) (2000) 953-962.
- [116] M. Jensen, P.F. Hansen, Autogenous deformation and change of the relative humidity in silica fume-modified cement paste, *Materials Journal* 93(6) (1996) 539-543.
- [117] T.C. Powers, T.L. Brownyard, *Studies of the Physical Properties of Hardened Portland Cement Paste*, Bulletin 22, Res. Lab. of Portland Cement Association, Skokie, IL, U.S, 1948.
- [118] D.P. Bentz, J. Conway, Computer modeling of the replacement of "coarse" cement particles by inert fillers in low w/c ratio concretes: hydration and strength, *Cement and Concrete Research* 31(3) (2001) 503-506.
- [119] C. Di Bella, M. Wyrzykowski, M. Griffa, P. Termkhajornkit, G. Chanvillard, H. Stang, A. Eberhardt, P. Lura, Application of microstructurally-designed mortars for studying early-age properties: Microstructure and mechanical properties, *Cement and Concrete Research* 78 (2015) 234-244.
- [120] P. Termkhajornkit, R. Barbarulo, G. Chanvillard, Microstructurally-designed cement pastes: A mimic strategy to determine the relationships between microstructure and properties at any hydration degree, *Cement and Concrete Research* 71 (2015) 66-77.
- [121] C. Di Bella, A. Michel, H. Stang, P. Lura, Early age fracture properties of microstructurally-designed mortars, *Cement and Concrete Composites* 75 (2017) 62-73.
- [122] M. Wyrzykowski, K. Scrivener, P. Lura, Basic creep of cement paste at early age-the role of cement hydration, *Cement and Concrete Research* 116 (2019) 191-201.
- [123] P.J. Barr, B.M. Kukay, M.W. Halling, Comparison of Prestress Losses for a Prestress Concrete Bridge Made with High-Performance Concrete, *Journal of Bridge Engineering* 13(5) (2008) 468-475.
- [124] S. Zingg, G. Habert, T. Lämmlein, P. Lura, E. Denarié, A. Hajiesmaeili, Environmental assessment of radical innovation in concrete structures, in: G. Habert, A. Schlueter (Eds.) *Sustainable Built Environment (SBE) Regional Conference*, Zurich, Switzerland, vdf Hochschulverlag AG, 2016, p. 687.
- [125] A. Leemann, F. Moro, Carbonation of concrete: the role of CO₂ concentration, relative humidity and CO₂ buffer capacity, *Materials and Structures* (2017) 50:30.

- [126] A. Leemann, R. Loser, B. Münch, P. Lura, Steady-state O₂ and CO₂ diffusion in carbonated mortars produced with blended cements, *Materials and Structures* (2017) 50:247.
- [127] T. Lämmlein, F. Messina, M. Griffa, G. Terrasi, P. Lura, Bond Performance of Sand Coated UHM CFRP Tendons in High Performance Concrete, *Polymers* 9(2) (2017) 78.
- [128] H.F. Taylor, Modification of the Bogue calculation, *Advances in Cement Research* 2(6) (1989) 73-77.
- [129] G. Terrasi, E. McIntyre, L. Bisby, T. Lämmlein, P. Lura, Transient Thermal Tensile Behaviour of Novel Pitch-Based Ultra-High Modulus CFRP Tendons, *Polymers* 8(12) (2016) 446.
- [130] E. Toumpanaki, J.M. Lees, G.P. Terrasi, Bond Durability of Carbon Fiber-Reinforced Polymer Tendons Embedded in High-Strength Concrete, *Journal of Composites for Construction* 22(5) (2018) 04018032.
- [131] E. Sakai, T. Kasuga, T. Sugiyama, K. Asaga, M. Daimon, Influence of superplasticizers on the hydration of cement and the pore structure of hardened cement, *Cement and Concrete Research* 36(11) (2006) 2049-2053.
- [132] G. De Schutter, L. Taerwe, Degree of hydration-based description of mechanical properties of early age concrete, *Materials and Structures* 29(6) (1996) 335.
- [133] A. Boumiz, C. Vernet, F.C. Tenoudji, Mechanical properties of cement pastes and mortars at early ages: Evolution with time and degree of hydration, *Advanced cement based materials* 3 (3-4) (1996) 94-106.
- [134] M. Vandamme, F.-J. Ulm, Nanogranular origin of concrete creep, *Proceedings of the National Academy of Sciences* 106(26) (2009) 10552-10557.
- [135] C.A. Jones, Z.C. Grasley, Short-term creep of cement paste during nanoindentation, *Cement and Concrete Composites* 33(1) (2011) 12-18.
- [136] Z. Hu, J. Ston, M. Wyrzykowski, P. Lura, K. Scrivener, Intrinsic viscoelasticity of C-S-H assessed from basic creep of cement pastes, *Cement and Concrete Research* 121 (2019) 11-20.
- [137] C. Di Bella, M. Wyrzykowski, P. Lura, Evaluation of the ultimate drying shrinkage of cement-based mortars with poroelastic models, *Materials and Structures* 50(1) (2017) 52.
- [138] M. Wyrzykowski, P. Lura, F. Pesavento, D. Gawin, Modeling of internal curing in maturing mortar, *Cement and Concrete Research* 41(12) (2011) 1349-1356.
- [139] Z.C. Grasley, C.K. Leung, Desiccation shrinkage of cementitious materials as an aging, poroviscoelastic response, *Cement and Concrete Research* 41(1) (2011) 77-89.
- [140] P. Lura, O.M. Jensen, K. van Breugel, Autogenous shrinkage in high-performance cement paste: An evaluation of basic mechanisms, *Cement and concrete research* 33(2) (2003) 223-232.
- [141] M. Wyrzykowski, P. Lura, Effect of relative humidity decrease due to self-desiccation on the hydration kinetics of cement, *Cement and Concrete Research* 85 (2016) 75-81.
- [142] B.t. Bissonnette, P. Pierre, M. Pigeon, Influence of key parameters on drying shrinkage of cementitious materials, *Cement and Concrete Research* 29(10) (1999) 1655-1662.
- [143] F. Meftah, J. Torrenti, W. Nechnech, C. de Sa, An elasto-plastic damage approach for the modelling of concrete submitted to the mechanical induced effects of drying, in: V. Baroghel-Bouny, P.-C. Aïtcin (Eds.) *International RILEM Workshop on Shrinkage of Concrete*, RILEM Publications s.a.r.l., Paris, France, 2000, pp. 341-354.
- [144] G. Pickett, The Effect of Change in Moisture-Content on the Crepe of Concrete Under a Sustained Load, *Journal Proceedings* 38 (1942) 333-356.
- [145] A.O. Abdelatif, J.S. Owen, M.F.M. Hussein, Modelling the prestress transfer in pre-tensioned concrete elements, *Finite Elements in Analysis and Design* 94(0) (2015) 47-63.
- [146] Abaqus Analysis User's Manual 6.12, 22.7.1, Dassault Systèmes 2012.

- [147] G. P. Terrasi, U. Meier, Long term bending creep behaviour of thin walled CFRP pretensioned high strength spun concrete poles under sustained load, in: R. El-Hacha (Ed.) Proceedings of the 7th International Conference on FRP Composites in Civil Engineering, International Institute for FRP in Construction, Vancouver, Canada, 2014.
- [148] G. Terrasi, G. Battig, R. Bronnimann, Pylons made of high-strength spun concrete and prestressed with carbon fibre reinforced plastic for high power transmission lines, *International Journal of Materials and Product Technology* 17(1) (2002) 32-45.
- [149] T.D. Lämmlein, F. Messina, M. Wyrzykowski, G.P. Terrasi, P. Lura, Low clinker high performance concretes and their potential in CFRP-prestressed structural elements, *Cement and Concrete Composites* 100 (2019) 130-138.
- [150] A. Nanni, FRP reinforcement for prestressed and non-prestressed concrete structures, *Developments in civil engineering No. 42: Fiber-Reinforced-Plastic (FRP) Reinforcement for Concrete Structures*, Elsevier, 1993.
- [151] F. Stoll, J. E. Saliba, L. E. Casper, Experimental study of CFRP-prestressed high-strength concrete bridge beams, *Composite Structures* 49(2) (2000) 191-200.
- [152] T. Hoshijima, K. Yagi, T. Tanaka, T. Ando, Properties of CFRP composites for concrete structures, *First International Conference on Composites in Infrastructure*, Tucson, Arizona, USA, 1996, pp. 227-241.
- [153] M.K. Tadros, N. Al-Omaishi, S.J. Seguirant, J.G. Gallt, Prestress losses in pretensioned high-strength concrete bridge girders, *NCHRP Report No. 496*, Transportation Research Board, Washington, DC, United States, 2003.
- [154] M.K. Tadros, A. Ghali, A.W. Meyer, Prestressed Loss and Deflection of Precast Concrete Members *PCI Journal* 30(1) (1985) 114-141.
- [155] P. Zia, H.K. Preston, N.L. Scott, E.B. Workman, Estimating prestress losses, *Concrete International* 1(6) (1979) 32-38.
- [156] H.K. Preston, J.M. Barker, H.C. Boecker jr, R. Dull, H.H. Edwards, T. Huang, J. Irargorri, H.P. Koretzky, P.E. Kraemer, D.D. Magura, Recommendations for Estimating Prestress Losses, *PCI JOURNAL* 20(4) (1975) 44-75.
- [157] R. Maaskant, T. Alavie, R. Measures, G. Tadros, S. Rizkalla, A. Guha-Thakurta, Fiber-optic Bragg grating sensors for bridge monitoring, *Cement and Concrete Composites* 19(1) (1997) 21-33.
- [158] L.A. Caro, J.R. Martí-Vargas, P. Serna, Prestress losses evaluation in prestressed concrete prismatic specimens, *Engineering Structures* 48 (2013) 704-715.
- [159] G.P. Terrasi, M.R. Wyrzykowski, P. Lura, Self-prestressed reinforced concrete elements, Patent No. EP3106446A1, 2016.
- [160] S.T. Kim, Y. Park, S.Y. Park, K. Cho, J.R. Cho, A sensor-type PC strand with an embedded FBG sensor for monitoring prestress forces, *Sensors* 15(1) (2015) 1060-1070.
- [161] J.M. Gilstrap, C.R. Burke, D.M. Dowden, C.W. Dolan, Development of FRP reinforcement guidelines for prestressed concrete structures, *Journal of Composites for Construction* 1(4) (1997) 131-139.
- [162] C. Bakis, L. Bank, V. Brown, E. Cosenza, J. Davalos, J. Lesko, A. Machida, S. Rizkalla, T. Triantafillou, Fiber-Reinforced Polymer Composites for Construction—State-of-the-Art Review, *Journal of Composites for Construction* 6(2) (2002) 73-87.
- [163] T. Lämmlein, F. Messina, M. Griffa, G. Terrasi, P. Lura, Bond Performance of Sand Coated UHM CFRP Tendons in High Performance Concrete, *Polymers* 9(12) (2017) 78.
- [164] Y.-J. Rao, Fiber Bragg grating sensors: principles and applications, in: K.T.V. Grattan, B.T. Meggitt (Eds.), *Optical Fiber Sensor Technology. Optoelectronics, Imaging and Sensing*, vol 2., Springer, Boston, MA, United States, 1998, pp. 355-379.

- [165] K.T.V. Grattan, T. Sun, Fiber optic sensor technology: an overview, *Sensors and Actuators A: Physical* 82(1) (2000) 40-61.
- [166] B.W. Russell, N.H. Burns, Measurement of transfer lengths on pretensioned concrete elements, *Journal of Structural Engineering* 123(5) (1997) 541-549.
- [167] S.P. Gar, J.B. Mander, S. Hurlebaus, Deflection of FRP Prestressed Concrete Beams, *Journal of Composites for Construction* 22(2) (2018) 04017049.
- [168] M. Faruqi, M.S. Khan, Deflection behavior of a prestressed concrete beam reinforced with carbon fibers at elevated temperatures, *Frontiers of Structural and Civil Engineering* 13(1) (2019) 81-91.
- [169] S.-X. Wang, L.-Z. Wu, L. Ma, Low-velocity impact and residual tensile strength analysis to carbon fiber composite laminates, *Materials & Design* 31(1) (2010) 118-125.
- [170] W. Steinman, *Energiestrategie 2050: Konzept, Stand und nächste Schritte*, Bundesamt für Energie (BFE), Bern, Switzerland, 2012.
- [171] E. Fitzer, A. Foley, W. Frohs, T. Hauke, M. Heine, H. Jäger, S. Sitter, *Fibers*, 15. Carbon Fibers, Ullmann's Encyclopedia of Industrial Chemistry (2000).
- [172] E. Griffing, E. Vozzola, M. Overcash, Life cycle inventory data for carbon fiber and epoxy systems and use in environmentally optimized designs, *LCA XIV San Francisco*, 2014.
- [173] ISO 14040: Environmental management–life cycle assessment–principles and framework, London: British Standards Institution (2006).
- [174] B.P. Weidema, C. Bauer, R. Hirschler, C. Mutel, T. Nemecek, J. Reinhard, C. Vadenbo, G. Wernet, Overview and methodology: Data quality guideline for theecoinvent database version 3, (2013).
- [175] *Ökobilanzdaten im Baubereich 2009/1:2014 KBOB c/o BBL Bundesamt für Bauten und Logistik*, Bern, Switzerland, 2014.
- [176] R. Frischknecht, N. Jungbluth, H.-J. Althaus, R. Hirschler, G. Doka, C. Bauer, R. Dones, T. Nemecek, S. Hellweg, S. Humbert, Implementation of life cycle impact assessment methods. Ecoinvent report No. 3, Ecoinvent Centre, 2007.
- [177] R. Frischknecht, S. Büsser-Knöpfel, *Swiss eco-factors 2013 according to the ecological scarcity method*, Federal Office for the Environment (FOEN), Bern. Switzerland, 2013.
- [178] G. Terrasi, C. Affolter, M. Barbezat, G. Bättig, Increasing the acceptance of high performance concrete prestressed with CFRP, in: M. Motavalli (Ed.) *Proceedings of the Fourth International Conference on FRP Composites in Civil Engineering*, International Institute for FRP in Construction, Zurich, Switzerland, 2008.
- [179] E. Zea Escamilla, H. Wallbaum, Environmental savings from the use of vegetable fibres as concrete reinforcement, 6th International Structural Engineering and Construction Conference. Zürich, Switzerland, 2011.
- [180] E. Griffing, M. Overcash, Carbon fibre HS from PAN, *Chemical Life Cycle Database*, www.environmentalclarity.com, 2010.
- [181] T. Suzuki, J. Takahashi, Prediction of energy intensity of carbon fiber reinforced plastics for mass-produced passenger cars, Ninth Japan International SAMPE Symposium JISSE-9, Tokyo, Japan, 2005, pp. 14-19.

Curriculum Vitae

Name Tobias Dominik Lämmlein
Date of Birth 20.09.1985, Darmstadt
Address Winterthurerstrasse 460
8051 Zürich
Email Tobias.Laemmlein@outlook.com
Nationality German

Education

05/2014 – 04/2019 **Swiss Federal Institute of Technology, Zurich**
PhD ETH
Title Doctoral Thesis : "Development of Novel Low-Clinker High-Performance Concrete Elements Prestressed with High Modulus Carbon Fibre Reinforced Polymers"

03/2010-03/2012 **Swiss Federal Institute of Technology, Zurich**
MSc ETH ME
Focus : Advanced Structures and Aerospace Engineering
Title Master Thesis : "Characterization of Capillary Flow and the Effect of Particle Toughened Resin Systems"

08/2010 – 01/2011 **Chalmers Tekniska Högskola, Gothenburg (Sweden)**
Exchange
Focus : Material Selection and Design

10/2005 – 03/2010 **Swiss Federal Institute of Technology, Zurich**
BSc ETH ME
Focus: Structural Mechanics
Title Bachelor Thesis : „Konstruktion eines Partikeldämpfers“

Practical Experience

04/2012 – 05/2019 **Empa Dübendorf**
Group Mechanical Systems Engineering
Research Assistant

09/2011 – 12/2011 **Swiss Federal Institute of Technology, Zurich**
Autonomous System Lab (ASL), Prof. Siegwart
10/2007 – 01/2010 Student Assistant
03/2007 – 06/2008 **RUAG Schweiz AG, Emmen**
04/2011-06/2011 Division Technology, Team Engineering Design
Internship

02/2006 – 03/2006 **Solidtec GmbH, Dieburg (Germany)**
Internship

Skills

Languages	German (native), English (fluent)
Continued Education	Publishing in Science, 2017 Discuss, Debate and Present, 2016-2017 Scientific Posters, 2014 Polymer materials for technical applications, 2012 Abaqus CAE, 2012

Conference Presentations

Bending Creep Behaviour of CFRP Prestressed Slender Concrete Elements 7 th Biennial Conference on Advanced Composites In Construction (ACIC) St John's College, University of Cambridge	2015
--	------

List of Publications

Low clinker high performance concretes and their potential in CFRP-prestressed structural elements T. D. Lämmlein , F. Messina, M. Wyrzykowski, G. P. Terrasi, P. Lura Cement and Concrete Composites 2019, Volume 100, pp. 130-138.	2019
Bond Performance of Sand Coated UHM CFRP Tendons in High Performance Concrete T. D. Lämmlein , F. Messina, M. Griffa, G. P. Terrasi, P. Lura Polymers 2017, 9(2), 78.	2017
Transient Thermal Tensile Behaviour of Novel Pitch-Based Ultra-High Modulus CFRP Tendons G. P. Terrasi, E. R. E. McIntyre, L. A. Bisby, T. D. Lämmlein , P. Lura Polymers 2016, 8(12), 446.	2016
Environmental assessment of radical innovation in concrete structures S. Zingg, G. Habert, T. D. Lämmlein , P. Lura, E. Denarié, A. Hajiesmaeili Expanding Boundaries: Systems Thinking for the Built Environment, ETH Zurich, pp. 682-687.	2016
Bending Creep Behaviour of CFRP Prestressed Slender Concrete Elements T. D. Lämmlein , G. P. Terrasi Proceedings of the 7th Biennial Conference on Advanced Composites In Construction (ACIC) held at St John's College, University of Cambridge, pp. 56-61.	2015
Value correction in the determination of transverse permeability values by using flow simulation in deformable porous media F. Klunker, M. Danzi, T. D. Lämmlein , B. Louis, P. Ermanni Proceedings of 11th International Conference Flow Processing in Composite Materials (FPCM-11), Auckland, New Zealand.	2012
Characterization of Reactive Resin Flow During High Temperature LCM Injection B. Louis, J. Maldonado, F. Klunker, T. D. Lämmlein , P. Ermanni Proceedings of SAMPE EUROPE 33rd International Technical Conference (SEICO 2012), pp. 26-27.	2012

